Fluorescence Spectroscopy of Trapped Molecular Ions

by

Kenneth Charles Wright

B.Sc., Dalhousie University, 1993

A THESIS SUBMITTED IN PARTIAL FULFILMENT OF
THE REQUIREMENTS FOR THE DEGREE OF

DOCTOR OF PHILOSOPHY

in

The Faculty of Graduate Studies

(Department of Chemistry)

We accept this thesis as conforming
to the required standard

THE UNIVERSITY OF BRITISH COLUMBIA

December 22, 2003

Abstract

This thesis describes the development of a unique instrument capable of detecting fluorescence emission from large gas phase molecular ions trapped in a three-dimensional quadrupole ion trap. The hypothesis that has formed the basis of this work is the belief that fluorescence spectroscopy can be combined with ion trap mass spectrometry to probe the structure of gas phase molecular ions. The ion trap provides a rarefied environment where fluorescence experiments can be conducted without interference from solvent molecules or impurities.

Although fluorescence was not detected during preliminary experiments, two significant experimental challenges associated with detecting the gas phase fluorescence of ions were discovered. First, gas phase ions were vulnerable to photodissociation and low laser powers were necessary to avoid photodissociation. Since fluorescence emission is directly proportional to laser intensity, a lower laser power limits the fluorescence signal. Second, the fluorescence emission was not significantly Stokes shifted from the excitation. The lack of Stokes shift meant the small fluorescence signal must be detected in the presence of a large amount of background scatter generated by the excitation. Initially, this background was seven orders of magnitude higher than the analytical signal ultimately detected.

A specially designed fiber optic probe was inserted between the electrodes of the ion trap to stop light scattered off the outside surfaces of the trap from reaching the detector. The inside surfaces of the ion trap were coated black to further reduce the amount of scattered light collected. These innovations helped reduced the background by six orders of magnitude and fluorescence emission from rhodamine-6G was detected.

Pulse counting experiments were used to optimize fluorescence detection. The effects of trapping level, laser power, and irradiation time were investi-

gated and optimized. The instrument developed in this work not only allows for the detection of fluorescent photons, but the sensitivity is high enough for the light to be dispersed and an emission spectrum recorded. The emission spectra of rhodamine-6G and 5-carboxyrhodamine-6G ions reported in this thesis represent the first spectra recorded from large molecular ions confined in a quadrupole ion trap. Finally, anti-Stokes fluorescence from rhodamine-6G was also detected.

Table of Contents

List of Tables

List of Figures

List of Abbreviations

Abbreviation	Description
5-CR 6G	5-carboxyrhodamine 6G
AC	alternating current
ADC	analog to digital converter
ASMS	American Society for Mass Spectrometry
CCD	charged coupled device
CID	collision-induced dissociation
CPS	counts per second
CW	continuous wave
DAC	digital to analog converter
DC	direct current
DIB	diffuse interstellar band
ECL	emitter coupled logic
EHD	electrohydrodynamic

Abbreviation	Description
ESI	electrospray ionization
FC43	perflourotributylamine
FITC-Gly-Gly-His	fluorescien-glycine-glycine-histidine
FITC-Gly-His	fluorescien-glycine-histidine
fl	focal length
FNF	filtered noise field
FRET	fluorescence resonance energy transfer
FT-ICR	fourier transform ion cyclotron resonance
GFP	green fluorescent protein
HPLC	high performance liquid chromatography
ICCD	intensified charged coupled device
ICR	ion cyclotron resonance
IVR	internal vibrational redistribution
MCP	microchannel plate
MS/MS	two successive mass selective operations
MS^n	n mass selective operations
m/z	mass/charge

Abbreviation	Description
O.D.	optical density
PAH	polycyclic aromatic hydrocarbon
PMT	photomultiplier tube
R6G	rhodamine 6G
RF	radio frequency
S/N	signal to noise ratio
TOF	time of flight
TTL	transistor transistor logic
UBC	University of British Columbia

Acknowledgements

Many thanks are extended to my academic colleagues and mentors. I wish to thank my supervisor Mike Blades for all his assistance. I also want to express my appreciation to Don Douglas who has been very generous with his time and laboratory equipment. Special thanks must go to John Hepburn, for providing many informative tutorials on molecular spectroscopy, allowing me to participate in group meetings, and especially for giving me the idea to coat the ion trap electrodes with carbon. Bruce Todd also deserves a special mention. Bruce has been a great source of technical information over the years.

I want to express my gratitude to the University of British Columbia and the Natural Science and Engineering Research Council for funding my work.

I also acknowledge the significant contribution provided by other members of the UBC Chemistry Department for their professional support and friendship during my years at UBC: John Ellis, Lance Jones, Elizabeth Varty, Brian Ditchburn, Elena Polishchuk, Ben Clifford, Tim Daynard and especially Lani Collins (sorry about that email!) you are wonderful people to know and work with.

For me, there cannot possibly be a better place to build an analytical instrument than the UBC Chemistry Department. The shops and service labs are staffed by truly excellent people. The members of the Electronic and Mechanical Engineering Services shops deserve a great deal of credit for the instrumental achievements described in this thesis. I will forever be indebted to the outstanding members of the Mechanical shop: Des Lovrity, Oskar Greiner, Ed Gomm, Ken Love, Ron Marwick, and Brian Snapkauskas. Truly kings among men. From the Electronics shop I want to thank Dave Bains, Jason Gozjolko, Rolly Chan, Mike Hatton, Milan Coschizza, Martin Carlisle and especially the dynamic duo of Brian Greene and Dave Tonkin.

"Greener" and "Fish" are not only excellent technicians and teachers, but have become great friends.

Finishing my work would have been very difficult without the superb treatment provided by my Dream Team of medical professionals: physicians Dr. Peter Grantham and Dr. Judy Stringer, rehabilitation specialist Dr. John Le Nobel, physiotherapist Tyler Dumont and chiropractor Dr. David Kavlheim. My lawyers Anthony Vecchio and Art Vertlieb also deserve thanks for their role in assembling this medical team.

Thanks must also go to my family and friends for their constant support. In particular I want to thank my parents, Don and Shirley, who have been very patient and my sister Elaine for all her hard work proofreading my thesis. Shane Greek has also been a great friend to have around.

Saving the best for last, I want to thank my wife Holly. Without Holly's emotional and financial support I could not have finished my work. Holly has been "plunking quarters" into me the past few years hoping that I would eventually "pay off". I may have hit a few snags along the way, but in the end I have achieved my goals: to make a significant contribution to science, secure a position at an excellent research facility, and most importantly to have a truly wonderful wife.

For Holly

Chapter 1

Introduction

1.1 Thesis Objective

Instrumentation development has long been a cornerstone of analytical chemistry. Critics of analytical chemistry often confuse instrumentation science with Edisonian tinkering. In fact, many instrument developments are hypothesis-driven. Hypotheses are formulated from the detailed knowledge of how instruments function and by having a fundamental understanding of the chemical and physical phenomena selected for study.

The hypothesis that has driven this work is the belief that fluorescence spectroscopy can be combined with ion trap mass spectrometry to probe the structure of gas phase molecular ions. The ion trap mass spectrometer provides a rarefied environment where fluorescence experiments can be conducted without interference from solvent molecules or impurities. Investigating the molecular fluorescence of trapped ions will be useful in many areas:

studying the conformation of biomolecules, identifying potential diffuse interstellar band (DIB) carriers, and for providing information that would be complementary to other molecular spectroscopies.

The gas phase three-dimensional structure of biomolecules could be investigated by monitoring conformationally dependent native fluorescence of proteins. Fluorescence resonance energy transfer (FRET)[1,2] experiments to probe the structure of gas phase biomolecules has also been proposed.[3] A FRET experiment involves the transfer of electronic excitation energy from a donor molecule to an acceptor chromophore. The energy transfer occurs by dipole-dipole resonance interactions and depends on the separation distance and relative orientation of the donor and acceptor molecules (FRET pairs). By selectively tagging a biomolecule with a FRET pair and monitoring the fluorescence emission, the three-dimensional structure of the biomolecule can be investigated.

Fluorescence spectroscopy and ion trap mass spectrometry could also be used to evaluate potential DIB carriers. The astrophysics community is interested in identifying the molecules responsible for the broad emission bands observed in the interstellar medium. Polycyclic aromatic hydrocarbon (PAH) cations are considered to be potential DIB candidates.[4,5] An ion trap could

be used to simulate interstellar conditions and investigate the fluorescence emission of PAH cations.

The advantages of combining ion trap mass spectrometry and fluorescence emission spectroscopy cannot be applied to any investigation without first developing a suitable instrument. The objective of this work was to develop an instrument capable of detecting fluorescence emission from large gas phase molecular ions confined in an ion trap mass spectrometer.

1.2 Background

The origin of mass spectrometry comes from J.J. Thomson's work at Cambridge University in the early twentieth century.[6] From his discovery of the electron (using a cathode ray tube) to his investigations using beams of positive ions, Thompson set the groundwork for the field of mass spectrometry and predicted its impact on chemistry many years before it was realized.

> "I have described at some lengths the applications of positive rays to chemical analysis: one of the main reasons for writing this book was the hope that it might induce others and especially chemists, to try this method of analysis. I feel sure that there are

> many problems in chemistry which could be solved with much greater ease by this than by any other method. This method is surprisingly sensitive - more so even than that of spectrum analysis, requires an infinitesimal amount of material and does not require this to be especially purified; the technique is not difficult if appliances for producing high vacua are available "
>
> J.J. Thompson[6]

F.W. Aston, a student of Thomson, built a mass spectrograph based on velocity focusing to study stable isotopes. Around the same time (1914-1918) A.J. Dempster, a Canadian working at the University of Chicago, developed the first sector mass spectrometer. Mass spectrometric techniques were soon applied to important problems such as the hydrocarbon analysis of aircraft fuel during World War Two. As scientists became aware of the potential of mass spectrometric analysis, fundamental studies in the field thrived and new instruments were developed. In the 1950's Wolfgang Paul and co-workers invented a new type of mass analyzer called a quadrupole mass spectrometer.[7]

Although 3D quadrupole ion traps (also known as Paul traps) are primarily used as mass spectrometers they have also been used to confine ions for spectroscopic interrogation.[8–13] It has been argued that trapped gas phase ions are close to the ideal spectroscopic sample of an isolated species at rest.[14] A quadrupole ion trap offers mass selectivity and excellent spatial and temporal confinement of ions without introducing perturbations that would impact negatively on the spectroscopy.[14] While these capabilities have been exploited to conduct fluorescence experiments with atomic and small molecular ions, little progress has been made with larger molecular ions.

For the purpose of this work molecules in the range of hundreds Daltons are considered to be large molecules. Many significant experimental challenges must be overcome in order to realize the advantages of using a quadrupole ion trap to confine large molecular ions for spectroscopic interrogation.

One problem common to all types of ions confined in an ion trap is low ion density (typically, $[ion] < 5 \times 10^{-10} M$). In order to detect fluorescence from such a small number of ions the fluorescence must be efficiently separated from the excitation. Atomic ions can be excited by a multiphoton process that would result in the resonant fluorescence having a wavelength

(λ) much less than the excitation (for a two photon excitation, emission λ = $\frac{1}{2}$ excitation λ). Single atomic ions have been detected this way.[8] Emission from atomic ions can also be detected by monitoring a transition lower in energy than the excitation.[3] Alternatively, since atomic ions and small molecules have excited state lifetimes ranging from several tens of nanoseconds to seconds, a pulsed excitation source can be used. The collection of the fluorescence emission is delayed allowing the small fluorescence signal to be detected without interference from the excitation pulse.[15] These spectroscopic techniques used to study atomic ions and small molecular ions trapped in the gas phase are not appropriate for larger ions. An excitation scheme similar to the multiphoton process used for atomic ions leads to rapid heating and photodissociation of molecular ions. Larger molecules typically have excited state lifetimes of a few nanoseconds and it is therefore very difficult to resolve temporally their emission from the excitation.[16]

In condensed phase experiments fluorescence detection is limited by the background emission from impurities and the elastic or inelastic scattering from the solvent or matrix.[17] An ion trap mass spectrometer can eliminate solvent and impurities from the probe volume. However, the lack of solvation presented unexpected difficulties. In condensed phase experiments any

excess vibrational energy acquired by a molecule is efficiently transferred to the surrounding medium. In gas phase experiments, however, internal vibrational redistribution (IVR) redistributes excess internal energy, but the molecule remains vibrationally excited. Vibrational cooling of the ions can take place through collisions with buffer gas molecules or by infrared emission but these processes are very slow and would likely not occur between absorption and emission events.

Continuous excitation, such as that provided by a continuous wave (CW) laser, causes rapid heating of the ions and leads to photodissociation. To avoid unwanted photodissociation, laser irradiances are typically four orders of magnitude lower than those that can be used in solution experiments. Since the molecule cannot relax to the lowest vibrational level of the excited stated before emission occurs, the fluorescence will not be significantly Stokes (wavelength) shifted from the excitation.

For solution experiments, filters that have sufficient optical density at the excitation wavelength and good transmission at the emission maximum are common. As the Stokes shift decreases it is more difficult to find a filter with enough attenuation at the excitation wavelength without also reducing the total fluorescence detected. The gas phase absorption spectrum of a molecule

may also be different from its solution absorbance spectrum. While a shift in absorbance maximum is an important effect to consider, it is a relatively minor problem to solve compared to those already mentioned.

The two main problems of photodissociation and the lack of a significant Stokes shift in the fluorescence emission were not fully appreciated when the instrument was first designed. While initial attempts to detect fluorescence from trapped ions were unsuccessful, many crucial lessons were learned. The knowledge acquired from these initial experiments ultimately led to a better understanding of ion trap instrumentation and the photophysics and spectroscopy of gas phase molecular ions. It was then possible to successfully redesign the instrument and detect fluorescence from large molecular ions. This new instrumentation not only allows for the collection of fluorescent photons, but the sensitivity is high enough for the light to be dispersed and a fluorescence spectrum to be collected.

1.3 Thesis Overview

This thesis describes the development of a unique instrument capable of detecting fluorescence emission from large gas phase molecular ions trapped

in a three-dimensional quadrupole ion trap. Chapter 2 reviews the theory of quadrupole ion traps and details the development of the ion trap mass spectrometer used to confine ions.

Chapter 3 provides a basic discussion of luminescence spectroscopy and describes the development of the optical system. It also contains a description of early experiments with PAH cations and ionic dyes. Although those experiments did not generate a detectable fluorescence signal, the vital knowledged acquired was used to rationalize improvements to the instrument.

Chapter 4 outlines the instrumental modifications and methods used in the first successful fluorescence experiments. Pulse counting experiments used to optimize fluorescence detection are also described. In addition, the effects of trapping level, laser power, and irradiation time are reported.

Chapter 5 details the instrumentation and methods used to collect the emission spectra of rhodamine 6G and 5-carboxyrhodamine 6G ions. Finally, Chapter 6 provides a summary of the thesis and describes potential applications of the instrument developed.

Chapter 2

Mass Spectrometry

A mass spectrometer consists of a source of gas phase ions, an analyzer that separates ions according to their mass/charge (m/z) ratio and a detector that determines the fraction of the total ion current carried by each of the ions. The mass/charge ratio of an ion is defined as:

$$m/z = \frac{mass(amu)}{elementary\,charge} \tag{2.1}$$

which has units of Thomson (Th).

There are many different combinations of ion sources, mass analyzers and detectors available. The mass analyzer and detector regions of a mass spectrometer are contained in a vacuum system while the ion source may be external to the vacuum chamber. A trapping device, the quadrupole ion trap, was chosen to mass select and confine molecular ions for optical spectroscopy. The final version of the instrument also employs two linear quadrupoles for

ion storage and ion transmission. The ion source originally utilized a thermal desorption probe and electron impact ionization but interference from neutral molecules motivated the change to an electrospray ionization (ESI) source.

According to Earnshaw's theorem no combination of static electric fields can be used to confine an electric charge. Quadrupoles are dynamic trapping devices that are capable of confining ions because they use time varying electric fields. Since the three-dimensional quadrupole and linear quadrupole can be used to confine ions they both can be called ion traps. In this thesis the three-dimensional quadrupole will be referred to as a quadrupole ion trap, ion trap, 3D quadrupole, or Paul trap. The linear quadrupole will be referred to as a linear trap or linear quadrupole. Of course, the 3D quadrupole and linear quadrupole are very similar.

The quadrupole potential used for mass selection and ion confinement is generated by applying radio frequency voltages (V_{rf}) to hyperbolic electrodes. The ideal electrode shapes are shown in Figure 2.1. These truncated electrodes will produce an almost perfect quadrupole field near the centre of the trapping volume.

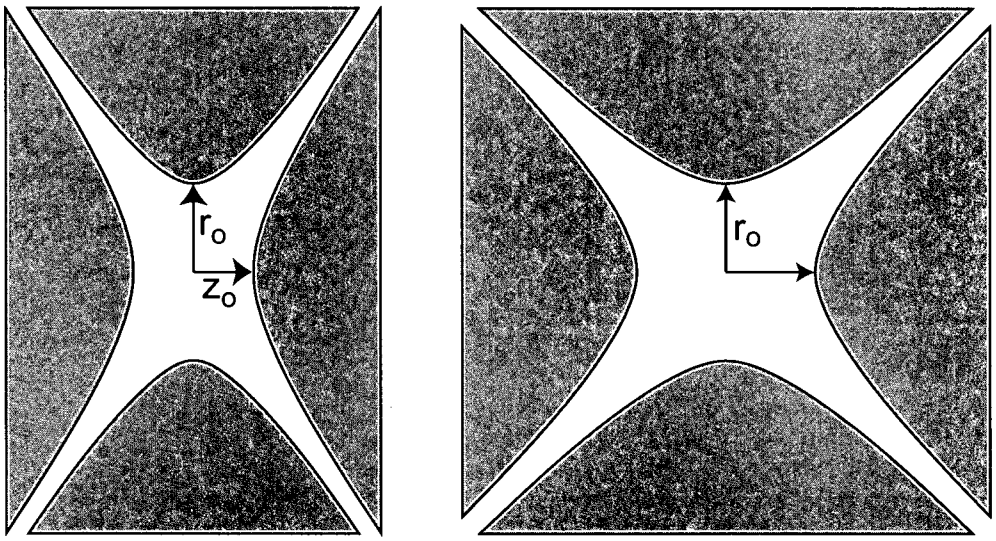

Figure 2.1: Ideal hyperbolic electrode shapes for the 3D quadrupole and the linear quadrupole (identical field radii (r_o) shown).

2.1 Quadrupole Ion Trap Theory

A quadrupole ion trap can be used as a mass selective ion storage device or as a versatile mass spectrometer. Although the ion trap may seem to be a very simple device to understand and operate, there are many subtleties that require closer attention. Descriptions of quadrupole ion trap theory and operation are reviewed in several textbooks and papers.[18–20] A qualitative description of the ion trap and its operation will precede a review of the relevant theory.

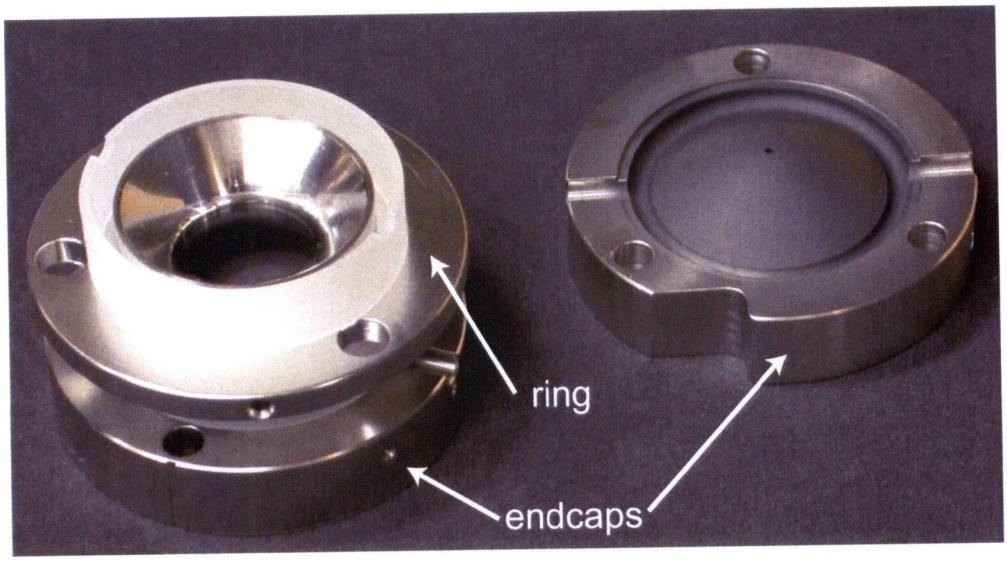

Figure 2.2: Ion trap electrodes. Endcap and ring electrode shown together on left. Single endcap electrode shown on right. White quartz spacers define electrode spacing when assembled.

Figure 2.2 shows the electrodes of the ion trap used in the instrument. Two identical endcaps are positioned symmetrically on either side of the ring electrode. A radio frequency (RF) potential (V_{rf}) is applied to the ring electrode while the endcaps are essentially grounded. Figure 2.3 shows a cross sectional view through the centre of symmetry of the ion trap used in this thesis.

The force (F) acting on an ion of charge e in an electric field ($\overrightarrow{E}$) is defined as:

$$F_u = -e\overrightarrow{E} = -e\left(\frac{\partial\phi}{\partial u}\right) \tag{2.2}$$

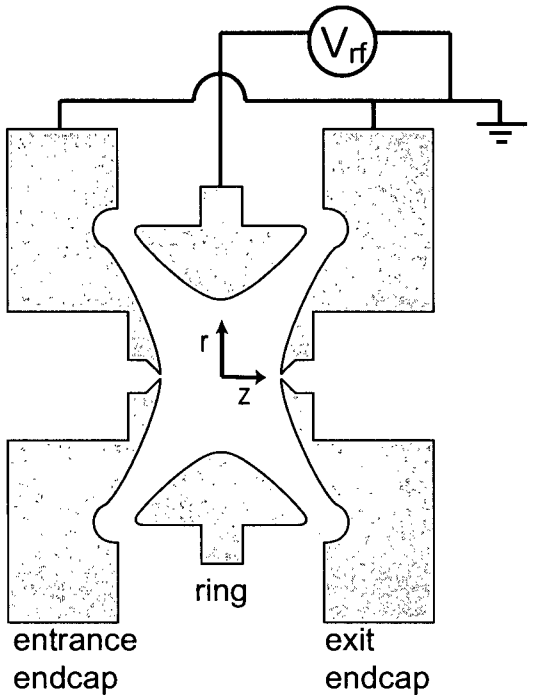

Figure 2.3: Cross-sectional view of ion trap electrodes. RF-potential (V_{rf}) applied to ring while endcaps are grounded.

where ϕ is the electric potential and u represents any direction. Knowing Newton's second law:

$$F_u = ma_u \tag{2.3}$$

one can easily predict the direction an ion will move in an electric field. When ring electrode has a positive potential, a positive ion will experience a force directed away from the ring and toward one of the endcaps. When the ring has a negative potential, the same ion will then be attracted to

the ring and move away from the endcaps. Trapped ions will experience small deviations in their trajectories, commonly referred to as micromotions, with the same frequency as the applied RF potential. This micromotion is superimposed on a larger trajectory as the ion completes a three-dimensional "figure-of-eight".[21] Ions will experience forces proportional to the charge they carry and the acceleration experienced as a result of these forces will depend inversely on their mass. Ions of different m/z ratios will complete figure-of-eights at unique secular frequencies. Ions can be ejected from the trap based on their secular frequencies and an external detector can be used to record a mass spectrum.

2.1.1 The Mathieu Equation

The general operating principles of a quadrupole mass spectrometer can be best understood after a formal treatment of the physics involved. The motion of ions in quadrupole fields are described by second-order differential equations. Conveniently, in 1868 E. Mathieu solved a second-order differential equation while studying the resonant frequencies of drums.[22] Mathieu's solution can be used by simply rearranging the equation describing the motion of ions into the canonical form of the Mathieu equation:

$$\frac{d^2u}{d\xi^2} + (a_u - 2q_u \cos 2\xi)u = 0 \tag{2.4}$$

The potential (ϕ) at any point within the quadrupole field can be described by the equation:

$$\phi_{x,y,z} = ax^2 + ay^2 + bz^2 \tag{2.5}$$

where a is the weighting constant for the equivalent x and y coordinates and b is the weighting constant for the z coordinate. Any electric field that does not contain point charges must be linear in all directions and satisfy the Laplace condition ($\nabla^2\phi = 0$). Therefore:

$$\frac{\delta^2\phi}{\delta x^2} + \frac{\delta^2\phi}{\delta y^2} + \frac{\delta^2\phi}{\delta z^2} = 0 \tag{2.6}$$

From substituting Equation 2.5 into Equation 2.6:

$$\nabla^2\phi = 2a + 2a + 2b = 0 \tag{2.7}$$

$$4a + 2b = 0 \tag{2.8}$$

$$b = -2a \tag{2.9}$$

and by substitution back into Equation 2.5 the potential at any point becomes:

$$\phi_{x,y,z} = ax^2 + ay^2 - 2az^2 \tag{2.10}$$

At this point it is convenient to make the usual substitutions ($x = r\cos\theta$ and $y = r\sin\theta$) to convert Equation 2.10 to cylindrical coordinates. The cylindrical coordinates are defined in Figure 2.3.

$$\phi_{r,z} = a(r\cos\theta)^2 + a(r\sin\theta)^2 - 2az^2 \tag{2.11}$$

$$\phi_{r,z} = ar^2(\cos^2\theta + \sin^2\theta) - 2az^2 \tag{2.12}$$

Since $\cos^2\theta + \sin^2\theta = 1$ Equation 2.12 becomes:

$$\phi_{r,z} = ar^2 - 2az^2 \tag{2.13}$$

If the ion trap was operated by applying the potential (ϕ) to the ring and the same potential 180° out of phase ($-\phi$) on the endcaps. The weighting factor (a) could be determined by substituting the known boundary conditions

into Equation 2.13. Since the endcaps are grounded, a constant (w) must be added to Equation 2.13 in order to satisfy the boundary conditions. It is important to note that this constant (w) does not appear in the equations of motion.

$$\phi_{r,z} = ar^2 - 2az^2 + w \tag{2.14}$$

The endcap spacing is defined as $2z_o$; r_o is inner radius of the the ring electrode and ϕ_o is the electric potential applied to the ring electrode while the endcaps are grounded. Therefore:

$$\phi(r_o, 0) = \phi_o = ar_o^2 + w \tag{2.15}$$

$$\phi(0, z_o) = 0 = -2az_o^2 + w \tag{2.16}$$

Subtracting Equation 2.16 from Equation 2.15 gives:

$$\phi_o = ar_o^2 + 2az_o^2 \tag{2.17}$$

$$a = \frac{\phi_o}{r_o^2 + 2z_o^2} \tag{2.18}$$

Substituting Equation 2.18 into Equation 2.15 gives:

$$w = \frac{2\phi_o z_o^2}{r_o^2 + 2z_o^2} \tag{2.19}$$

The potential in the ion trap can be finally expressed by the following equation:

$$\phi_{r,z} = \frac{\phi_o}{r_o^2 + 2z_o^2}(r^2 - 2z^2) + \frac{2\phi_o z_o^2}{r_o^2 + 2z_o^2} \tag{2.20}$$

Since there are no terms in Equation 2.20 that include both r and z, the equations of motions in each direction can be treated independently. The force experienced by an ion in any direction (u) can be expressed as:

$$F_u = ma_u = -eE_u \tag{2.21}$$

$$m\left(\frac{d^2u}{dt^2}\right) = -e\left(\frac{\partial\phi}{\partial u}\right) \tag{2.22}$$

The equations of motion are therefore:

$$m\left(\frac{d^2r}{dt^2}\right) = -e\left(\frac{2\phi_o r}{r_o^2 + 2z_o^2}\right) \tag{2.23}$$

$$m\left(\frac{d^2z}{dt^2}\right) = e\left(\frac{4\phi_o z}{r_o^2 + 2z_o^2}\right) \tag{2.24}$$

The applied potential will now be defined as a combination of a DC potential, U, and an RF potential, $V\cos\Omega t$, where Ω is the angular frequency of the RF potential ($\Omega = 2\pi f$). Here, V is the 0-peak voltage of the RF potential.

$$\phi_o = U + V\cos\Omega t \tag{2.25}$$

After substituting Equation 2.25 into Equations 2.23 and 2.24 and rearrangement, the equations of motion become:

$$m\frac{d^2r}{dt^2} + \left(\frac{2eU}{r_o^2 - 2z_o^2} + \frac{2eV\cos\Omega t}{r_o^2 + 2z_o^2}\right)r = 0 \tag{2.26}$$

$$m\frac{d^2z}{dt^2} - \left(\frac{4eU}{r_o^2 - 2z_o^2} + \frac{4eV\cos\Omega t}{r_o^2 + 2z_o^2}\right)z = 0 \tag{2.27}$$

Substitutions with the dimensionless Mathieu parameter ξ are now necessary.

$$\xi = \frac{\Omega t}{2} \qquad \textit{and} \qquad \frac{d^2}{dt^2} = \frac{\Omega^2}{4}\frac{d^2}{d\xi^2} \tag{2.28}$$

Therefore:

$$\frac{d^2r}{d\xi^2} + \left(\frac{8eU}{m(r_o^2 - 2z_o^2)\Omega^2} - \frac{-8eV\cos 2\xi}{m(r_o^2 + 2z_o^2)\Omega^2}\right)r = 0 \tag{2.29}$$

$$\frac{d^2z}{d\xi^2} + \left(\frac{-16eU}{m(r_o^2 - 2z_o^2)\Omega^2} - \frac{16eV\cos 2\xi}{m(r_o^2 + 2z_o^2)\Omega^2} \right) z = 0 \tag{2.30}$$

The equations describing the motions of ions in a quadrupole ion trap can now be arranged into the canonical form of the Mathieu equation:

$$\frac{d^2r}{d\xi^2} + (a_r - 2q_r \cos 2\xi)\, r = 0 \tag{2.31}$$

$$\frac{d^2z}{d\xi^2} + (a_z - 2q_z \cos 2\xi)\, z = 0 \tag{2.32}$$

where

$$a_r = \frac{8eU}{m(r_o^2 + 2z_o^2)\Omega^2} \qquad and \qquad q_r = \frac{-4eV}{m(r_o^2 + 2z_o^2)\Omega^2} \tag{2.33}$$

$$a_z = \frac{-16eU}{m(r_o^2 + 2z_o^2)\Omega^2} \qquad and \qquad q_z = \frac{8eV}{m(r_o^2 + 2z_o^2)\Omega^2} \tag{2.34}$$

2.1.2 Regions of Ion Trajectory Stability

The solution to the Mathieu equation can now be used to describe the motion of ions using the values for the Mathieu parameters a_u and q_u. The solutions

to the Mathieu equation are shown graphically in Figure 2.4. Figures 2.4 and 2.5 were adapted from a March paper.[23] Ions with q_z and a_z values falling within the shaded regions have trajectories that are stable in the z-dimension. The same is true for the r-dimension. Ions falling outside of these regions of stability will have trajectories that will increase until the ion hits an electrode or is ejected from the trap. An ion that is stable in the z-dimension but unstable in the r-dimension will likely hit the ring electrode. An ion which is stable in the r-dimension but becomes unstable in the z-dimension will be ejected from the trap through holes in the endcap electrodes. Ions which are stable in both dimensions will remain trapped.

To determine which ions are trapped it is useful to overlap the regions shown in Figure 2.4. The area labelled "Region I" in Figure 2.5 highlights a region where ions are stable in both dimensions. Since most ion traps have no DC potential applied to the electrodes (i.e. $U = 0$) they operate on the q-axis of this stability region. Figure 2.5 also shows that the right boundary of this stability region is defined by $q_z = 0.908$.

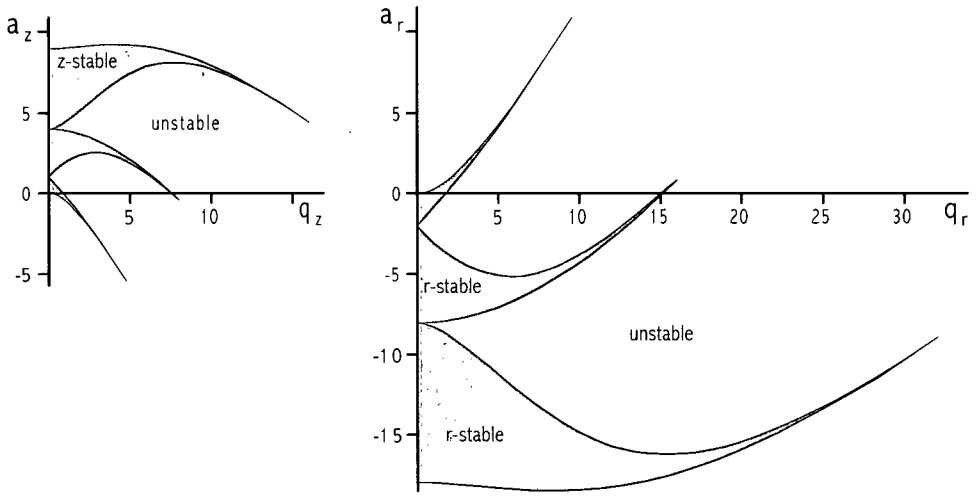

Figure 2.4: Regions of stability defined by a and q. "z-stability" on left and "r-stability" on right. Adapted from a March paper.[23]

2.1.3 Secular Frequencies and Resonant Excitation

Trapped ions complete their stable trajectories with angular frequencies, called secular frequencies (ω_u), defined by the following relationship:

$$\omega_u = \frac{1}{2}\beta_u \Omega \tag{2.35}$$

where:

$$\beta_u \approx \sqrt{\left(\frac{q_u^2}{2}\right)} \qquad (q < 0.4 \quad and \quad U = 0) \tag{2.36}$$

Equation 2.34 shows that q_u depends on the mass (m) and charge (e) of the ion, the amplitude (V) and frequency (Ω) of the applied voltage, and the

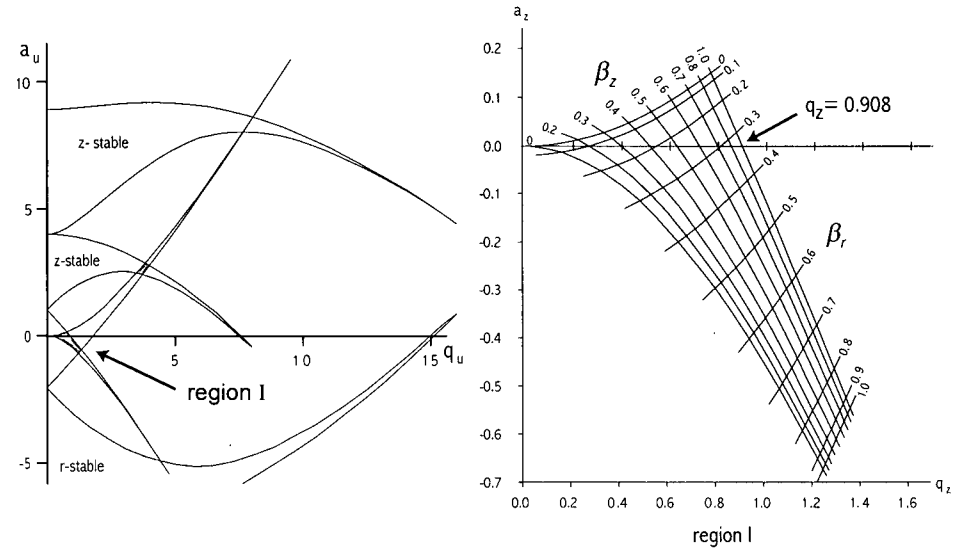

Figure 2.5: Stability in both dimensions defined by the overlap of r-stability and z-stability. The right boundary of Region I is defined by $\beta_z = 1$ (or $q_z = 0.908$ when $U = 0$). Adapted from a March paper.[23]

dimensions of the ion trap (r_o and z_o). For a given set of trapping parameters ions will therefore have unique frequencies depending on their m/z ratio. Ions with a specific m/z can be manipulated by applying a dipolar excitation across the endcap electrodes at a frequency corresponding to their unique secular frequency. This is called resonant excitation.

Resonant excitation is the basis for many ion manipulation techniques that make ion trap mass spectrometry so powerful. Resonant excitation can be used to improve the mass resolution[24] and extend the mass range[25] of an

ion trap mass spectrometer.

2.1.4 Stretched Ion Traps

In the solution to the Mathieu equation outlined in Section 2.1.1 the relationship between the electrode dimensions r_o and z_o were not defined. For a pure quadrupole field one must use perfectly shaped hyperbolic electrodes and the following relationship must be maintained:

$$r_o^2 = 2z_o^2 \tag{2.37}$$

Real electrodes must be truncated adding higher order fields (hexapolar and octupolar) to the mainly quadrupolar field experienced by the ions. Contributions to higher order fields from truncating electrodes are very small and usually do not affect the operation of the ion trap. It was discovered that increasing the distance between the endcaps would add a significant amount of higher order fields($1 - 2\%$ of V) and that these higher order fields could be used to improve ion trap performance.[26] An ion trap with a z_o greater than that dictated by Equation 2.37 is said to be "stretched".

The ion trap used in the instrument was manufactured by Teledyne

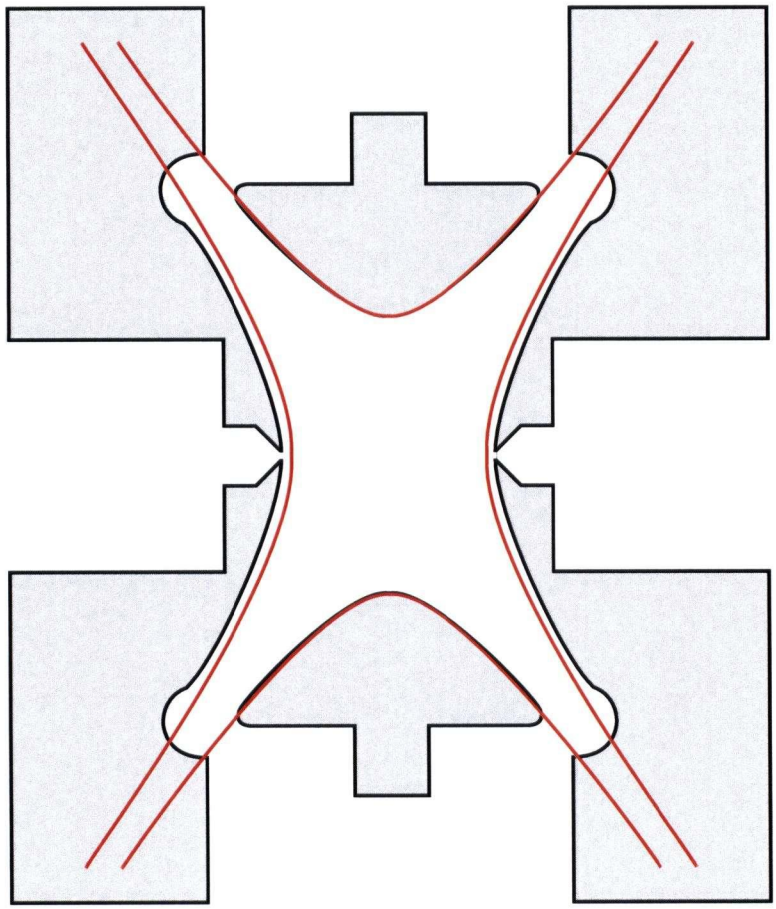

Figure 2.6: The endcaps of the Teledyne 3DQ Discovery are stretched to improve performance. The red line defines "ideal" electrode geometry. The internal diameter of the ring electrode is 2 *cm*.

(Mountain View, USA). Figure 2.6 shows the ideal electrode shape and spacing compared with the actual spacing used in the Teledyne 3DQ Discovery.

The electric potential of a stretched trap is still mostly quadrupolar, especially near the centre of the trap. Ion trajectories and secular frequencies in a stretched trap can be described adequately by considering only the quadrupolar component of the electric field. The higher order fields become more significant as an ion moves farther away from the centre of the trap. When the trajectory of an ion increases it will experience greater effects of hexapolar and octupolar fields. The trajectory of any ion can increase either by coming into resonance with the applied RF-potential (near $q_z = 0.908$) or as the result of resonance excitation. These higher order field contributions are exploited by instrument manufactures to improve the resolution of ion trap devices. The role of higher order fields and other aspects of quadrupole theory will be used to explain the operation of a quadrupole ion trap.

2.2 Ion Trap Operation

Quadrupole ion traps are most commonly used as mass spectrometers. To produce a mass spectrum the majority of commercial traps use some version of a mass selective instability mode. The selectivity of an ion trap can be improved by using a powerful technique called collision-induced dissociation

(CID) to preform tandem mass spectrometry. A relatively high pressure buffer gas is used in ion trap mass spectrometers; this is avoided in other mass spectrometers.

2.2.1 Mass Selective Instability

The majority of ion trap mass spectrometers are operated in what is called a "mass selective instability mode".[27] Trapped ions are sequentially ejected from the ion trap based on their m/z. The ion current measured with an electron multiplier external to the trap is plotted against m/z to produce a mass spectrum.

This mode of operation can be understood by considering the stability diagram (Figure 2.5) and that the q_z value of an ion is directly proportional to the applied RF-potential V (Equation 2.34). For an ion trap operated with only an RF-potential, the ion q_z value will determine its stability. Ions with q_z values below 0.908 will be trapped. To eject an ion from the trap the RF-potential applied to the ring is increased until that ion reaches the stability boundary ($\beta_z = 1$ line, Figure 2.5). At $\beta_z = 1$ the secular frequency of an ion in the z-dimension will come into resonance with the applied potential and its trajectory will quickly increase until it is ejected from the trap through

holes in the endcap electrodes. Lower mass ions have higher q values for a given V so low mass ions will be ejected before heavier ions. Linear ramping of V will produce a signal linear in m/z at the detector, which is a mass spectrum. The mass resolution will depend on how quickly ions come into resonance and the difference in secular frequencies between mass units ($n\ Th$ and $(n+1)\ Th$).

The difference in secular frequencies between mass units depends on the frequency of the RF-potential, trap size, and the q_z at which the ions are ejected. Ion traps are usually designed to give unit mass resolution from $0 - 650\ Th$ and the frequency of the RF-potential is normally close to $1\,MHz$. The RF-potential of ion trap used in this work has a frequency of $909090.90\,Hz$. As a comparison, a ring potential at $60\,Hz$ would be appropriate for the trapping of micron sized particles.

Resonance excitation (Section 2.1.3) can be used with a mass selective instability scan to improve the mass resolution or to extend the mass range of the ion trap. The Teledyne 3DQ ion trap has a potential applied across the endcaps to excite ions just before they reach the stability boundary. This pre-ejection excitation increases the trajectory of the ions and keeps them farther away from the centre of the trap where space charge from heavier ions may

affect their trajectories and secular frequencies. The electric field experienced by the ions farther away from the centre of the trap is also stronger and this helps to eject all ions of a particular m/z faster. The Teledyne 3DQ can easily achieve unit mass resolution from $0 - 650$ Th.

Mass Range Extension

The mass range of the ion trap used can be extended by ejecting ions at lower q_z values. Ejection at a lower q_z is accomplished by applying a different frequency across the endcaps during the mass selective instability scan. Instead of ions being ejected at $q_z = 0.908$, ions can be ejected at a lower RF-voltage. Therefore, for a given RF-power supply the mass range of an ion trap can be increased. Mass range extension is not without problems. First, ejecting heavier ions requires a greater amplitude for the endcap excitation. If operational amplifiers are used to supply the endcap excitation then the mass limit will depend on their maximum output. Even if there is no issue with the power supply, the resolution will degrade as the ejection q_z is lowered because the secular frequencies of adjacent mass units will be closer together.

Currently, ion trap manufacturers extend the mass range of their ion traps

by lowering the frequency of the RF-potential applied to the ring electrode. In this way the resolution is not necessarily degraded as the mass range is extended. The frequency of the RF-potential is fixed for the ion trap used in this work.

Mass Calibration

Mass calibration is accomplished by using known standards. The initial version of the instrument used an electron gun to ionize a calibration gas (FC43) that was leaked into the vacuum chamber. When the instrument was converted to include an ESI source, appropriate calibration solutions had to be sprayed in. These calibration methods are very straightforward. The most important aspect of mass calibration is appreciating just how many operational parameters can affect it. While conducting ion trap experiments it is often difficult to change only one parameter without changing another.

Scan Speed (Th/s), resonant excitation (determined by: frequency, magnitude, rate of change), trap pressure, electrode temperature, and the total number of ions trapped all affect the mass calibration. Some of these parameters are merely hardware and software effects. However, the effects of background pressure and ion density are fundamental to ion trap mass spec-

trometry.

2.2.2 Buffer Gas and Collisional "Cooling"

Quadrupole ion traps are operated at a relatively high pressure for a mass spectrometer. Sector, time of flight (TOF), Fourier transform ion cyclotron resonance (FT-ICR), and even linear analyzing quadrupole mass spectrometers are designed to minimize ion-neutral collisions. Ion traps are typically operated with a helium buffer gas pressure in the $0.01 - 1$ *mtorr* range. This is one to three orders of magnitude higher than pressures used in other mass spectrometers. Ion-neutral collisions are necessary for ions to be efficiently trapped and for optimizing ion trap performance.[27]

The exact ion-neutral collision frequency will depend on the buffer gas pressure and the collisional cross-sections of the ion and the buffer gas. For a molecule in the hundreds of Dalton range the mean time between collisions could be as short as $1\mu s$. An ion will lose a small amount of kinetic energy during each of these collisions. Ions may be created in the trapping volume or they may be injected into the trapping volume from an external source. Ions further away from the trap centre are more likely to be lost from the trap even if they should be stable. The initial position and kinetic energy

of an ion is a critical factor in determining if it will be trapped. Collisions with the buffer gas help trap ions and keep them closer to the centre of the ion trap. This decrease in trajectory amplitude and kinetic energy is often referred to as "collisional cooling". It is important to note that these ions are not rotationally or vibrationally "cool". Trapped ions are considered to be at the same temperature as the buffer gas.[28]

A buffer gas improves ion trap performance by concentrating ions near the centre of the trap. Ions a particular m/z, near the centre of the trap, will experience the same fields and therefore have the same secular frequency. As outlined in Section 2.2.1, ions are separated based on their secular frequencies.

2.2.3 Mass Selective Ion Isolation

Filtered Noise Fields

Section 2.1.3 describes how an ion can be ejected from the ion trap with a dipolar excitation applied across the endcaps at the secular frequency of the ion. It is also possible to isolate an ion of a particular m/z while ejecting all others by applying a waveform which Teledyne called a filtered noise field (FNF). A FNF is made up of many frequencies except the secular frequency

corresponding to the ion which is to be isolated. The ability to isolate ions of a single m/z and trap them for an almost indefinite period of time is the principal advantage of using an ion trap for optical experiments. Pure solutions were used for most of the experiments described in this thesis so mass selective ion isolation was usually unnecessary. Only the ion of interest was usually trapped. This technique could be used if the molecule to be interrogated with optical experiments was contained in a more complex mixture.

Trapping Times

Theoretically an ion can be trapped indefinitely. Unfortunately, time limitations are imposed by the commercial ion trap software. The Teledyne 3DQ was manufactured in the early 1990's and the data acquisition hardware available at that time had some limitations. Synchronous voltage scanning and data collection was limited by the buffer capacities of the digital to analog and analog to digital converters (DAC's and ADC's). While the Teledyne software is very versatile, the maximum trapping time is only 15 seconds. This 15 second time limit was a severe handicap during earlier stages of the instrument development.

Mass Range for Ion Confinement

The mass range of the ion trap discussed in Section 2.2.1 refers to the mass range of the ion trap as a mass spectrometer. The largest m/z ion that can be ejected from the trap and detected represents the high mass limit of the spectrometer. As an ion storage device the mass limit of the trap is much greater. The stability region shown in Figure 2.5 asymptotically approaches the origin where $q_z = 0$. An ion trap may therefore appear to have no mass limit and that infinitely heavy ions could be trapped.

The trapping capacity of an ion trap can be thought of as a potential well. A deep potential well would result in strong focusing of the ions. Ions with very low q experience a shallow potential well and are not trapped effectively. Another problem with very massive and/or multiplied charged ions is their kinetic energy. Heavier ions require a greater number of collisions with buffer gas neutrals before they are slowed enough to be trapped. The trapping efficiency of large ions therefore approaches 0% as q_z approaches zero.

2.2.4 Collision-Induced Dissociation and Tandem Mass Spectrometry

Collision-induced dissociation can be used to determine the structures of ions and to increase the selectivity of ion identification. CID of an ion in a quadrupole ion trap is another powerful technique based on resonance excitation. Resonance excitation is used to increase the trajectory of an isolated ion. As the ion moves away from the centre of the trap it will experience an increasing electric field and therefore greater acceleration. Collisions with the buffer gas will be more energetic and the internal energy of the ion will slowly increase until dissociation occurs. The fragmentation pattern of an ion can be used to elucidate structure. Selectivity of ion identification can be enhanced by using CID for tandem mass spectrometry.

Tandem mass spectrometry is the process of completing two or more mass selective operations in series before the ions are ejected from the trap and detected. Two successive mass selective operations are called "MS/MS" and n mass selective operations are called "MS^n". Tandem mass spectrometry can be used to differentiate ions which have the same m/z but different fragmentation patterns. The molecular ion (precursor) is first isolated and

then CID is used to create fragments known as product ions which are then mass analyzed to produce an MS/MS spectrum. If MS/MS is not selective enough for a particular application, a product ion can be isolated and fragmented (MS^3) to further increase the selectivity of the technique. When combined with chromatography, MS/MS usually provides sufficient selectivity for most applications. Police and customs agencies around the world routinely use tandem mass spectrometry to screen for drugs and explosives.

2.3 Linear Quadrupoles

Linear quadrupoles can be used as ion guides, ion storage devices, and mass analyzers. In the instrument developed, two linear quadrupoles are the key elements of the ion optic system that moves ions from the atmospheric electrospray ionization (ESI) source to the ion trap.

2.3.1 Linear Quadrupole Theory

Most linear quadrupoles consist of four symmetrically positioned rods as shown in Figure 2.7. Round rods can be used to approximate the ideal

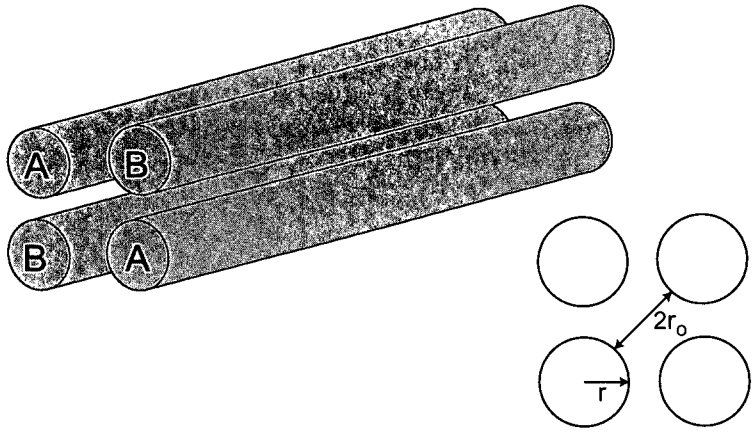

Figure 2.7: Linear quadrupole rod set. $2r_0$ is the distance between poles and r is the rod radius.

hyperbolic shape using the following relationship:

$$r = 1.1487 r_o \tag{2.38}$$

where r is the rod radius and $2r_o$ is the distance between the electrodes. Figure 2.8 demonstrates how rods having a circular cross-section can approximate the ideal hyperbolic shape. Analyzing quadrupoles must be machined to very high tolerances if reasonable resolution is to be obtained. Linear quadrupoles used as storage devices or for ion transmission can be constructed with far less precision.

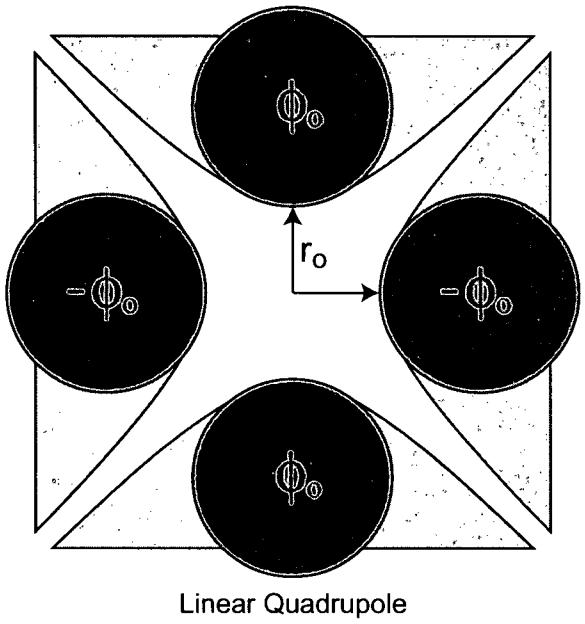

Figure 2.8: End view of linear quadrupole rod set and "ideal" hyperbolic shape. Round rods are used to approximate the hyperbolic shape of ideal quadrupole electrodes.

An electric potential (ϕ_o) is applied to one set of rods while the same potential 180° out of phase ($-\phi_o$) is applied to the other rod set (Figure 2.8). The Mathieu equation and solution are also used to describe the linear quadrupole. The Mathieu parameters for the linear quadrupole are:

$$a_x = -a_y = \frac{8eU}{mr_o^2\Omega^2} \qquad and \qquad q_x = -q_y = \frac{4eV}{mr_o^2\Omega^2} \tag{2.39}$$

The x-dimension can be defined by a line passing through the centres of the rod ends labeled A in Figure 2.7 and the y-dimension would then be defined by a line passing through the centres of the rod ends labeled B in Figure 2.7. The z-dimension is therefore parallel to the rods. Since there is no quadrupole field in the z-dimension the linear quadrupole does not focus ions in the z-dimension.

Linear quadrupoles operated at high vacuum pressures will quickly focus a beam of ions towards the centre of the device. This property, first discovered by Douglas[29], is extremely useful for ion transmission. Collisional focusing in the linear quadrupole concentrates the diffuse ion beam from the ion source so that it may be efficiently focused through small apertures.

2.3.2 Linear Quadrupole Operation

Only an RF-potential was applied between the poles of the quadrupoles used in our instrument (*i.e.* $U = 0$). RF-only linear quadrupoles should transmit a wide mass range of ions. Lenses positioned at both ends of the linear quadrupole are used to trap ions. To trap positive ions, the lenses are biased with a higher DC voltage than the quadrupole rods. All four rods of the linear quadrupole are biased with the same potential so as not to affect the

quadrupole field (*i.e.* $U = 0$). Ions are pulsed out of the linear quadrupole by lowering the voltage on one lens (exit lens). To use a linear quadrupole in ion transmission mode the entrance lens, quadrupole rods, and exit lens are biased with decreasing voltages so positive ions will be accelerated in the desired direction.

Although RF-only linear quadrupoles can be operated at high vacuum pressures they must be kept clean. This may seem to be an obvious point but poor practices in this area are common. Sometimes plastics are used as insulators in high pressure regions of a mass spectrometer because the outgassing of these materials has little effect on the measured vacuum pressure. However, contaminants from these plastics can lead to the formation of unwanted adducts when ions are stored for long periods of time ($> 1\ s$). Contaminated electrodes and mounting hardware can also hold a static charge and can have a negative impact on ion storage and transmission.

2.4 The Ion Source

Many different ion sources can be coupled to an ion trap mass spectrometer. In early versions of the instrument an electron gun was used to ionize neutral

molecules, which had been thermally desorbed from a heated tungsten filament. The final version of the instrument uses electrospray ionization (ESI) to generate ions external to the ion trap. Although the thermal desorption probe ultimately had to be replaced, much was learned about the performance of the ion trap and the photophysics of trapped gas phase molecular ions.

Analyte solutions used in this work were prepared using HPLC grade solvents. For the PAH experiments saturated solutions were used to load analyte molecules onto the thermal desorption probe. For the ESI experiments dilute solutions were prepared in three dilution steps. While volumetric flasks were always used to prepare the first two stock solutions the final solutions used for ESI were prepared less precisely. Of course, the integrity of the molecules was confirmed by mass spectrometric analysis for each optical experiment. Also, the exact composition of the stock or ESI solutions are not relevant to the optical experiments preformed on trapped ions. Only the ions confined in the ion trap and neutral molecules present in the vacuum are important.

2.4.1 Thermal Desorption and Electron Impact Ionization

The thermal desorption probe designed and built for the initial experiments consisted of a long stainless steel tube used to support two wire electrodes (see Figure 2.9). A tungsten filament was spot welded between the wires at the vacuum end of the probe. To load the probe with molecules the filament was soaked in an analyte solution and allowed to dry. The probe was then inserted into the vacuum system through a ball valve and the tungsten filament was positioned between the exit endcap and the ring electrode. A current was passed through the wire electrodes to heat the tungsten filament, thus desorbing the analyte molecules into the internal volume of the ion trap. Before the vacuum system pumped away all the neutrals, an electron gun was used to pulse a beam of electrons into the ion trap ionizing some fraction of the molecules. This electron impact ionization can be represented by the following equation:

$$M + e^- \rightarrow M^+ + 2e^- \tag{2.40}$$

This ion source was very easy to use and efficiently filled the ion trap

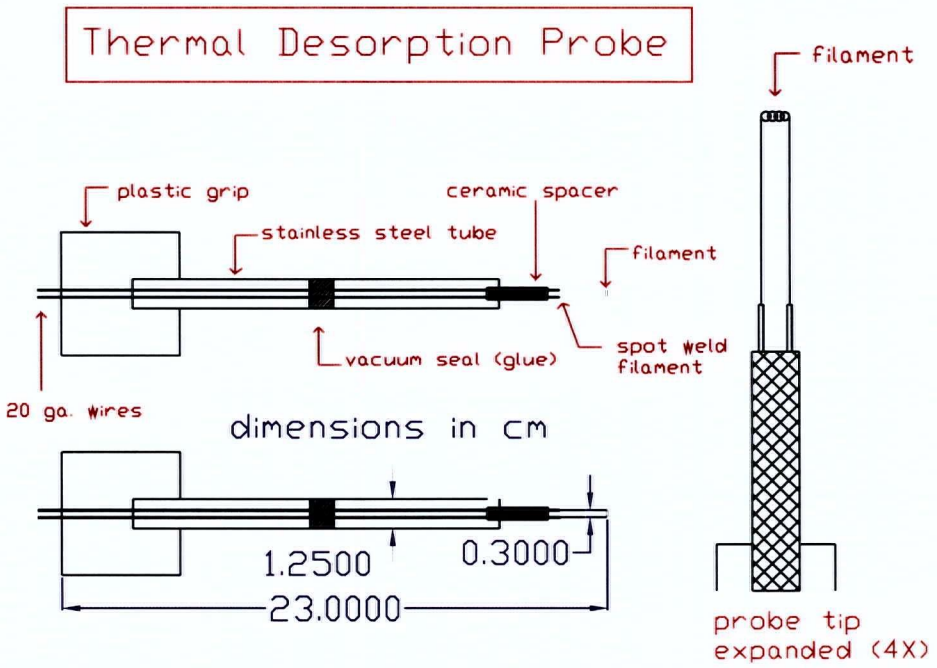

Figure 2.9: Thermal desorption probe.

with ions. Unfortunately, thermal desorption also created a significant background of neutral molecules in the vacuum system. It was suspected that any emission from trapped ions was buried under the emission from neutrals (gas phase or adsorbed to surfaces). Changing to an external ESI source eliminated the problem of a neutral background and allowed a new class of molecules to be investigated.

2.4.2 Electrospray Ionization

Electrospray is a method used to transfer ions present in solution to the gas phase. Many articles on ESI fundamentals have been written,[30–32] and a book edited by Cole[33] is an excellent reference. The general design of the ESI front-end was provided by Dr. Don Douglas (UBC Chemistry) as a part of a collaboration.

Figure 2.10 is a schematic of the ESI front-end used here. A glass capillary carries a solution of ions from the syringe pump to the stainless steel sprayer where a high potential induces electrohydrodynamic (EHD) spraying.[34–36] Air is used to pneumatically assist the spraying process when solutions having a high surface tension (*i.e.* mostly water) are used. Pneumatically assisted electrospray is called ionspray. Typically, a potential of 3000V-5000V between the the sprayer and the curtain plate will produce a spray containing highly charged droplets. Some of these droplets evaporate and pass through the sampling orifice. Evaporation, enhanced by using a counterflow of dry nitrogen gas, will eventually lead to the formation of gas phase ions. Ions and neutrals now pass through the orifice and into the vacuum system where the expansion is sampled by the skimmer. Bare ions (no solvent) are then confined in the first RF-only linear quadrupole (Q_0).

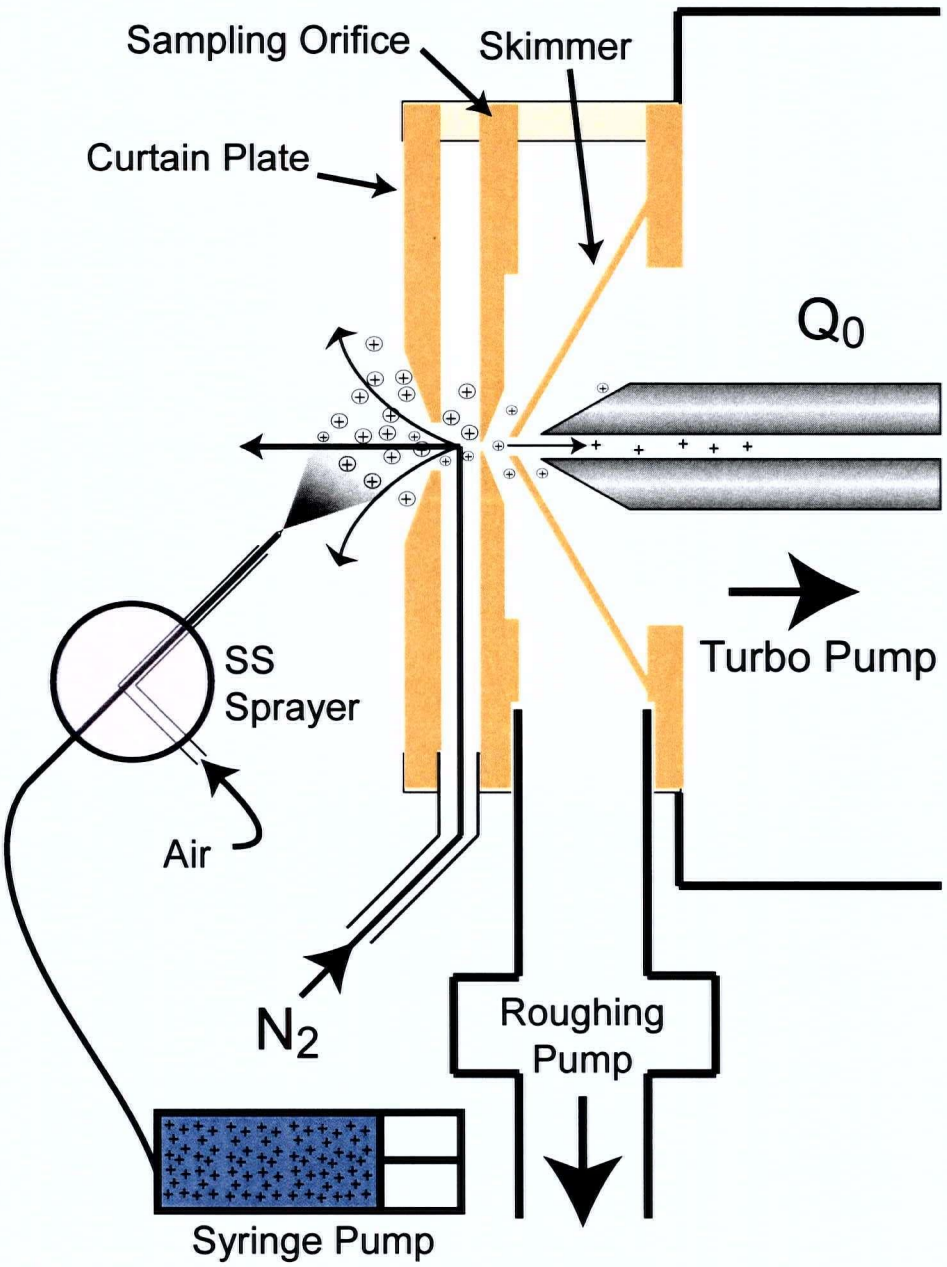

Figure 2.10: ESI Front-end.

Electrospray ionization is a "soft" ionization technique that allows thermally labile ions to be transferred to the gas phase without falling apart. Besides eliminating neutral analytes from the ion trap the ESI source can be used to generate ions from wide variety of molecules including dyes, peptides and proteins.

2.5 MS Instrumentation

A commercial ion trap (Teledyne 3DQ Discovery) was significantly modified to provide the ion trap mass spectrometer component of the instrument. All of the initial modifications involved gaining optical access to the trapping volume of the ion trap. The final version of the instrument has an external electrospray ion source. Although a great deal of time was needed to couple this external ion source to the Teledyne system, successful completion of the optical experiment may not have been possible without this new ion source. Figure 2.11 is a diagram of the mass spectrometer used to confine ions for optical spectroscopy. Ions generated using ESI are transmitted to the ion trap using two RF-only linear quadrupoles (Q_0 and Q_1). Transmission of ions from the ESI source to the ion trap requires a large pressure drop and

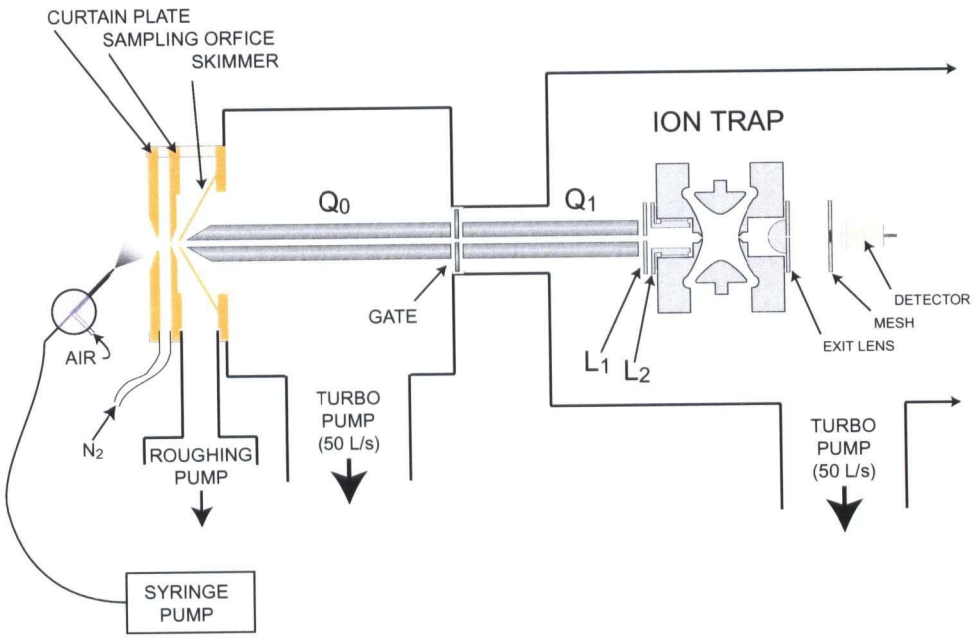

Figure 2.11: Mass spectrometer.

ion optics to accelerate the ions towards the trap.

2.5.1 Vacuum System

For optical experiments the ion trap is usually held close to 1 $mtorr$. The pressure drop from atmosphere is achieved in three stages. The area between the sampling orifice and skimmer is pumped using a Leybold D8A roughing pump providing 190 L/min of pumping speed. The pressure achieved in this region is approximately 950 $mtorr$. The next stage of pumping uses a $50L/s$

turbomolecular pump (Leybold Turbovac 50) to keep Q_0 at a pressure of approximately 7 $mtorr$. Finally, the vacuum chamber containing Q_1 and the ion trap was pumped with another 50 L/s Leybold Turbovac 50. Both turbo pumps were backed using an Edwards E2M-18 2-stage roughing pump (343 L/min).

The pressure in the ion trap is increased for optical experiments by leaking in a helium buffer gas. A Granville Phillips (Boulder, USA) variable leak valve was used to control the pressure of helium. Between optical experiments the helium pressure is decreased to prolong the life of the turbo pumps. Some helium (1 to $5 \times 10^{-5} torr$) is still leaked into the system when the instrument is not in use to prevent the backtreaming of pump oil which would otherwise contaminate the vacuum system.

Surfaces contaminated with pump oil, or other organic molecules, can hold a static charge. A severely contaminated vacuum system can degrade the performance of a mass spectrometer. The transmission efficiency of the electrospray front-end was especially vulnerable to contamination. In fact, the ion trap could not be filled to capacity in 15 s (time limit of ion trap software) until all of the plastic was removed and a thorough cleaning of the front-end was completed. This cleaning of the front-end also included an

ESI & Ion Guide Operating Voltages		
Component	Voltage	Power Supply
Sprayer	3500	Kepco #188-0021
Curtain Plate	195	VG Micromass PQ Lens Supply
Sampling Orifice	80	VG Micromass PQ Lens Supply
Skimmer	46	VG Micromass PQ Lens Supply
Q_0 Offset	35	Xantrex LXQ 60-1
Gate	39	Chem. E-Shop Lens Supply #00728
Q_1 Offset	30	Xantrex LXQ 60-1
L1	30	Chem. E-Shop Lens Supply #00728
L2	30	Chem. E-Shop Lens Supply #00728

Table 2.1: Suitable operational voltages for singly charged ions.

improvement of the ion optics.

2.5.2 Ion Optics

The ion optics used to transmit ions from the ESI source to the ion trap are very straightforward. To accelerate a cation, an electric field must be established in the desired direction. Table 2.1 shows the voltages used to trap a 450 Th singularly charged cation. The voltage drop between the first few ion optics is large because of the high pressures in these regions. Once past the skimmer, voltage drops are much lower.

For most experiments, ions were accumulated in Q_0 by keeping the Gate voltage $3-5\,V$ higher than the Q_0 offset. The offsets applied to the linear quadrupoles were applied to all four rods. This should not be confused with

the DC potential U in Equation 2.39. Ions stored in Q_0 are pulsed into the ion trap by briefly lowering the Gate potential.

The linear quadrupoles are the key elements of the ion optics. The collisional focusing in the high pressure Q_0 narrows the beam of ions collected from the skimmer. Collisional focusing allows more ions to pass through the small hole in the entrance endcap. The RF-potential applied to the linear quadrupoles was generating using a single SCIEX (Toronto, Canada) power supply. The RF-supply operated at 1 MHz and was capacitively coupled to Q_1 which was, in turn, capacitively coupled to Q_0. The impedance of the capacitors creates a voltage divider. The amplitude of the RF-potential on Q_0 is approximately 75% of the amplitude on Q_1.

Externally generated ions must lose kinetic energy after they are injected into the ion trap through collisions with the buffer gas.[37] Ions injected with too much kinetic energy will not be trapped. Therefore, the voltage drop between the Gate and the grounded entrance endcap must be kept low. The RF-voltage applied to the ring electrode during ion injection is also critical.

To optimize injection of a particular ion, the RF-voltage applied to the ion trap ring electrode should correspond to a q_z of between 0.1 and 0.2 for that ion.[37] The phase of the potential is obviously important but a pulse of

ions from Q_0 will persist for many RF-cycles so no synchronization is possible or necessary. The ions should also be shielded from the entrance endcap as much as possible before injection so that voltages applied to the ion trap do not disrupt the ion beam. Early versions of the ESI front-end included an aperture between L1 and L2 that was connected to the ring electrode. The ion trap could not be filled to capacity until this aperture was insulated from the endcap and connected to L2 as shown in Figure 2.11. This modification of L2 and the cleaning described in Section 2.5.1 increased the ion transmission by at least two orders of magnitude. This increase in ion transmission allowed the ion trap to be filled to capacity.

As ions are scanned out of the ion trap during a mass scan they are accelerated towards the detector with an exit lens. The exit lens is biased to -300 V. The exit lens also shields ions from the exit endcap as they leave the trap. The ions pass through the mesh electrode before they hit the detector. The mesh electrode is biased to $+300V$ when a mass scan is not in progress to prevent unwanted ion from hitting the detector.

2.5.3 Ion Trap Control

The commercial control software of the Teledyne 3DQ Discovery is versatile. The Teledyne 3DQ uses a mass selective instability mode enhanced with early resonant ejection (Section 2.2.1). The frequency and amplitude of resonant excitation, scan speed, injection voltage, trapping voltage, trap temperature, and multiplier voltage can all be controlled with the software. As previously discussed, the main limitation is the 15 s time limit for a single mass spectrometric sequence. The data processing package supplied by Teledyne also has limitations so a LabVIEW program (National Instruments, Austin, USA) was developed to process mass spectra.

The Teledyne 3DQ was delivered with a $0-650\,Th$ mass range. The mass range was extended to approximately $2000\,Th$ by changing the gain of the two amplifiers which supply the resonant excitation to the endcaps. When operated with an extended mass range, the mass scan speed was reduced from the default 12000 Th/s to 1000 or 2000 Th/s. The buffer gas pressure must also be lowered to extend the mass range. Unfortunately, lowering the buffer gas pressure also lowers the trapping efficiency and fewer ions can be trapped.

Chapter 3

Spectroscopy and Optics

It was hypothesized that combining the sensitivity of fluorescence spectroscopy with the selectivity of ion trap mass spectrometry would produce a mass spectrometer with unique detection capabilities. The fluorescence from a single barium ion had been detected in an ion trap[8] and fluorescence emission from molecular cations insolated in a frozen noble gas matrix had been characterized. If one atomic ion could be detected then surely a million fluorescent molecular ions could also be detected. The ion trap's rarified environment and long trapping times seemed to be ideal for ultra-sensitive fluorescence spectroscopy.

Fluorescence spectroscopy is a very sensitive technique when used with condensed phase experiments. Generally, the limit of detection for fluorescence experiments is $\approx$ 1000 times lower than absorption spectroscopy.[38] It is intrinsically easier to measure a small fluorescence signal against a zero

background than to detect small differences in two large signals in an absorption experiment. The intensity of the fluorescence signal (I_f) is given by the following equation:

$$I_f = 2.303\phi_f I_o \epsilon c d \tag{3.1}$$

where ϕ_f is the fluorescence quantum efficiency, I_o is the excitation intensity, ϵ is the wavelength dependent molar absorptivity, c is concentration and d is path length. Another advantage of fluorescence spectroscopy is that the signal I_f can be increased by using the high intensity output of a laser for excitation (I_o). Furthermore, since trapped ions can be contained almost indefinitely, the signal from many absorption and emission events can be integrated to increase the total amount of fluorescence detected . While I_f is obviously important, the limit of detection is really dependent on the signal to noise ratio (S/N) and the magnitude of the background signal.

Fluorescence is normally significantly red shifted from the excitation so the excitation does not directly contribute to the background. In condensed phase experiments, the background signal is usually dominated by Rayleigh and Raman scattering from the solvent, and fluorescence from the solvent and impurities.[17] Since the ion trap eliminates any solvent or impurities from the probe volume, it was theorized that detection limits may be even better than

those obtained in solution.

Modifying an ion trap to allow optical access for both excitation and emission, while preserving the functionality of the mass spectrometer, was expected to be the main instrumental challenge of this project. Unfortunately, several aspects of gas phase spectroscopy were not anticipated and the experiment proved impossible without major instrumental modifications. This chapter describes the development of the optical system used to detect fluorescence emission from large gas phase molecular ions trapped in a quadrupole ion trap mass spectrometer. While initial experiments failed to detect fluorescence, they led to an improved understanding of the fundamental processes involved. This chapter describes how the knowledge gained from these early experiments was used to develop a successful instrument.

3.1 Optical Access to the Trapping Volume

In order to gain optical access to the trapping volume, modifications to the vacuum chamber and ion trap electrodes were necessary. A new vacuum chamber was machined with three optical ports to allow the laser radiation to enter and exit the chamber. It also allowed any fluorescence emission to

exit the chamber. Two slots in the entrance endcap and one slot in the exit endcap allowed the laser beam to enter and exit the trapping volume, and allowed emission from inside the trap to be collected.

Brian Snapkauskas (UBC Chemistry Mechanical Engineering Shop) machined a new vacuum chamber from a solid block of aluminium. The chamber was then black anodized (Altech Anodizing Ltd., Delta, Canada) to reduce light scatter. Custom flanges were built to hold glass windows. These flanges were then welded at angles that corresponded to the asymptotes of the hyperbolic electrodes. To avoid problems with reflections, the laser entrance window was replaced with a quartz Brewster window on the end of a long black anodized tube.

Laser light from the Spectra Physics (Mountain View, USA) Stablite 2017 argon ion laser was spatially filtered before being passed into the ion trap. A long focal length (500 mm fl) plano-convex lens was used to focus the laser. Two cone shaped 3 mm apertures, located behind the Brewster window, were used for the spatial filtering. The beam waist is $\approx 1\,mm$ in diameter at the centre of the ion trap. It would be easier to pass a more tightly focused laser beam through the ion trap without hitting an electrode, but fewer ions would be excited because the ion cloud radius is at least 2 mm in diameter.

A CW laser was chosen over a pulsed laser because the CW laser can deliver more photons to the probe volume without causing unwanted multiphoton absorption.

Figure 2.2 shows the Teledyne electrodes without optical access slots. In order to create a line of sight through the ion trap, 5 *mm* wide slots were cut from the outside edge of the endcap to the edge of the channel surrounding the hyperbolic surface. The modifications made to the electrodes and vacuum chamber did not degrade the performance of the instrument as a mass spectrometer.

3.2 Optical Detection

The original optical collection system used several singlets for confocal imaging and to correct for chromatic abberations. The first singlet (*i.e.* lens) was positioned inside the vacuum system close to the slot cut into the entrance endcap. The aperture used for confocal imaging was positioned at the back focal point the first lens (usually inside the vacuum system). Outside the vacuum system, two plano-convex lenses separated by the sum of their focal lengths were used to correct for chromatic abberations and to focus the

collected light onto the entrance slit of the spectrograph. The optical configuration was aligned by irradiating a small amount of dye solution, which was held in the centre of the ion trap with the vacuum system open and the trap electrodes removed. A software program was written to calculate the exact front and back focal lengths of the lenses as a function of wavelength.

The 0.150 m spectrograph used for this work has a 600 $groove/mm$ grating blazed at 500 nm (Acton SpectraPro-150, Acton, USA). The spectrograph is a Czerny-Turner type with a flat focal plane, an f-number of 4.0, and a dispersion of 9 nm/mm. The optical system was designed with the last lens having an f-number of 4.0 so that the grating would be fully illuminated. The charged coupled device (CCD) detector used for all preliminary experiments with the spectrograph was a 1024×512 CCD (TE/CCD 1024 EEV UV1, Princeton Instruments, Tucson, USA). The optical setup used with the thermal desorption probe (Section 2.4.1) is shown in Figure 3.1.

3.3 First Experiments with PAH Cations

PAH cations were the first analytes investigated. PAH cations were chosen because they are toxic in the environment even at low levels and sensitive

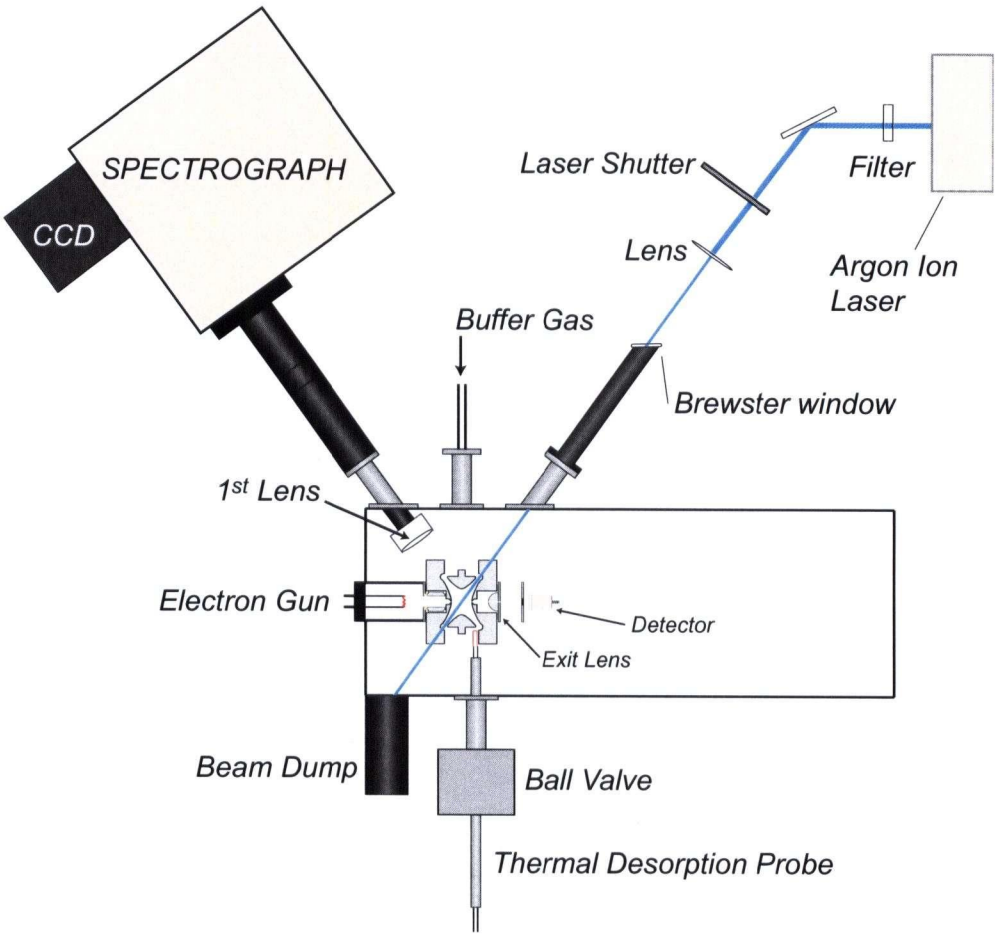

Figure 3.1: Instrumentation used to study PAH cations. (*N.B.* only part of the laser is shown)

methods to detect them are needed.[39] Their mass spectrometric identification can be complicated by the fact that there is often more than one geometric isomer corresponding to the same m/z in a mass spectrum. It was predicted that fluorescence detection of trapped PAH cations would be a more sensitive and selective analytical technique than ion trap mass spectrometry alone.

3.3.1 Methods

Two PAH molecules were chosen based on the matrix isolated absorption spectra of their cations[40] (see Figure 3.2). As shown in Equation 3.1, fluorescence intensity (I_f) is directly proportional to molar absorptivity (ϵ). The absorption of tetrabenzo[acfh]napthalene and benzo[ghi]perylene corresponds to the wavelengths available with the argon ion laser (i.e. $488\,nm$ and $514\,nm$). Obviously, in order to detect fluorescence it must be possible to excite the cations. Tetrabenzo[acfh]napthalene was synthesized in the UBC Chemistry department by Tim Daynard who followed a procedure found in the literature.[41] Benzo[ghi]perylene was purchased from Aldrich Chemical Company (St. Louis, USA).

Benzene solutions of the PAH molecules were applied to the tungsten filament of the thermal desorption probe (Section 2.4.1). The probe was

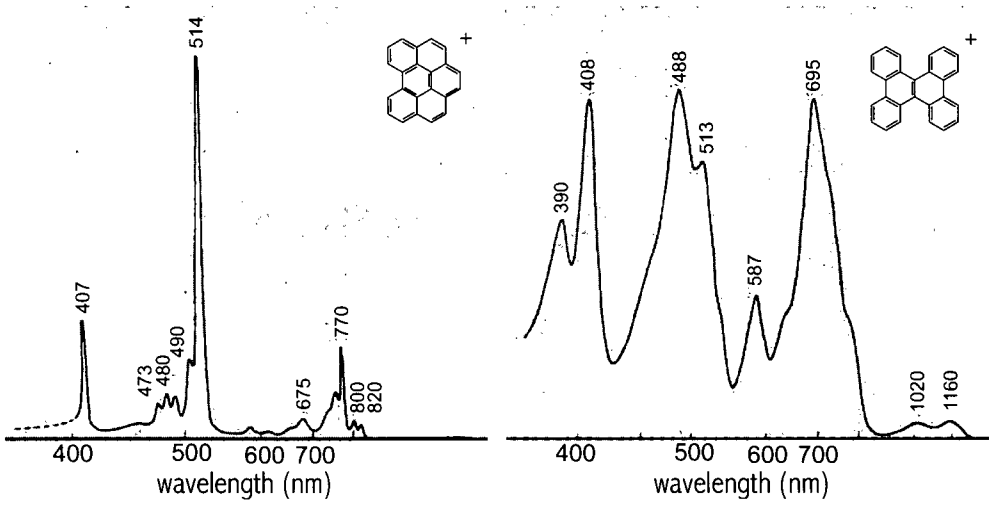

Figure 3.2: The matrix isolated cation absorption spectra of Benzo[ghi]perylene (left) and Tetrabenzo[acfh]napthalene (right).(from *Electronic absorption spectra of radical ions.*, volume 34 of *Physical sciences data.* Elsevier, New York, 1988.)

then inserted into the vacuum chamber with the filament positioned between the ring and exit endcap. A current was passed through the filament and neutral PAH molecules were thermally desorbed into the trapping volume. Radical cations were then created using a beam of $70\,eV$ electrons from an electron gun (Equation 2.40).

The original Teledyne instrument was equipped with an electron gun positioned behind what is now referred to as the entrance endcap. Electrons were accelerated into the ion trap by pulsing an electrostatic lens at the end of the electron gun. The duration of the electron pulse is software controlled

which allows one to control the number of ions created. It was very easy to fill the ion trap to maximum capacity by increasing the duration of the ionization pulse. The trapping level during the ionization step was normally kept close to $q_z = 0.3$ for these first optical experiments.

The light given off by both filaments, which was a major limitation, was initially overlooked. The tungsten filaments of the electron gun and thermal desorption probe give off a significant amount of light. The filament supply for the Teledyne's electron gun was modified to include a high current mechanical relay. A similar relay was used with the thermal desorption probe. These relays were gated on and off so that light from the filaments would never reach the CCD. As well, the laser light was gated on and off using a crude but effective shutter constructed in the lab from a business card and a solenoid. Figure 3.3 shows the usual timing for the experiment.

Only dark current and read noise were initially considered to be limiting sources of noise in this experiment. It was expected that the Stokes shift in the gas phase fluorescence might be different than the Stokes shift observed in the matrix experiments, however the fluorescence was still expected to be red shifted significantly from the laser line. If this were true, the fluorescence measurement could be made against a zero background, as detector noise

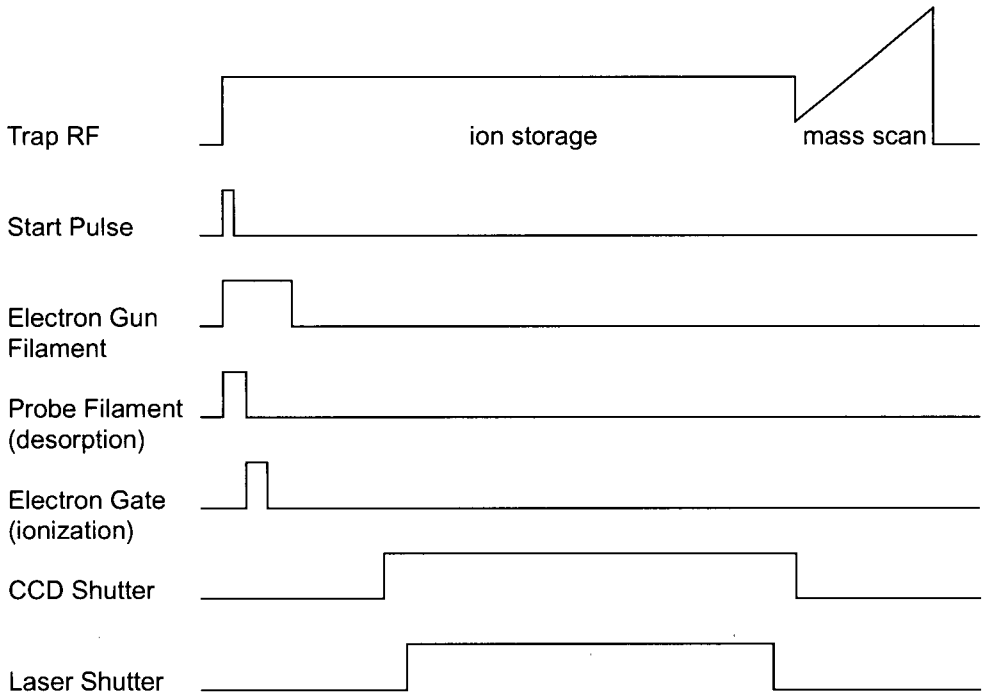

Figure 3.3: Timing diagram for early optical experiments on PAH cations using the thermal desorption probe. The start pulse is TTL, the next three are either on (high) or off (low), and the shutters are open (high) or closed (low).

was the only background noise expected. The CCD was cooled to $-50°C$ to reduce its dark current and full vertical hardware binning was used to reduce the read noise. Since noise in a CCD follows Poisson statistics, the rms noise is the square root of the background. In the low-light regime, the significant noise sources are read noise and dark current noise. The total background noise for a CCD is given by the following equations:

$$dark\ noise = \sqrt{dark\ current} \tag{3.2}$$

$$total\ background\ noise = \sqrt{(read\ noise)^2 + (dark\ noise)^2} \tag{3.3}$$

3.3.2 Photodissociation

The first optical experiments were conducted before the CCD detector was available. Absorption was detected by observing photodissociation of the PAH cations. Photodissociation was used to align the laser beam with the centre of the ion cloud as well as to determine the dimensions of the ion cloud. Figures 3.4 and 3.5 show typical photodissociation spectra.

Initially, photodissociation was a welcomed indication that the ions were absorbing, but unfortunately, photodissociation also limited the laser power that could be used. In solution experiments, much higher laser powers can

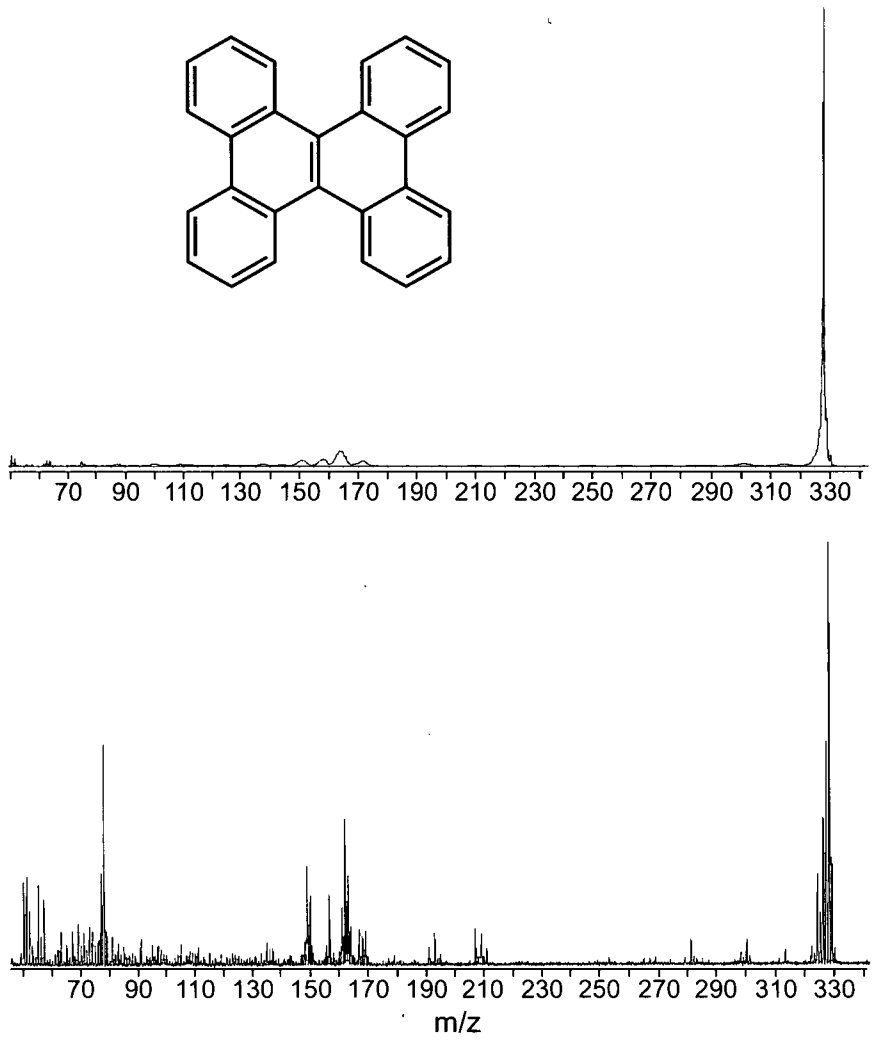

Figure 3.4: Tetrabenzo[acfh]napthalene. The upper mass spectrum without photodissociation and the lower mass spectrum with photodissociation (488 nm, 0.25 W)

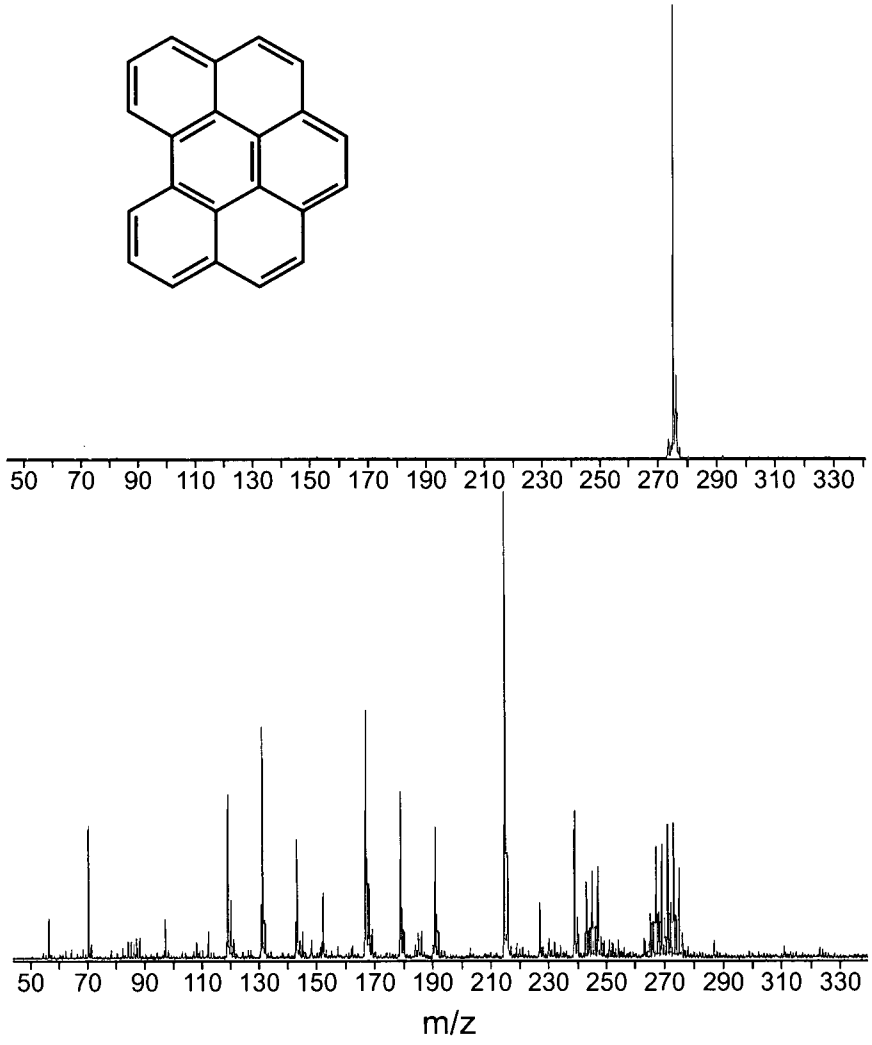

Figure 3.5: Benzo[ghi]perylene. The upper mass spectrum without photodissociation and the lower mass spectrum with photodissociation (514 nm, 0.6 W)

be used before photodissociation becomes a problem. Laser powers as high as $70,000\,W/cm^2$ are used in droplet experiments[42] but only 1 to $5\,W/cm^2$ could be used in the ion trap without quickly fragmenting all of the ions. A typical ion cloud has a diameter of at least 2 mm so the argon ion laser would only be able to deliver 25 to $35\,W/cm^2$ to the entire ion cloud.

In solution experiments, photodissociation is thought to be a single photon event where one photon can excite the molecule to a dissociative excited state.[17] For many fluorescent molecules it is routinely estimated that a fluorescent molecule can withstand, on average, close to one million absorption and emission cycles before dissociating. This mechanism is not consistent with the increased susceptibility of trapped ions to photodissociation.

3.3.3 Background Scatter

When optical detection was first attempted, the laser power was kept just below the level that would cause photodissociation. The only emission detected away from the laser line turned out to be plasma lines from the laser tube. The plasma emission was scattered off of the ion trap electrodes and collected as unwanted background. This problem was easily solved by placing a filter in the laser beam which was designed to pass only the laser line.

Filters for $488\,nm$ and $514\,nm$ were obtained for this purpose (03-FIL-202 and 03-FIL-204, Melles Griot, Rochester, USA).

The scatter from the laser line was overwehelming. No matter how well the laser beam was spatially filtered (or otherwise cleaned up), unwanted Rayleigh and Raman scattering from the last window into the vacuum system (entrance window) caused problems. The integration time for the optical experiment was limited to 1-3 s because the CCD would saturate if the spectrograph's grating was positioned with laser wavelength hitting the CCD. A solution to this problem was to position the grating in the spectrograph so that the laser wavelength was not incident upon the CCD. By doing this the integration time can be extended to $10\,s$. As a result, the total integration time was limited by the amount of light collected, the well capacity of the CCD and the stray light from the laser excitation wavelength.

The Raman scattering and fluorescence generated by the laser beam as it passed through the entrance and exit windows was significant. This background can reflect off the outside and inside ion trap electrode surfaces. Even with confocal imaging of the centre of the ion trap, it is not possible to eliminate all of this unwanted scatter. Since the fluorescence is expected to be Stokes shifted from the laser line this background scatter was not expected

to interfere with the fluorescence experiment.

To further reduce unwanted background generated by the laser, the exit window was replaced with a specially designed beam dump. The dimensions of the beam dump were chosen so that the laser beam would be completely contained as it reflected around the interior of the device. The exit window was only necessary for photodissociation experiments used to determine ion cloud size.

3.3.4 Unwanted Neutrals

To this point, no fluorescence from the ions was detected. To address the problem of background scatter from the electrodes, efforts were taken to improve the collection optics. The first collection optic outside the trap was doubled in diameter to 1 inch. The purpose of this change was to collect more light exiting the trap and to reduce the depth of field of the image created by this lens. Decreasing the depth of field improves the confocal imaging at the expense of losing light from the fringes of the ion cloud. Several optical configurations were used to image the ion cloud. A minimum number of optics is desirable because approximately 5% of the light will be lost by reflections at each lens surface. More optics are needed if confocal imaging

is to be efficient and chromatic abberations are to be minimized.

Optimizing an optical system without a detectable signal was very difficult. Especially problematic was adjusting the lens and aperture inside the vacuum system. Before the adjustment could be evaluated, the vacuum system would need to pump down for a few hours. After many months of optical changes and adjustments, a signal other than unwanted laser scatter was finally detected. Unfortunately, this signal was extremely chaotic and was present even without ions in the trap. Figure 3.6 is an example of the background collected in an experiment with a total integration time of 100 s.

The varying component of the background was attributed to neutral PAH molecules that remained in the probe volume after they were desorbed. The improved ion optics was partly responsible for making it possible to detect emission from neutrals. After discussing the high neutral background with a Teledyne scientist it was revealed that a recent software change could be responsible. In their last software update Teledyne decided to reduce the heating of the ion trap without informing their customers. For all previous PAH experiments, the ion trap was kept hot enough to evaporate any PAH molecules that adsorbed to the electrodes. With this latest software change the neutral background would remain a problem because it was no longer

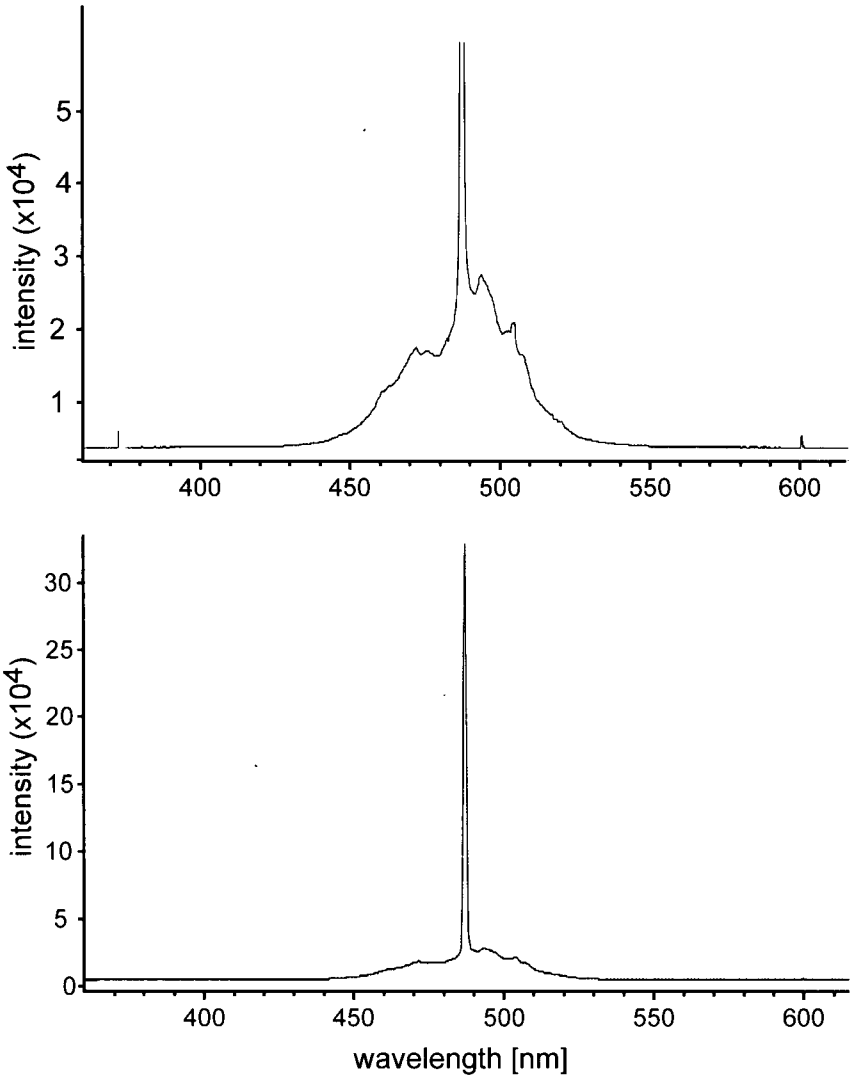

Figure 3.6: Chaotic background from laser scatter and neutral emission. Tetrabenzo[acfh]napthalene excited at 488 *nm*. Upper spectrum is magnification of lower spectrum.

possible to keep the electrodes hot enough.

Reverting to old versions of the software may have been possible, but the instrument was already being converted to incorporate the ESI source. Although not ideal for fluorescence experiments the thermal desorption instrument could have been used to collect absorption spectra of PAH cations. Photodissociation would be used to indicate absorption. The astrophysics community was, and still is, interested in identifying diffuse interstellar band (DIB) carriers and PAH cations are prime candidates. The absorption spectra of the PAH cations would be useful for evaluating potential candidates. A tunable laser source would be needed for such experiments.

3.3.5 Results from PAH Experiments

Although fluorescence from PAH cations was not detected, these experiments were still very useful. The susceptibility of gas phase ions to photodissociation was a problem that had not been anticipated. The emission of neutral molecules suggested that ion emission may be significantly closer to the laser line than originally predicted. If the fluorescence is not Stokes shifted away from the laser generated background, then the fluorescent measurement would no longer be against a zero background. Without a zero background,

the main sensitivity advantage of fluorescence spectroscopy is lost.

Another group reported that fluorescence from similar PAH cations could not be detected in a molecular beam experiment.[4] Lower temperatures, less photodissociation, and longer integration times should make molecular beam experiments easier than ion trap experiments. Maier reported experiments where two thirds of ions that were fluorescent in matrix experiments did not fluoresce in the gas phase.[43] Furthermore, it has been predicted that fluorescence experiments of large gas phase molecular ions may not be possible in an ion trap.[14] There were many aspects of the fluorescence experiment that remained unknown and further investigation was clearly necessary.

The problem of emission from neutral molecules was solved by changing to an electrospray ion source. However, there were many other issues which were not addressed by this major instrumental change: photodissociation would still limit the laser intensity, absorption spectra have not been recorded, the fluorescence quantum efficiency (ϕ_f) for gas phase ions remained unknown, and ion fluorescence (if present) may be totally obscured by background scatter.

3.4 Preliminary Experiments Using ESI

The decision to add an electrospray source to the ion trap mass spectrometer represented a significant shift in both experimental techniques and goals. It was clear that fluorescence spectroscopy of trapped molecular ions may not be a particularly sensitive technique. However, fluorescence spectroscopy could still be combined with ion trap mass spectrometry to probe the structure of molecular ions. The structure of gas phase biomolecules is of particular interest.[44] Using an ESI source allowed these ions to be investigated. It would have been impossible to trap biomolecules using the thermal desorption probe since thermal desorption would destroy most biomolecules.

Initially, the ESI source could not efficiently deliver ions to the ion trap. The benefits of the ESI source were difficult to appreciate when the total number of ions that could be trapped was reduced by ay least two orders of magnitude. While successful fluorescence experiments were not possible until the ESI front-end was properly optimized (Section 2.5.2), further photodissociation experiments led to a better understanding of the photophysics of trapped ions.

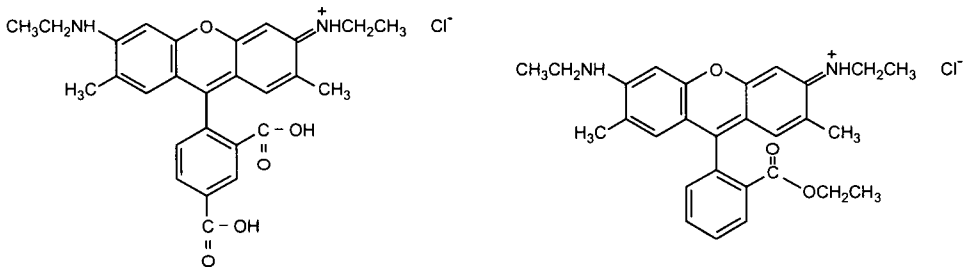

Figure 3.7: Structures of 5-CR 6G and R6G. These molecules have very similar structures.

3.4.1 Ionic Dyes

The first molecules investigated were the ionic dyes Rhodamine 6G (R6G) and 5-carboxyrhodamine 6G (5-CR 6G). These dyes have very similar structures (Figure 3.7). The dyes were chosen because they are ions in solution and they have a high fluorescence quantum efficiency in solution ($\phi_f > 0.9$). R6G was purchased from the Eastman Kodak Company (Rochester, USA) and 5-CR 6G was purchased from Molecular Probes Inc.(Eugene, USA). For all experiments using these dyes, 1 μM, (in 50:50 water methanol solutions) were used for spraying (Section 2.4.2). The gas phase absorption spectra and quantum efficiencies were unknown.

Gas Phase Absorption of 5-CR 6G Ions

A photodissociation experiment was devised to measure the absorption of gas phase 5-CR 6G ions. Ideally, a tunable laser should be used for this experiment but the argon ion laser was the only one available. Trapped ions were irradiated at five different wavelengths. The following conditions were kept constant for each wavelength: trapping level(q_z), buffer gas pressure, irradiation time, and laser power. The percentage decrease in the molecular ion peak was then plotted against wavelength. The gas phase absorption spectrum was approximated by connecting these points with a smooth line. Figure 3.8 shows the gas phase absorption compared to the solution absorption, measured with a Hewlett Packard (Palo Alto, USA) 8452A diode array UV-Vis spectrophotometer. The gas phase absorption is blue shifted 22 nm from the solution spectrum.

The gas phase 5-CR 6G ions are clearly absorbing at the argon ion wavelengths (476.5, 488.0, 496.5, 501.7, and 514.5 nm). Differences in fluorescence quantum efficiencies at these wavelengths could affect the amount of photodissociation observed. Measuring fluorescence emission and photodissociation at each wavelength could be used to generate a more accurate absorption spectrum.

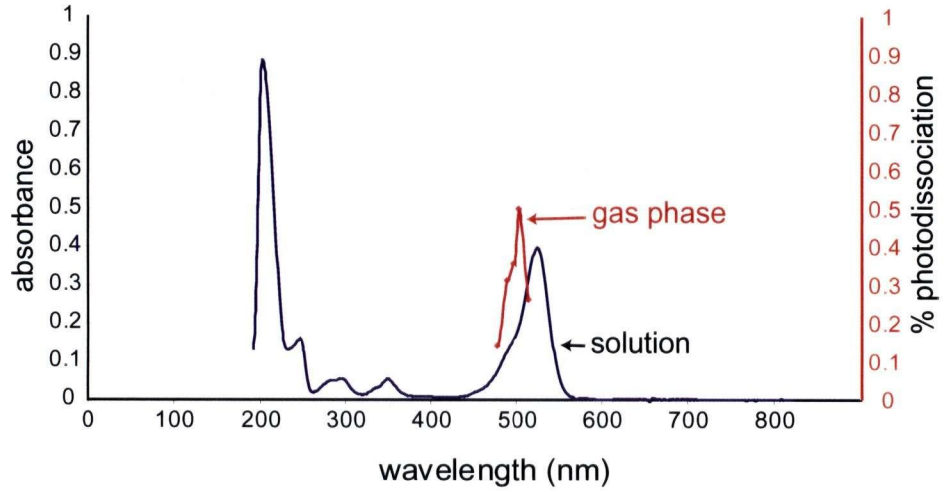

Figure 3.8: The solution and gas phase absorbance of 5-CR 6G. The gas phase absorbance was approximated by measuring the percentage of the molecular ion which was photodissociated (right vertical axis). The same laser power was used at each wavelength. The gas phase absorbance is blue shifted $\approx$ 22 nm relative to the solution absorbance.

Adduct Ions

The first mass spectra obtained using the ESI source usually included adduct ions. It was assumed that adduct ion formation was the unavoidable consequence of the electrospray process. Adduct ions are non-covalent complexes of the molecular ion of interest and an impurity or solvent molecule. The unwelcome molecule was likely water or methanol. Problems with the ion optics delayed the development of an accurate mass calibration method so

a definitive identification of the adduct was not made. The intensity of the adduct peak varied from 1-5% of the molecular ion peak.

Photodissociation of the molecular ion required a certain amount of laser power depending on the irradiation time, buffer gas pressure and trapping potential. Photodissociation of the molecular ion could be completely avoided by using low enough laser power or short enough trapping times, but the adducts were much more fragile. In contrast, the adduct ion could not survive even the lowest possible laser power setting. The fragile nature of the adduct ions suggests that the trapped 5-CR 6G ions gain vibrational energy very quickly upon irradiation.

Since the adduct ions did not survive any amount of irradiation, they could not affect the fluorescence experiment. It was later determined that leaks in the Q_0 vacuum chamber were causing the adduct ions to form. After eliminating these leaks the adducts were no longer observed.

3.4.2 Photodissociation Studies

The fluorescence signal was still undetectable; fluorescence (if any) was buried in the noise. To detect fluorescence, the signal would have to be increased or the noise would have to be decreased. Increasing the collection efficiency of

the optical system could increase the fluorescence signal. Only 0.16% of the ion cloud can be imaged through the $5\,mm$ slot cut into the entrance endcap. Increasing the size of the slots in the ion trap electrodes would allow for larger collection optics, but significant changes to the electrodes would degrade the performance of the instrument as a mass spectrometer. Larger collection optics may also collect a disproportionately greater amount of background scatter. It was therefore believed that larger collection optics would not help separate the fluorescence from the excitation background.

The fluorescence signal could be enhanced by increasing excitation intensity (see Equation 3.1). However, increasing the laser intensity will cause photodissociation of the ions. At this point, a better understanding of the photodissociation mechanism was needed to optimize the fluorescence experiment.

Photodissociation *vs.* Laser Power

Photodissociation was obviously dependent on laser power and irradiation times. When ions were trapped at lower RF-voltages (*i.e.* lower q_z) they could withstand greater laser powers without dissociating. The ion cloud is more diffuse at lower q_z values, so the benefit of using higher laser pow-

ers would be mitigated by a lower ion concentration. Simply changing the trapping potential and laser powers was not enough to produce a detectable fluorescence signal.

The degree of photodissociation varies with laser power. Lower laser powers can be used to generate modest fragmentation, while higher laser powers can be used to increase the fragmentation. Figure 3.9 shows the photodissociation of 5-CR 6G at two different laser powers. A more detailed picture of the photodissociation mechanism can be seen by monitoring the molecular ion (precursor) and the first fragment ion (product) as the laser power is slowly increased. Figure 3.10 shows that the photodissociation does not start until a critical threshold is reached. The precursor ion then decreases nearly linearly with laser power. The first fragment increases in intensity before it is photodissociated at higher laser powers.

If photodissociation was caused by a single photon absorption, there would not be a threshold as seen in Figure 3.10. This minimum energy required for photodissociation indicates that there must be a cooling mechanism to counteract the heating caused by the laser irradiation. Radiative emission would certainly help dissipate energy gained from absorption, but the quantum efficiency would have to change with laser power to produce

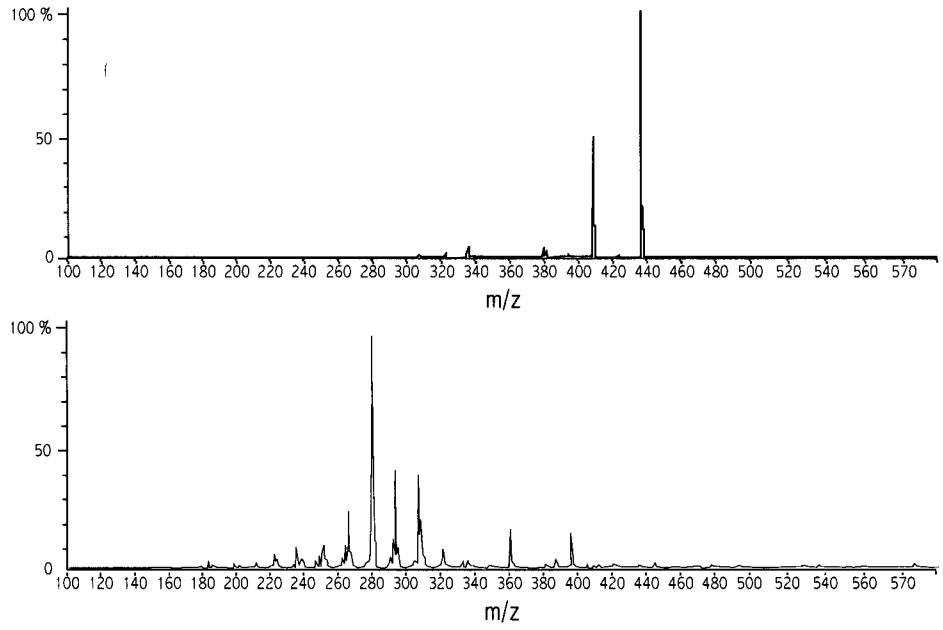

Figure 3.9: Mass spectra showing the photodissociation of 5-CR 6G at two different laser powers. Laser power is 0.15 W for upper trace and 0.5 W for lower trace.

the threshold.

Trapped ions undergo collisions with neutral helium atoms with a mean time between collisions on the order of $1\,\mu s$ if the buffer gas pressure is $1\,mtorr$. Typically, photon absorption occurs in $10^{-15}s$ and fluorescence emission happens within $1-3\ ns$ after absorption. Collisions with neutral buffer gas would not affect the fluorescence spectroscopy but could help cool the ions between absorptionevents. If photodissociation is the result of a

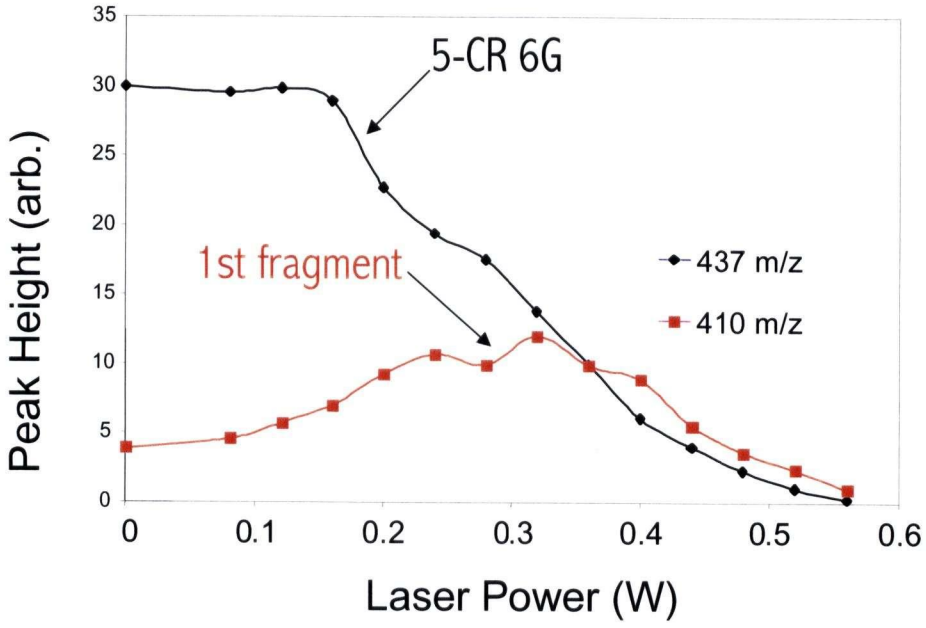

Figure 3.10: Peak height of 5-CR 6G's molecular ion and first fragment *vs.* laser power. Photodissociation of the molecular ion produces a first fragment which itself is photodissociated at higher laser powers.

slow heating process requiring the absorption of many photons, collisions with buffer gas molecules could help cool the ions.

Photodissociation *vs.* Pressure

The effect of buffer gas pressure was determined by measuring the laser power required to dissociate the precursor ion by 50% at different pressures.

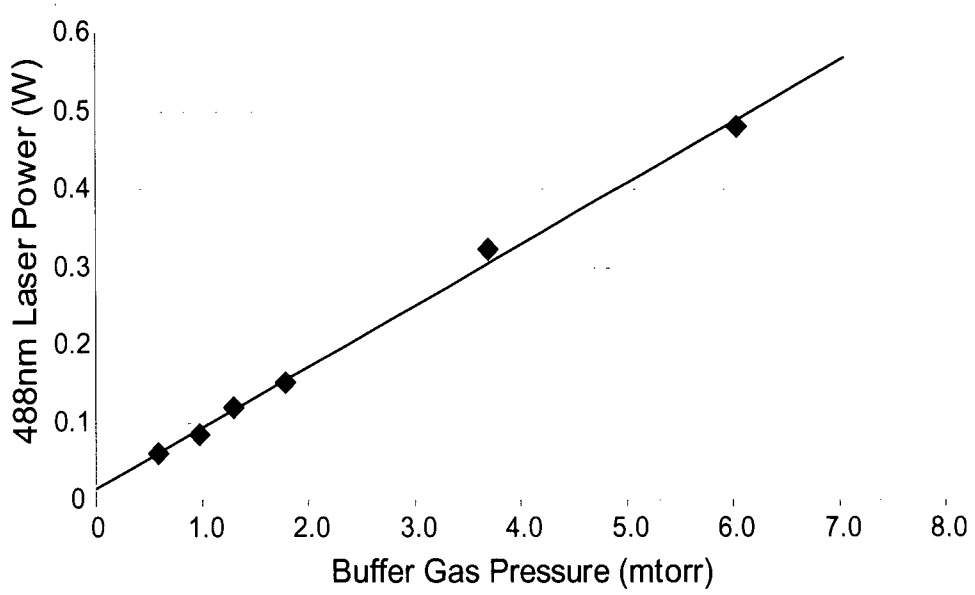

Figure 3.11: The laser power required to photodissociate 50% of the 5-CR 6G molecular ion is plotted *vs.* helium buffer gas pressure. Higher laser powers are required to photodissociate ions trapped at higher buffer gas pressures.

Higher laser powers were required to fragment ions held at higher buffer gas pressures (see Figure 3.11). The pressure dependence suggests that the photodissociation of trapped ions is a slow process that can be affected by the buffer gas.

The purpose of studying the photodissociation of trapped ions is to find ways to prevent it. Increasing the buffer gas pressure allows a higher laser power to be used before ions are destroyed by photodissociation. Typical ion

trap mass spectrometers are operated with buffer gas pressures from 1×10^{-5} to 1×10^{-3} *torr*. During fluorescence experiments the vacuum system and mass spectrometer should be operated close to their high pressure limits. This will allow a significantly higher laser power to be used and therefore produce a much higher fluorescence signal.

Helium is the buffer gas most commonly used in ion traps. As discussed in Section 2.2.2, the buffer gas improves the performance of the ion trap. Helium is used because a heavier collision partner would cause greater deviations in the trajectory of the ion with which it collides. To kinetically cool a trapped ion it is better to have many collisions with a light buffer gas, than to have fewer collisions with a heavier one. On the other hand, if a heavier buffer gas could decrease the internal energy of the ions more effectively it ought to be used in fluorescence experiments.

To investigate the effect of heavier buffer gases on photodissociation some minor instrumental changes were necessary. The plumbing on the high pressure side of the leak valve was changed to accommodate several different gas lines. Each gas cylinder had its own regulator and could be isolated from the leak valve. A roughing pump was also included so that the high pressure side of the leak valve could be evacuated to ensure the buffer gas could be

changed cleanly. This configuration permitted quick changes between the different gases tested.

To accurately monitor the pressure in the ion trap a model 120AA Baratron gauge (model 120AA: MKS Instrumentation Inc., Andover, USA) was used. The pressure gauge normally used with the ion trap is an ionization gauge (model 342: Granville-Phillips, Boulder, USA). Ionization gauges depend on the ionization potential of the gas which is being measured and are not as accurate as Baratron gauges. A Baratron gauge will also accurately measure the pressure of a mixture of gases while the output of the ionization gauge would depend on the exact ratio of gases present. Figure 3.12 shows the results for three gases: argon, nitrogen, and helium. Heavier gases are more effective at cooling the ions and could therefore be used to improve the fluorescence experiment.

The internal energy of trapped ions is increased by the absorption of photons. These ions can be cooled by collisions with the buffer gas and by emitting radiation. If the heating rate exceeds the cooling rate, the ions will eventually fragment. When the ion trap is filled to capacity or the ions are held at a low RF-potential, the ion cloud will be large and ions will oscillate in and out of the laser beam. When an ion is in the beam it will be heated

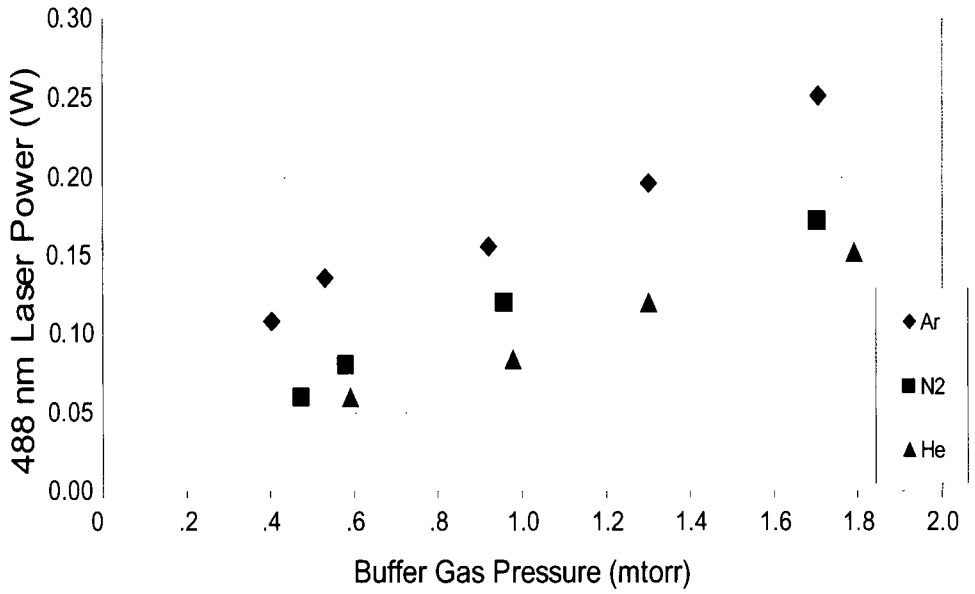

Figure 3.12: The laser power required to photodissociate 50% of the 5-CR 6G molecular ion is plotted *vs.* buffer gas pressure for argon, nitrogen and helium gasses. Using a heavier buffer gas can decrease the amount of photodissociation and allow a higher laser power to be used.

by absorption and cooled by collisions with the buffer gas. Outside the laser beam the ion will only cool. The more time the ion spends outside the laser beam the more difficult it will be to photodissociate.

Chopping the Laser Beam

Another experiment was designed to prevent photodissociation involved chopping the laser beam. A mechanical chopper (SR540, Stanford Research Sys-

tem Inc., Sunnyvale, USA) was used to give ions more time to cool. Even though the background noise increases with laser power, the S/N should still increase as more fluorescence and background are collected. Figure 3.13 demonstrates the effect of chopping the laser beam at two different laser powers. A chopping frequency of zero corresponds to continuous radiation.

The molecular ion signal increased with chopping frequency until a steady value was reached. The chopping allowed the ions more time to cool through collisions with the buffer gas. Chopping the laser beam should increase the S/N of the fluorescence measurement by allowing a higher laser power to be used. Unfortunately, increasing the trap pressure and chopping the laser beam was still not enough of an improvement to detect fluorescence.

Although the fluorescence experiment was not successful, the chopping experiments were still interesting. Dunbar had already completed similar experiments in the mid 1980's.[45] Dunbar's experiments were performed in an ion cyclotron resonance (ICR) trap.[45–47] An ICR trap uses magnetic fields to confine ions[48] at low operating pressures. The main advantage to using an ICR trap to conduct photodissociation experiments is the low operating pressures ($0.5 - 3 \times 10^{-8}$ *torr*) where heating rates can be measured without interference from collisional cooling. For fluorescence experiments

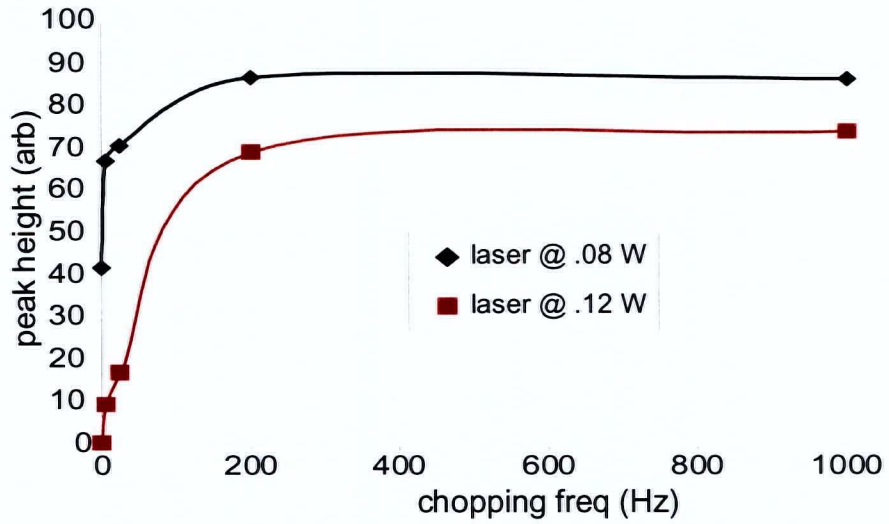

Figure 3.13: The 5-CR 6G molecular ion peak height is plotted *vs.* the frequency at which the 488.0 nm laser excitation was chopped for a 3 s experiment. Results for two laser powers are shown ($0.08W$ upper trace and $0.12W$ lower trace). Chopping the laser beam provides more time for the ions to cool thus reducing photodissociation.

collisional cooling is a welcomed benefit to working with the higher pressure of a quadrupole ion trap.

3.4.3 Fluorescently Tagged Peptides

Photodissociation limits the intensity of the laser light that can be used to excite gas phase molecular ions. Also, any fluorescence emission was likely

not significantly Stokes shifted from the excitation wavelength. It was hypothesized that attaching a fluorescent molecule to a small peptide might address one or both of these problems. If the fluorescent molecule could dissipate excess vibrational energy to the peptide, it may be able to withstand more excitation and emission cycles without dissociating. Unlike collisions with the buffer gas, the peptide tag may help dissipate excess vibrational energy when the molecule is in the excited state and induce a greater Stokes shift in the emission. In condensed phase experiments the solvent or matrix removes excess vibrational energy of the excited state.

Two very similar tagged peptides (see Figure 3.14 for structures), fluorescein-glycine-histidine (FITC-Gly-His) and fluorescein-glycine-glycine-histidine(FITC-Gly-Gly-His), were purchased from Molecular Probes Inc.(Eugene, USA). For these experiments, $1\,\mu M$ in 50:50 water methanol solutions of the peptides with 0.1% acetic acid were used. Adding acetic acid ensures that the molecules are positively charged in solution and easily sprayed.

The peptides seemed to withstand a greater amount of laser power than the dye molecules used in previous experiments. Of course, this decrease in photodissociation may be caused by a lower molar absorptivity and comparing molecules is difficult. There was some evidence that the peptide

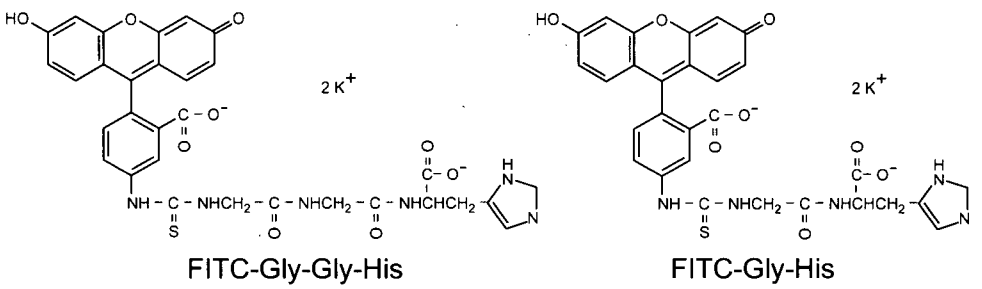

Figure 3.14: Structures of fluorescently tagged peptides FITC-Gly-Gly-His (ion is 659.6 Th) and FITC-Gly-His (ion is 602.6 Th).

tag was acting as a heat sink for the dye, but fluorescence emission could not be detected. As the laser power was increased the tagged peptides appeared to be losing histidine and then glycine. To break the peptide bonds the molecule must have transferred energy from the dye tag to the peptide. Only detectable fluorescence emission could prove that this energy transfer was happening fast enough to affect the excite state.

Differences between the CID fragmentation and the photodissociation were also observed (see Figure 3.15). Although a costly addition to a mass spectrometer, a photodissociation capability could be used to increase the selectivity of an ion trap. An important qualification is that one would need to find a chemical system where MS^n was not already selective enough. PAH analysis would be one case where photodissociation would certainly be more

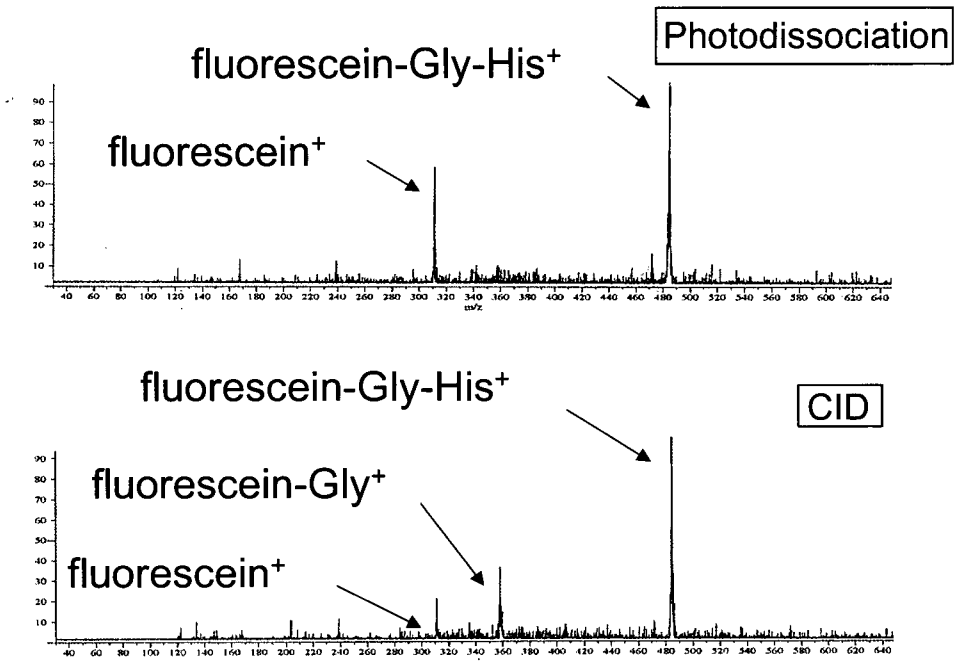

Figure 3.15: Photodissociation spectrum of FITC-Gly-His (top) and it's CID spectrum (bottom).

selective than CID.

3.5 Requirements for a Successful Fluorescence Experiment

The methods, technology and instrumentation used to this point were not adequate to allow the detection of fluorescence from molecular ions confined

in a quadrupole ion trap. The original instrumentation and methods were not adequate because critical aspects of this experiment were not anticipated when the project began. Photodissociation limits the laser intensity and this alone would make gas phase fluorescence measurements at least three or four orders of magnitude less sensitive than solution measurements. The problem of separating the fluorescence from the excitation was also not expected.

While it was expected that the Stokes shift of the emission in the gas phase would be different than in solution, the fluorescence was still expected to be wavelength separated from the laser generated background. The laser background, composed of Raman scattering and fluorescence from the windows, was very significant. At this point, it was thought that the fluorescence emission was not Stokes shifted away from the laser generated background and the gas phase experiment was no longer a zero background measurement.

If the fluorescence experiment was to be successful, major improvements to the instrumentation were needed. If fluorescence emission was to be detected then the S/N would have to be increased dramatically. The total number of ions trapped must also be increased. The trapping efficiency was improved by optimizing the ion optics of the ESI front-end. The main problem yet to be solved was reducing the amount of background light collected.

A new optical system and new detectors were necessary.

Chapter 4

Pulse Counting Experiments

It was not possible to detect fluorescence emission from trapped molecular ions with the methods and instrumentation described in the previous chapter. It did not appear that wavelength dispersion with a spectrograph could separate the fluorescence from the background generated by the excitation. The background signal was much too high and any fluorescence would likely be too close in wavelength to the excitation. For fluorescence to be detected, new instrumentation and a new approach would be necessary.

In an attempt to solve this problem methods used to detect small signals in other fields of analytical chemistry were considered. Lock-in amplification is one technique that can dramatically improve the S/N when measuring a small signal in the presence of a large, noisy background. Basically, the analytical signal of interest is modulated and the entire signal (background + analytical signal) is multiplied by a wave, which has been generated at

the same frequency as the modulation and with a fixed phase. The result of this multiplication (demodulation) is that the signal is recovered with only a small fraction of the original noise. Only noise that happens to fall within the narrow bandwidth of the lock-in amplifier will be detected. This technique would also be able to detect any emission that was resonant with the excitation.

For example, lock-in amplification is used to detect fluorescence emission from atoms in flames. The excitation source is modulated at a certain frequency so that the emission from the atoms become modulated at that same frequency. Most of the background generated by the flame stays constant (DC), or only varies at low frequencies, while the analytical signal is modulated to a much higher frequency and can be detected against an almost zero background. Unfortunately, in the ion trap fluorescence experiments it is the excitation source (laser) that is creating the unwanted background and modulating the laser would also modulate the background and nothing would be gained.

Modulating the fluorescence without modulating the background signal may be achieved by using a technique known as sample modulation. For the most part, sample modulation has never been a very effective or pop-

ular technique. In molecular absorption and luminescence spectroscopy the sample and reference cells can be moved in and out of the the light path to modulate the signal. In atomic emission, fluorescence, and absorption experiments the sample introduction system can be turned on and off. These techniques are not very effective because the signal modulation is usually too slow (low frequency) to separate the analytical signal from the DC background. If a nebulizer is used to inject a sample into a plasma (or flame) the act of modulating the sample can also modulate the plasma background emission at the same frequency. However, in an ion trap the ions are already moving at well defined secular frequencies.

In an ion trap experiment, sample modulation could be achieved by moving the ions in and out of the laser beam. In most of the experiments described so far, the ions are already moving in and out of the laser beam. To enhance the modulation the laser beam would be tightly focused and a resonance excitation voltage applied across the endcap electrodes (Section 2.1.3). A higher voltage for the resonance excitation would result in a greater percentage of the ions moving in and out of the beam on every cycle but it would also heat the ions. Hence the resonant excitation would have to be kept modest to avoid CID (Section 2.2.4).

The use of sample modulation and lock-in amplification requires a detector that will generate an analog signal if amplitude modulation, as described above, is to be used. An obvious choice is a sensitive photomultiplier tube (PMT). Experiments with PMT detection had already been attempted but were unsuccessful because of the high level of background. With the existing optical system, the PMT operating voltage would have to be kept so low that its detection efficiency would be severely compromised. To obtain a sufficient analog fluorescence signal the PMT gain should be as high as possible. However, the maximum achievable gain was also limited by the large background. Before lock-in amplification and sample modulation can be applied to separate the fluorescence signal from the background, the background must first be reduced by other means.

To reduce the background, a new optical collection system was designed. Confocal imaging was abandoned, and all of the collection lenses were replaced with a fiber optic probe. The fiber optic probe was designed to be inserted between the entrance endcap and ring electrodes of the ion trap. The fiber optic probe blocked any stray light reflected off of the outside of the trap electrodes. Unfortunately, laser generated background continued to scatter off the inside of the electrode surfaces.

An additional approach to reducing the background was to incorporate instrumentation used for Raman spectroscopy into the fluorescence experiment. Small signals are detected very close to laser lines in Raman spectroscopy. A relatively new type of holographic notch filter has been developed for Raman experiments that can block a very narrow bandwidth. To attenuate the scatter from the inside electrode surfaces such a filter was obtained (HSPF-488.0-1.0, Kiaser Optical Systems, Inc.). This filter was designed to have an optical density (O.D.) greater than 6.0 at 488.0 *nm* and a bandwidth of less than 10 *nm*. To achieve the rated performance the light to be filtered must be perfectly collimated and hit the filter at a specific angle. The fiber optic probe was designed to accommodate a holographic notch filter. Experiments using the notch filter are described in Chapter 5.

4.1 Fiber Optic Probe

The switch to a fiber optic probe for light collection eliminates serious weaknesses of the previous optical system. Most importantly, the background scatter from the outside of the electrodes no longer reached the detector. Also, the old system was difficult to align and vulnerable to inadvertent mis-

alignment when other parts of the instrument were being manipulated. The fiber optic probe was very easy to align and its correct positioning could be quickly verified. Using optical fibers to collect and guide light is simple and effective.

The fiber optic probe was designed with the following criteria: it must fit through the slot cut into the endcap electrode, collect light efficiently, be compatible with a holographic notch filter, and be vacuum tight so that an exit window is not necessary. An exit window would mean two more interfaces where signal would be lost to reflections. To make the probe durable and vacuum tight the fibers were contained in a stainless steel tube.

The fibers must protrude several centimeters from the stainless steel tube to prevent arcing from the high voltage on the ring electrode. Making a vacuum seal on the outside of the tube (1/4 inch outside diameter) is easy and commercially available tube connectors (SS-4-UT-1-4, Swagelok, Solon, USA) were used for this purpose. To make the inside of the probe vacuum tight an epoxy (Torrseal, Varian, Inc., Walnut Creek, USA) was used to fill the spaces between the fibers. A prototype was constructed. After these fibers were glued, they were cut and polished using lapping paper attached to a rotating disk. Unfortunately, the cutting and polishing heated the fiber

optic bundle excessively and the epoxy melted and contaminated the ends of the fibers. This meant a window had to be used to make the vacuum seal after all. The new fiber optic probe was designed so any one inch diameter optic could be used to make the vacuum seal. The fibers used for the bundle were chosen so the probe would collect light efficiently.

Superguide fused silica fiber optic (SFS400/440T, Fiberguide Industries, Stirling, USA) was purchased with the following specifications: $400\,\mu m$ core diameter, $40\,\mu m$ thick cladding, and a $40\,\mu m$ thick Thermacoat jacket. This fiber has a numerical aperture of 0.22 which corresponds to an acceptance angle of 12.7°. The Thermacoat jacketing material was chosen because it can withstand $-190°C$ to $300°C$ and is thin. The thinnest possible jacketing was chosen because only light hitting the core will be transmitted through the fiber. The temperature stability of the jacketing material will allow the probe to be used in experiments where the ion trap electrodes are heated or cooled. To keep the probe durable, the jacketing material was not removed. Seventy individual lengths of fiber were cut and polished using both silicon carbide (9μ) and aluminum oxide (0.3μ) lapping paper with a commercial polishing device (Ultrapol 1200, Ultra Tech Mfg., Inc., Santa Ana, USA).

The fiber optic probe is shown in Figure 4.1. The input end of the probe

is easily aligned with the ion cloud because the fiber bundle just fills the access slot cut into the entrance endcap. At the other end of the probe, the filter holder attaches to a one inch tube lens system (Thorlabs, Inc., Newton, USA) and can be coupled directly to any detector equipped with a compatible flange. Any one inch diameter filter, or window, can be used to make the vacuum seal. The optic is simply held against an o-ring positioned at the bottom of the filter holder. The probe is attached to the vacuum system using a KF-25 flange.

To estimate the collection efficiency of this probe the total cross-sectional area of the bundle must be compared to the area represented by the fiber cores. Assuming the fibers are efficiently packed, the empty spaces between the fibers will represent 9.31% of the cross-sectional area. The core is 400 μm in diameter and the total diameter of the fiber, including the cladding and jacketing, is 480 μm. Therefore, the area of the core is 69.4% of the total fiber cross-section. Assuming a 5% loss to reflections and negligible attenuation within the fibers, the entire probe will transmit 60% of the light striking it with an angle of incidence below 12.7°.

The fiber optic probe is positioned approximately 2 cm from the centre of the ion trap. The total effective cross-sectional area of the probe is simply

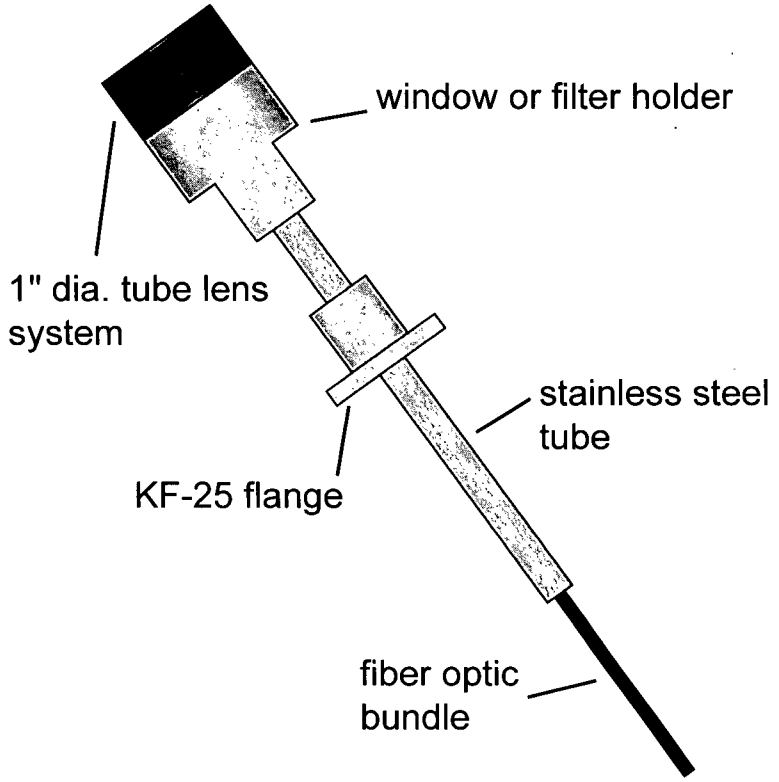

Figure 4.1: Fiber optic probe.

70 times the cross-sectional area of one core ($0.088\,cm^2$). The emission originating from the centre of the trap can be approximated by the surface area of a sphere with a 2 cm radius. The probe's effective area is approximately 0.18% of this sphere's surface area. Adding losses from reflections at both ends of the probe, this probe transmits $\approx$ 0.16% of the light originating at the centre of the trap.

4.1.1 PMT Detector for the Fiber Optic Probe

A PMT housing (model SWH/RFI, Electron Tubes Limited, Rockaway, USA) and a PMT (R1477-06, Hamamatsu, Hamamatsu City, Japan) were used for these experiments. The PMT housing has an RF-shielded socket assembly which helps reduce noise pick-up from the ion trap electronics. The R1477-06 has a high sensitivity multialkali photocathode with a spectral response from 180 nm-900 nm (peak at 450 nm). A special flange was built in the UBC Chemistry Mechanical Engineering Shop to couple the PMT housing to the fiber optic probe. The high voltage for the PMT was supplied by a Stanford Research Systems, Inc.(Sunnyvale, USA) power supply (model PS350/5000 V - 35 W).

The background noise was reduced considerably by using the fiber optic

probe. The exact level of reduction cannot be measured because different PMTs and housings were used before the probe was added. In addition, improved spatial filtering of the laser beam and other adjustments to the excitation optics had also reduced the amount of unwanted background.

4.2 Coating the Ion Trap Electrodes

While assembling the instrumentation for lock-in amplification detection Dr. John Hepburn was consulted. This invaluable discussion lead to the idea of coating the ion trap electrodes with carbon. The hemispheres of electron momentum spectrometers are coated with carbon to adsorb any traces of pump oil. Coatings on ion trap electrodes could potentially degrade the performance of the instrument as a mass spectrometer. If the surfaces in an electron momentum spectrometer can be coated with carbon, it was thought that ion trap electrodes could also be coated.

A commercial product, Aquadag, was used to coat the inside surfaces of the ion trap electrodes. Aquadag is an aqueous-based colloidal dispersion of $5\,\mu m$ diameter carbon particles produced by Acheson Colloids Company (Port Huron, USA). Aquadag is used as a commercial lubricant because it

adheres well to most metal surfaces and has a long wear life. The fine particle size produces a very stable suspension for commercial applications. The fine particle size also produces a very black coating; particles with diameters exceeding $10\,\mu m$ would produce a shiny grey coating. Aquadag is commonly applied to metal surfaces using a brush or by immersing the metal into a diluted suspension of the particles. Changing the shape or roughening the surface of the ion trap electrodes would degrade the performance of the ion trap as a mass spectrometer.

To produce an even coating, the Aquadag was diluted in ethanol (50:1 by volume) and sprayed onto the electrodes using a nebulizer. The metal surface was kept hot during the coating process to avoid creating rings of dried carbon. A hot plate was used to heat the electrodes to between $80°C$ and $100°C$. The electrode temperature was monitored using a thermocouple during the spraying process. A spare set of ion trap electrodes was coated to test the impact of the coating on mass spectrometer performance.

The coated set of electrodes was evaluated for a week and they did not negatively impact on the ion trap performance as a mass spectrometer. The coating was then applied to the endcaps which had been modified for optical experiments. Flash photography was used to demonstrate the effectiveness

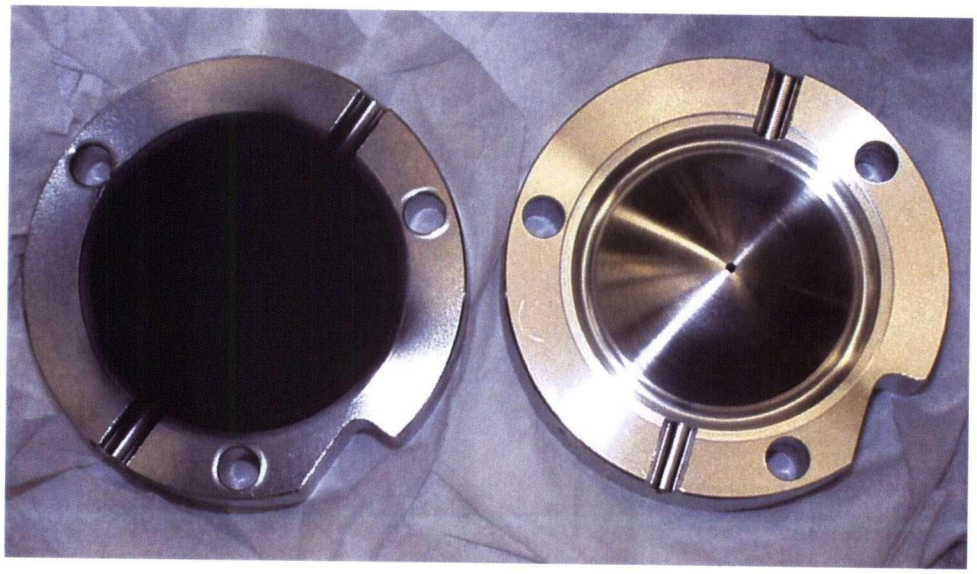

Figure 4.2: Endcap electrodes with (left) and without (right) carbon coatings. Carbon coating reduces scatter off the inside electrode surfaces.

of the coating (see Figure 4.2). The black coating on the electrodes reduced the background by $\approx$ 3000 times. Figure 2.2 shows the coated spare endcap electrodes and an uncoated ring electrode; it is easy to appreciate how uniform the coating is in this figure.

To prepare for the lock-in amplification experiment R6G was sprayed into the trap and irradiated with 488.0 nm light from the argon ion laser. The output of the PMT was monitored directly with an oscilloscope (TDS 340A Tektronix, Beaverton, USA). Individual pulses were detected indicating that

the PMT was now operating in a pulse counting regime. The output of the PMT was no longer a DC current as was the case in past experiments. Since the analytical signal was not sufficient to create a DC current output, amplitude modulation and lock-in amplification cannot not be used.

While it was difficult to see changes in the PMT output by visually monitoring the oscilloscope, there appeared to be a higher frequency of pulses with ions in the trap. Pulse counting hardware was attached to the PMT to get a precise measure of its output. A F-100E pre-amplifier and discriminator was connected to the PMT, and the output of the F-100E was connected to a PRM-100 precision ratemeter. Both devices were manufactured by Advanced Research Instrumentation, Corp (Wheat Ridge, USA).

This preliminary experiment resulted in the first successful detection of emission from trapped molecular ions using the instrument described in this thesis. The first signal to background ratio was approximately 2:1. At this point it was clear that emission was being detected from trapped R6G ions. However, it was possible that the emission was Rayleigh scattering and not fluorescence.

A long pass filter (CG-OG-530, CVI Laser Corporation) was placed in front of the PMT and the laser background dropped dramatically and the

S/N ratio improved to greater than 20 for 10 *s* experiments. The signal enhancement from using a long pass filter is evidence that the emission detected is indeed fluorescence. Without a fluorescence emission spectrum, it is difficult to predict how much fluorescence is also being blocked by the filter. A problem was encountered during these preliminary experiments: the probe was poorly aligned with the centre of the trap because the KF-25 flange and the filter holder were not parallel. This alignment problem was quickly fixed by Des Lovrity of the UBC Chemisrty Mechanical Engineering Shop.

4.3 Pulse Counting Instrumentation

At this point the instrument was adjusted to accommodate pulse counting experiments. The pulse counting experiments had to be synchronized with the ion trap control software. Software was developed to control the pulse counting experiment and to record data. Figure 4.3 shows the configuration of the instrument used for pulse counting experiments. Proper spatial filtering of the laser beam and the use of a Brewster window are important aspects of the instrumental design. However, it is the fiber optic probe and carbon coated electrodes, and to a lesser extent the internal beam dump, that

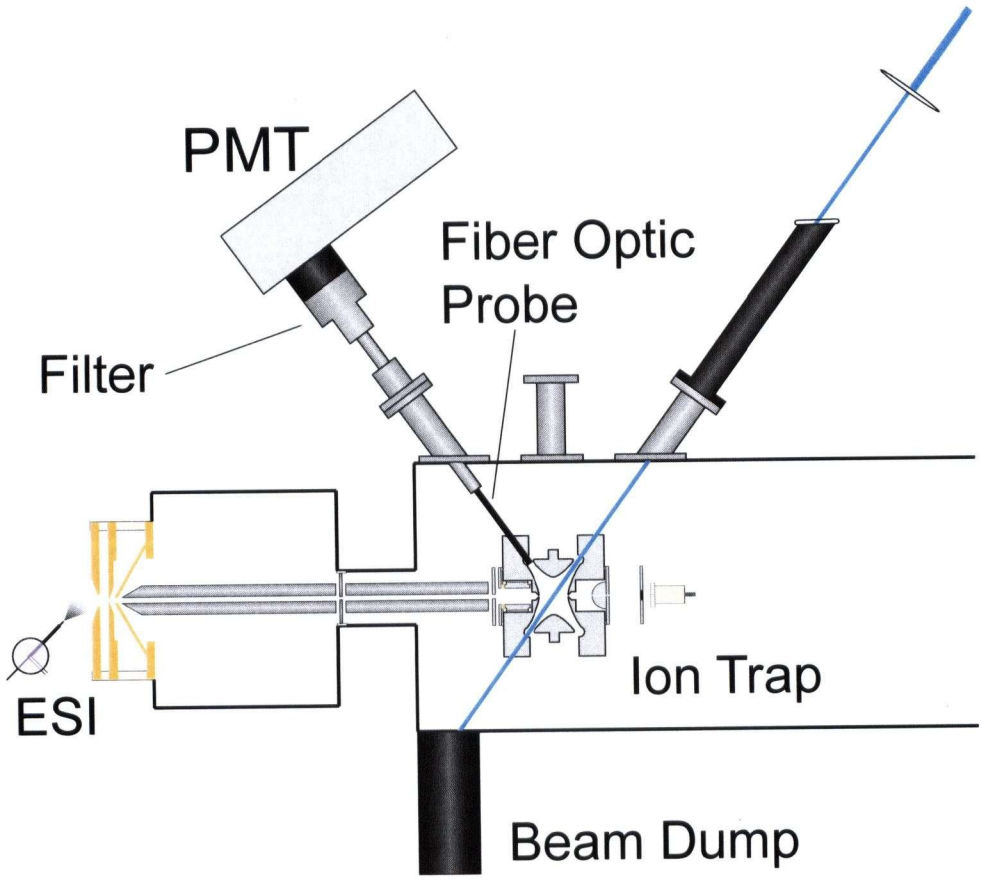

Figure 4.3: Instrumental configuration for pulse counting experiment.

resulted in exceptional performance. Figure 4.4 is a block diagram showing the more important peripherals used in the experiment.

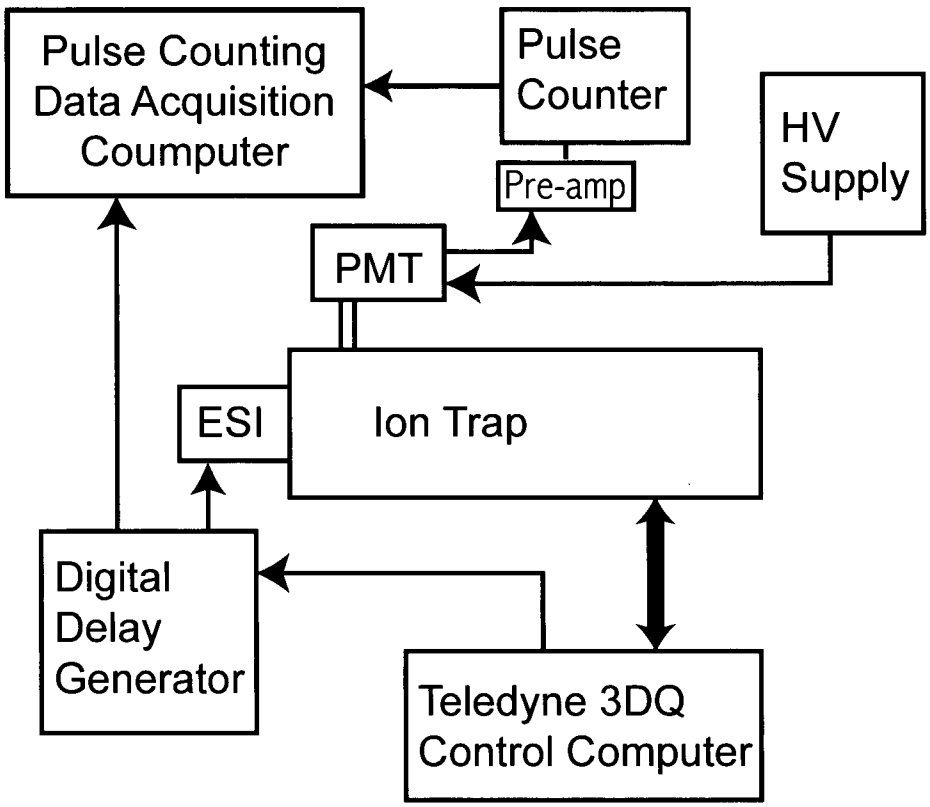

Figure 4.4: Instrumental block diagram for pulse counting experiment.

4.3.1 Data Collection for Pulse Counting

A data acquisition board (AT-MIO-16, National Instruments, Austin, USA) was borrowed so that LabVIEW could be used to develop the software necessary for the pulse counting experiment. The PRM-100 ratemeter is an excellent counter with a pulse pair resolution of less than $10\,ns$. Unfortunately, it does not have a convenient way of outputting count rates. To get around this problem, two counters on the AT-MIO-16 board were used to count TTL pulses generated by the PRM-100 ratemeter.

For every current pulse from the PMT that is above the threshold set by the discriminator, the PRM-100 receives an ECL pulse from the F-100E preamplifier. The PRM-100 converts the ECL pulses into TTL pulses. Counters in the PRM-100 then count the TTL pulses and the rates are displayed on the front panel of the ratemeter. The PRM-100 outputs rates based on a time scale set on the front panel. There was no way to set the counting period exactly without writing a complete instrument driver for the PRM-100. Instead, the TTL pulses generated by the PRM-100 were counted directly using a counter on the AT-MIO-16 data acquisition board.

The counting period was easily and accurately synchronized with the ion trap experiment. The Teledyne electronics can generate a pulse at the

beginning of every trapping sequence. This "start" pulse triggers a digital delay generator. The digital delay generator then sends a pulse to the gate lens between Q_0 and Q_1 allowing ions to enter the ion trap. The gate pulse drops the gate voltage by 19 V and lasts for 1 ms for all experiments. At a chosen delay after this, a pulse is sent to the data acquisition board to define the pulse counting period. The counters of the AT-MIO-16 can be gated on and off themselves. The pulse from the digital delay generator is sent to the gate input of one counter and at the same time sent to the input of a second counter. The input of the "gated" counter is, of course, the TTL output of the ratemeter. The software program can record how many pulses are detected in a given counting period. The software also controls how many counting periods are measured in each experiment. The software saves the data from each counting period in an array and calculates the mean and standard deviation. Since the time between ion injection into the trap and pulse counting begins is small (usually $< 10\,ms$), the laser is kept on all the time. The timing diagram of the experiment is shown in Figure 4.5.

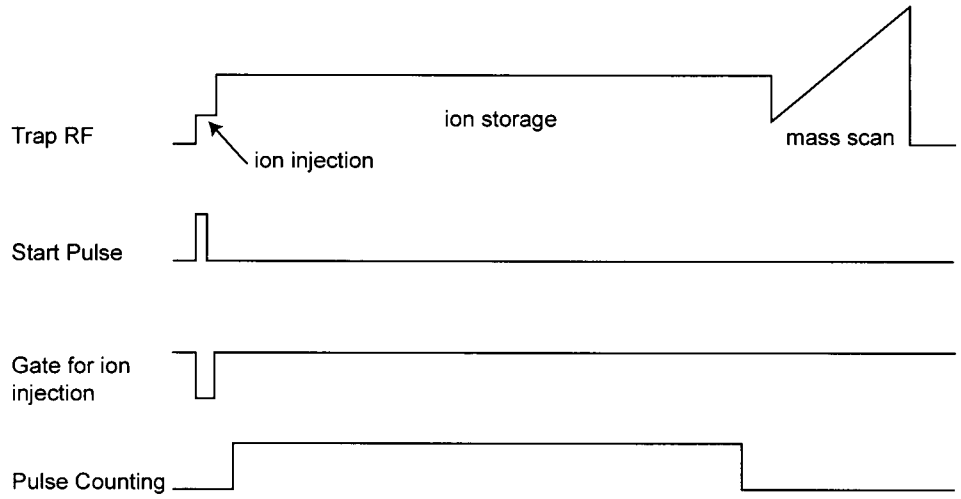

Figure 4.5: Timing diagram for pulse counting experiments. For a 1 s optical experiment the following timings were used: ion injection for 10 ms, ion storage for 1 s, mass scan of 50 ms, Q_o injection gate of 1 ms, and pulse counting for 1 s.

4.3.2 PMT Cooling

It is important to note that the R1477-06 PMT was not designed for pulse counting experiments. The R1477-06 was designed for maximum sensitivity while a pulse counting PMT would be designed to have very low dark counts. Most of the dark counts arise from thermionic emission from the PMT's photocathode. At room temperature, the dark counts from the R1477-06 were much higher than the laser background when a filter was being used. To improve the S/N of the measurement, the dark counts were reduced by

lowering the temperature of the photocathode. To cool the photocathode the entire PMT housing was cooled using solid CO_2. With $1000\,V$ applied to the PMT, cooling to $-1°C$ reduced the dark noise to $\approx$ 700 counts per second (CPS) compared to $\approx$ 2700 CPS at room temperature.

Cooling the PMT can cause condensation problems. To prevent condensation on the inside of the PMT housing, the base was filled with molecular sieves and the entire housing was sealed in a glove bag filled with nitrogen. To prevent condensation on the outside of the PMT window, the lens tube system between the probe and the PMT was also filled with nitrogen. A pulse counting PMT which would not require such cooling was ordered. While waiting for the new PMT, several pulse counting experiments were conducted.

4.4 Fluorescence vs. Laser Power

The first pulse counting experiments measured the laser power dependence of the fluorescence signal. The R6G ions were held at the same trapping voltage for each laser power (i.e. $q_z = 0.5$). The counting period was 1 s and ten measurements were made at each laser power. Mass spectra were

also recorded for each laser power. Background measurements were made without ions in the trap. To ensure nothing interfered with the background subtraction, only the pulse sent to the gate lens was stopped; every other instrumental setting remained constant. R6G ions were excited with 488.0 *nm* light from the argon ion laser for all pulse counting experiments described in this thesis. The long pass filter (CG-OG-530, CVI Laser Corporation) was used to attenuate the laser generated background in all pulse counting experiments.

4.4.1 Instrumental Parameters

The various instrumental parameters used in this experiment are noted in Table 4.1. These settings remain the same for all of the pulse counting experiments except were indicated. Helium was used as a buffer gas in all of the fluorescence experiments.

4.4.2 Results and Discussion

As expected, the fluorescence signal initially increased with increasing laser power. At higher laser powers, photodissociation begins to reduce the number of ions and the fluorescence signal decreases. The amount of fragmentation

ESI & Ion Guide	
Component	Voltage (V)
Sprayer	3750
Curtain Plate	195
Sampling Orifice	80
Skimmer	46
Q_0 Offset	35
Gate	38.5
Q_1 Offset	30
L1	30
L2	30
N_2 flow	1.4 L/min
Syringe Pump	1$\mu L/min$

MS Operating Pressures	
Zone	Pressure
Orifice/Skimmer	950 $mtorr$
Q_0	7.0 $mtorr$
Ion trap	1.4 $mtorr$
Teledyne Software Settings	
Injection q_z	0.16
Detector Voltage	1000 V
Scan Speed	12000 Th/s
Resonant Excitation	
549 kHz offset 5.0 $V(48\mu V/DAC)$	
Linear Quads	300 V

Table 4.1: Instrument settings.

was determined in the mass spectrum acquired at the end of every optical experiment. When evaluating the effect of photodissociation, it is important to know that the amount of fragmentation only indicates what has happened to the ions by the end of the irradiation period.

Figure 4.6 shows the mass spectrum of R6G and fragments recorded for each laser power. The fluorescence signal as a function of laser power is plotted in the insert of Figure 4.6. Curiously, the maximum fluorescence signal corresponded to some photodissociation. The fluorescence signal is directly proportional to both ion concentration and laser power. Increasing the laser power initially increased the signal, but after a certain threshold (Figure 3.10) the signal decreased as the ion concentration was reduced by

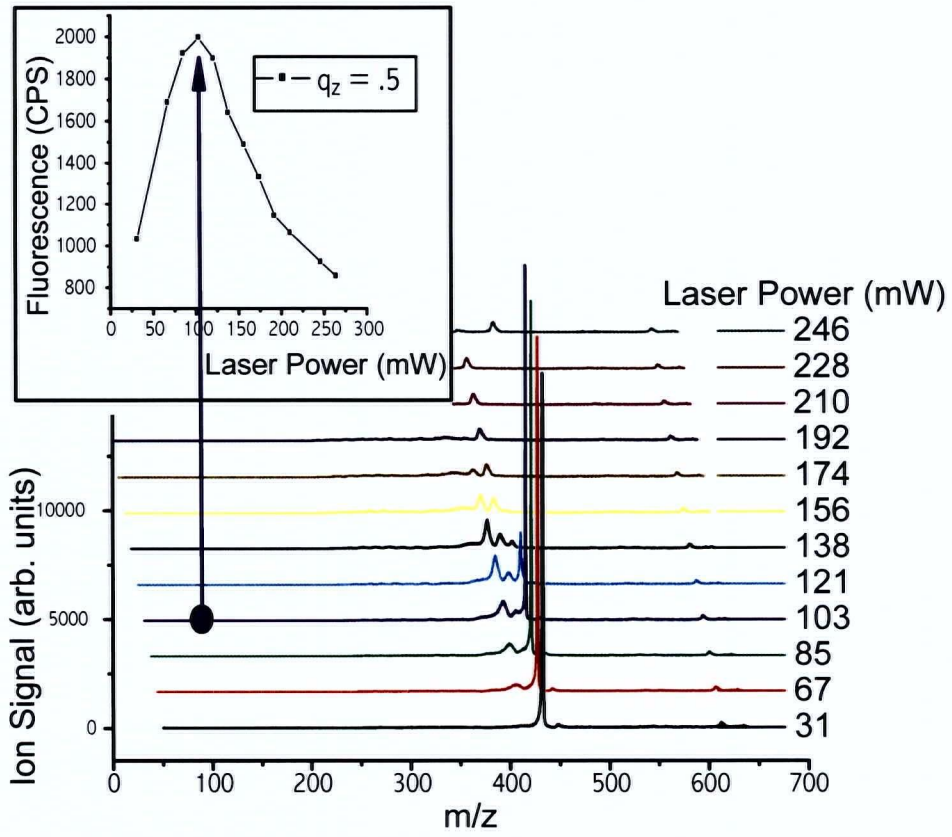

Figure 4.6: Background subtracted fluorescence signal of R6G *vs.* 488.0 *nm* laser power (insert) and corresponding mass spectra. Maximum fluorescence signal corresponds to some photofragmentation of R6G.

photodissociation. The maximum fluorescence signal corresponded to some photodissociation, but the dissociation occurred gradually over the whole irradiation period. Further experiments were needed to explain why the maximum signal corresponded to some photodissociation.

The mean S/N ratio of the fluorescence signal for these experiments is 33. The standard deviation calculated for the ten measurements at each laser power was used as the noise in the measurement. The fluorescence signal is the total signal minus the background signal that was collected with no ions in the trap. Fluorescence signals reported in this thesis always have the background subtracted.

The background signal is a combination of detector dark counts and background light from the laser scatter and room lights. S/N ratios are not to be confused with signal to background ratios. The standard benchmark for a signal to be detected is a S/N= 3. The signal does not have to be three times the background, but rather three times the total noise in the measurement. Figure 4.7 shows the fluorescence signal, background signal, and measured S/N ratio plotted against laser power. The S/N ratio is still very good even when the background is larger than the signal.

There are many possible sources of error in most analytical measurements. The laser intensity may fluctuate, but the total photon flux for a 1 s experiment should be very constant if the laser is operating properly. When operated in an analog mode, all pulse height fluctuations will end up on the PMT output as noise. In a pulse counting mode, pulse height fluctuations,

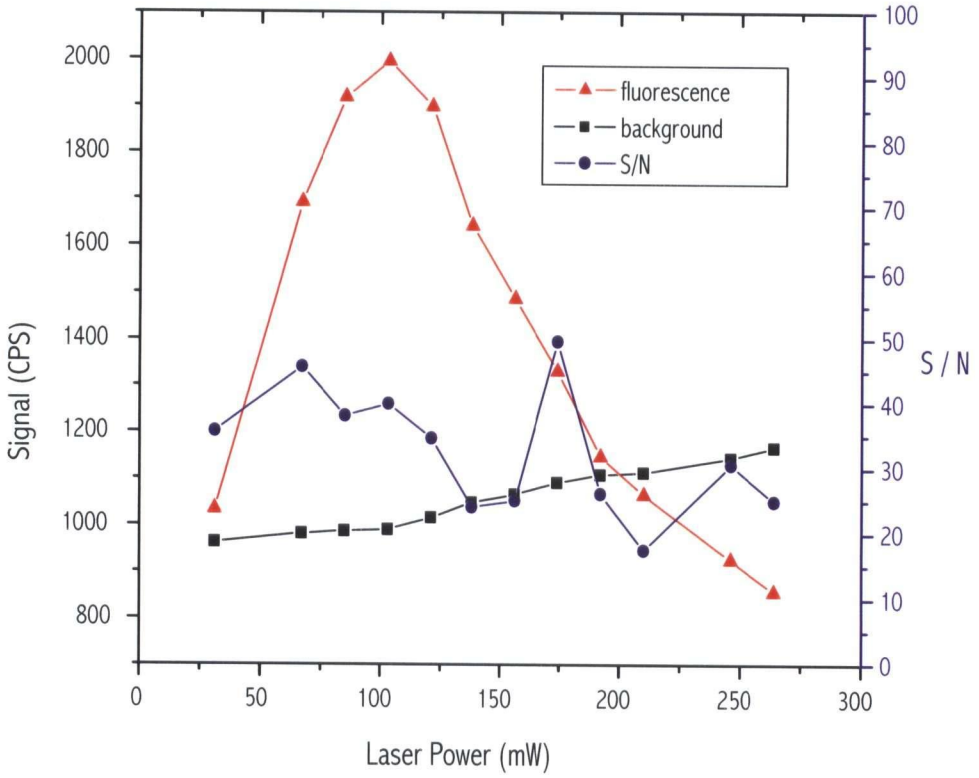

Figure 4.7: Fluorescence signal of R6G and background signal *vs.* laser power (left axis). S/N ratio *vs.* laser power (right axis).

unless very large, will not affect the count rate. The PMT gain is set high enough so that the discriminator level of the pulse counting system can be easily set higher than the amplifier noise. For this reason, pulse counting experiments have a significant S/N ratio advantage over analog detection.

In photon counting experiments, where signal pulses are detected for a certain period of time, there will always be fluctuations in the count rate.

These fluctuations, called shot noise, can be expressed as a Poisson distribution. The shot noise is simply the square root of the number of counts and represents the lowest achievable noise level in a photon counting experiment. Shot noise contributions from the fluorescence (S), background light (N_b), and dark counts (N_d) are given by the following relationships:

$$\begin{array}{lll} \text{noise from signal} & = n_s & = \sqrt{S} \\ \text{noise from background light} & = n_b & = \sqrt{N_b} \\ \text{noise from dark counts} & = n_d & = \sqrt{N_d} \end{array}$$

Since this fluorescence measurement is background subtracted, the total noise (n_{tot}) in the measurement is given by the following equation:

$$n_{tot} = \sqrt{n_s^2 + 2(n_b^2 + n_d^2)} \tag{4.1}$$

The factor of 2 in Equation 4.1 arises because background noise ($n_b^2 + n_d^2$)is present in the signal and in the subtracted "blank" measurement. The background shown in Figure 4.7 is dominated by dark counts of $\approx$ 740 CPS. The S/N would be improved by using a pulse-counting PMT that had fewer dark counts. However, the S/N measured for these fluorescence experiments were very close to the best that could be achieved in a pulse counting experiment (*i.e.* the most of the noise is from the shot noise of the signal itself and not

from the background signal).

4.5 Fluorescence *vs.* Trapping Level (q_z)

In this experiment the effect of the trapping level was examined. The instrumental parameters used in the previous experiment were not changed (Table 4.1). As with all of the pulse counting experiments discussed in this thesis, R6G was the molecule interrogated. For this experiment the laser power was held constant at $120\,mW$ while the trapping level (q_z) was varied.

4.5.1 Results and Discussion

The results of the experiment are shown in Figure 4.8. The fluorescence signal initially increases with q_z and then reaches a broad maximum before decreasing. As the trapping voltage, and therefore q_z, was increased, the ion cloud becomes smaller. A smaller ion cloud means the ions are more concentrated. As expected, the increased concentration leads to a higher signal since fluorescence is directly proportional to concentration. However, as the ion cloud shrinks the ions spend more time in the laser beam. An ion spending a greater percentage of time inside the laser beam experiences

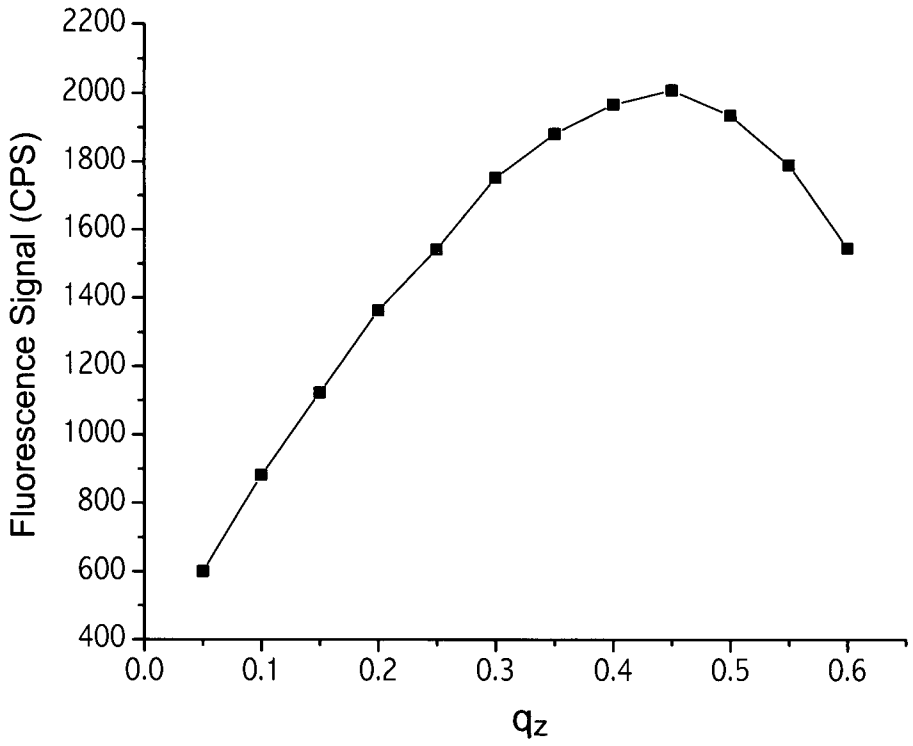

Figure 4.8: Background subtracted fluorescence signal from 5-CR 6G *vs.* q_z for a fixed laser power.

greater heating rates. Increased heating rates will eventually cause enough photodissociation to decrease the total fluorescence signal detected at high laser powers.

Another factor that could play a role in this measurement is the collection efficiency of the fiber optic probe. As the ion cloud size decreases, the collection efficiency may be improved because the ions will be emitting closer

to the centre of the trap. Changes in collection efficiency are not expected to have a large effect. While a lens outside of the ion trap would not be able to collect more light through the optical access slot, a lens mounted on the end of the probe may improve collection. One important consideration is that a lens on the end of the probe may also collect an even greater amount of scattered light.

It is clear that the laser power or trapping level can be optimized to give a maximum fluorescence signal. For a global optimization, the signal dependance on the laser power had to be monitored at several different trapping levels.

4.6 Fluorescence *vs.* Laser Power and q_z

To optimize the fluorescence experiment, the signal dependence on the laser power was measured at six different trapping levels. The instrumental parameters have not changed and are given in Table 4.1. As with the previous experiments, each data point is an average of ten 1 s measurements.

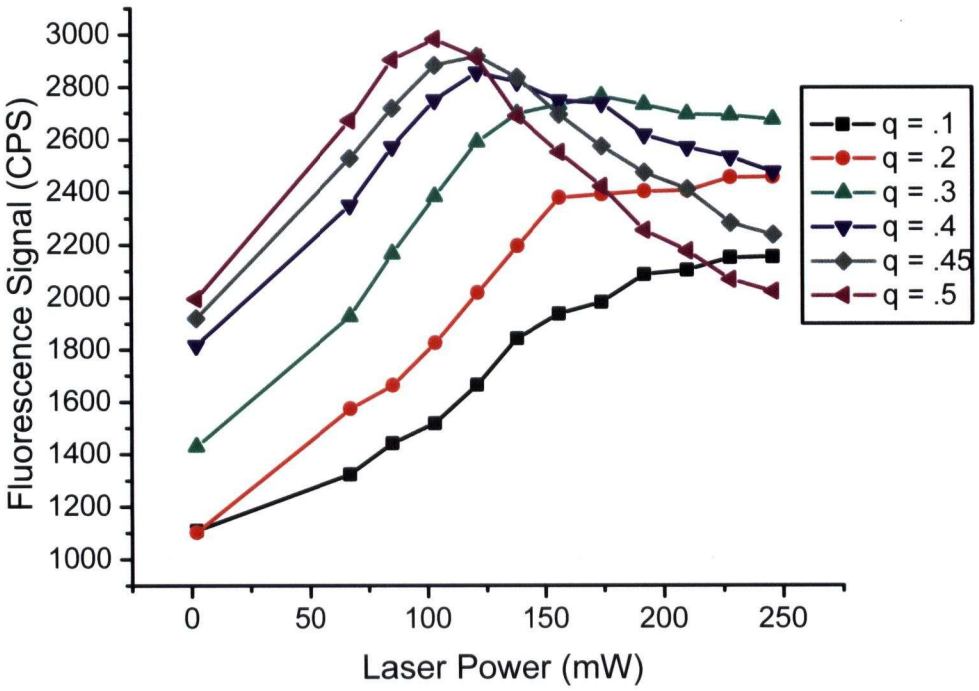

Figure 4.9: Background subtracted fluorescence signal from 5-CR 6G *vs.* laser power for six trapping levels (q_z). Higher count rates are obtained for smaller ion clouds (larger q_z) and lower laser power.

4.6.1 Results and Discussion

The results of these experiments are shown in Figure 4.9. For low trapping levels the fluorescence signal increases fairly linearly and then appears to level off. At higher trapping levels (*i.e.* higher q_z), the fluorescence decreases after reaching a maximum.

For low q_z values, the ion cloud is so diffuse that very little photodis-

sociation occurs at the laser powers used. As the trapping level increases photodissociation begins to limit the maximum fluorescence signal which can be collected. As q_z increases, lower laser powers are needed to achieve the maximum signal. A more significant observation is that greater fluorescence signals can be achieved by using smaller, more concentrated ion clouds (*i.e.* higher q_z) and lower laser powers.

Using smaller ion clouds and lower laser power is superior to using higher laser power with diffuse ion clouds for several reasons. Increasing the laser power may increase the fluorescence but it also increases the heating rate and causes photodissociation. As well, more background scatter is generated at higher laser powers thus decreasing the S/N ratio of the measurement. As previously discussed, light collection may also be more efficient for smaller ion cloud sizes. Finally, it is likely that photodissociation has a greater than linear dependance on laser power because many photons are required to dissociate an ion.

4.7 Irradiation Time

All pulse counting experiments described thus far have used 1 s storage times. In this experiment, the fluorescence signal was measured for each 1 s interval of a 10 s total storage time. Since the laser was on for the entire experiment the storage time was equivalent to the irradiation time. The experiment was repeated for two different laser powers and ten measurements were averaged for each interval. For both experiments, R6G ions were held at a trapping level corresponding to $q_z = 0.45$. After 10 s of irradiation at the lower laser power ($31\,mW$), almost no photodissociation was observed in the mass spectrum. The second laser power ($174\,mW$) was chosen so that 80% of the molecular ions would be photodissociated at the end of the 10 s irradiation time.

4.7.1 Results and Discussion

The results are displayed in Figure 4.10. For the higher laser power, the fluorescence signal is initially quite high but quickly decreases. The drop in signal is clearly the result of photodissociation. For the lower laser power, the fluorescence signal is very constant for each interval. The signal is constant because the concentration of ions is not decreasing from photodissociation.

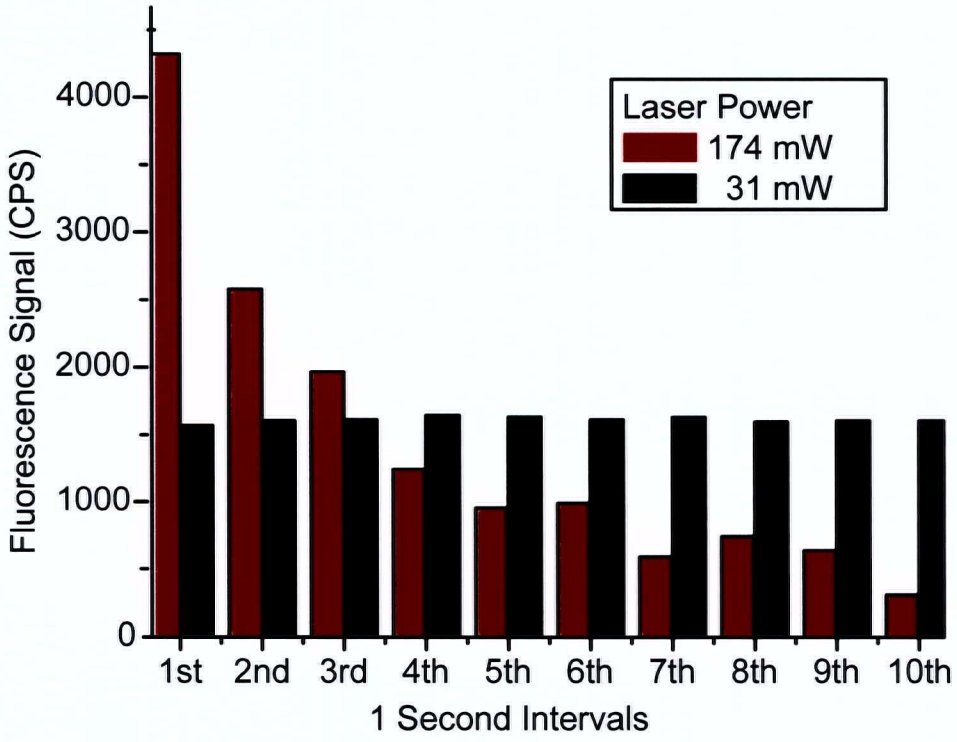

Figure 4.10: Fluorescence measured in 1 s intervals of a 10 s experiment with high laser powers (causing fragmentation) and lower laser power (no fragmentation).

The total amount of fluorescence collected for the entire 10 s is slightly higher for the lower laser power. Also, the lower laser power created less background scatter. For the full 10 s, the lower laser power measurement has $\approx$ 10% higher S/N ratio. However, using a lower laser power for a 10 s experiment is obviously not the way to improve the S/N ratio of the fluorescence experiment. To make best use of 10 s of measurement time, it would be better to use ten separate ion storage cycles and make ten 1 s measurements at the higher laser power. Shorter irradiation times and higher laser powers will give better S/N ratios until the trapping time becomes so short that the ion trap is no longer completely filled between experiments.

4.8 Final Optimization

For complete optimization of the fluorescence experiment the full range of trapping potentials was investigated. In Section 4.6, only trapping levels up to $q_z = 0.5$ were considered. Pressure effects were also evaluated.

A new PMT specifically designed for pulse counting was used for the remaining pulse counting experiments. The Hamamatsu R4632 has a much lower dark count than the R1477-06. The PMT housing was cooled to $\approx 15°C$

using a Peltier cooler. To avoid condensation problems, the PMT was not cooled further. This modest cooling reduces the dark counts from 50 CPS at room temperature to 30 CPS at 15°C. The reduction of dark counts from 700 CPS, with the R1477-06, to 30 CPS with the R4632 significantly improved the S/N of the measurements. Using the R4632 pulse counting PMT the total background was reduced to 35 CPS consisting of: 30 CPS dark counts, 4 CPS laser generated background, and 1 CPS from room lights for most measurements. All other instrumental parameters (Table 4.1) remain unchanged except for pressure.

4.8.1 Complete Optimization at Two Pressures

The photodissociation studies reported in Section 3.4.2 show that increasing the buffer gas pressure increases the cooling rate of absorbing ions and decreases photodissociation. Thus, higher pressures allow the use of higher laser powers. For the same concentration of ions, higher laser powers must increase the fluorescence signal. Unfortunately, the photodissociation results provide the only evidence that increased pressure will lead to improved fluorescence detection.

Increasing the pressure in the current instrument affects more than just

the cooling rates of trapped ions. It also affects the focusing properties of the ESI front-end, especially Q_1, and injection efficiency into the ion trap (Section 2.5.2). Increasing the pressure in the trap will cause more ions to be trapped. Attempts to trap equal numbers of ions at each pressure would be complicated by the fact that ion ejection and detection is also pressure dependent.

For this experiment, the laser power was optimized for each trapping level (q_z) tested. As before, the maximum signal reported for each q_z was the average of ten 1 *s* experiments. The optimization was conducted at 1 *mtorr* and 0.55 *mtorr* of helium buffer gas.

4.8.2 Results and Discussion

The results of the optimization experiment are shown in Figure 4.11. A trapping level corresponding to $q_z = 0.65$ gives the maximum fluorescence signal at both pressures. The higher pressure experiment gives greater fluorescence signals at every q_z value. Increased cooling rates, from more frequent collisions with helium atoms, must contribute to this effect. However, the main reason for superior signals at the higher pressure is the increase in the total number of trapped ions. The mass spectra clearly show more ions being

trapped at 1 *mtorr* compared to 0.55 *mtorr*. Although this experiment does not prove that higher fluorescence signals can be obtained at higher buffer gas pressures, subtle differences in the results do illustrate some interesting complexities of the fluorescence experiment.

At both pressures, the fluorescence signal increases linearly with q_z at low q_z values. At 0.55 *mtorr*, the linear portion of the graph has a lower slope and begins to roll off at lower q_z values. Two related effects are responsible for this difference. First, the ion cloud size is much larger for the higher pressure; there are simply more ions in the ion cloud. At the lower pressure, the smaller ion cloud will requires less compression (lower q_z) to become fully illuminated by the laser beam. As the ion cloud becomes fully illuminated there is less concentration advantage to further increasing q_z (compressing the ion cloud) and the slope of the graph decreases. Furthermore, space charge effects are more serious for larger numbers of trapped ions.

Space charge effects are caused by the electric fields generated by the ions themselves. At low ion numbers, the motions of trapped ions are primarily affected by only the quadrupole field. When the ion trap is filled to capacity the ion-ion repulsions become much more significant. The mass spectra shown in this experiment are severely "space charged". The ion-ion repul-

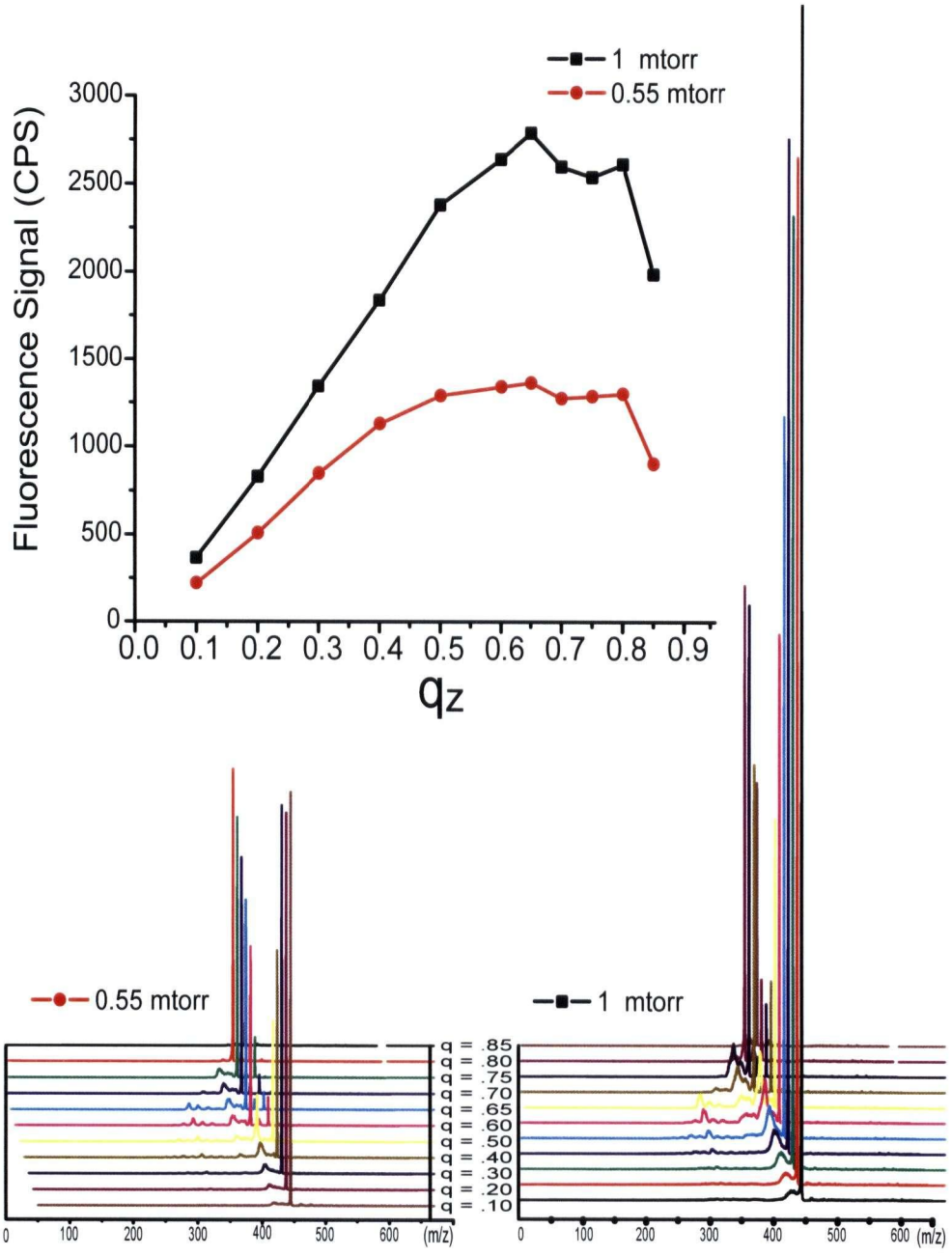

Figure 4.11: Optimization of q_z and corresponding mass spectra. The upper graph shows 5-CR 6G fluorescence signal *vs.* q_z for two different buffer gas pressures (1 *mtorr* and 0.55 *mtorr*). The mass spectra for both pressures are plotted on the same vertical scale.

sions interfere with ion ejection during the mass scan and ions appear in the mass spectrum as broad peaks. Especially sensitive to space charge effects are low concentration ions which have a slightly lower mass to charge ratio than an abundant ion. Space charge effects are also partially responsible for the longer linear portion of the high pressure curve. Larger ion clouds will require stronger trapping fields (higher q_z) to overcome the space charge effects and fully compress the ion cloud.

At both pressures, there is a noticeable suppression of the fluorescence signal for q_z values of 0.7 and 0.75. This decrease in signal is the result of a decrease in ion concentration. The ion concentration is lowered at these q_z values because trapped ions are resonantly excited at $\beta_z = 0.5$. This resonance is attributed to higher order fields caused by truncating and/or stretching electrodes. Normally the $\beta_z = 0.5$ resonance does not affect ion trap performance because ion numbers are kept low and trapping times used for mass spectrometric analysis are much less than 1 s. At high ion concentrations the cloud size increases and the ions are subjected to stronger fields farther away from the centre of the trap. This "dip" in the fluorescence signal is more pronounced at higher pressures because the ion cloud is larger and a greater number of ions is affected by the $\beta_z = 0.5$ resonance.

At very high q_z the fluorescence signal drops quickly. It turns out that the first few fragment ions created by photodissociation are also fluorescent. Since they are of lower mass, these fragments have higher q_z values than the precursor ion. As the q_z value of the intact R6G ions approaches the stability limit defined by $\beta_z = 1$ and $q_z = 0.908$, the trajectories of the lower mass fragment ions are no longer stable. The sharp decrease of the fluorescence signal occurs because the fragment ions are no longer contributing to the fluorescence signal since they are ejected from the trap as soon as they are formed.

4.9 Fluorescence From Fragments

To prove that a particular photodissociation product is fluorescent, it must be isolated in the ion trap. Ion isolation is achieved using a filtered noise field (FNF, Section 2.2.3). After all other ions have been removed from the ion trap, a standard pulse counting experiment can be performed. First, the precursor R6G ions are irradiated until enough of the desired fragment is formed. A FNF is then applied to eject all other ions. Finally, the counter on the data acquisition board is gated on and fluorescence data is recorded. CID

was not used to generate fragments because some photodissociation products are not observed in the CID spectrum.

The mass scan for this experiment is shown in Figure 4.12. After ion injection, the RF-voltage is increased so that the R6G ions are held at a trapping level corresponding to $q_z = 0.65$. The laser power is held constant for the entire experiment and depends on which fragment is being analyzed. After 1 s of irradiation a sufficient amount of the desired fragment is produced. Since the application of the FNF requires 100 ms, photodissociation must be stopped while the FNF is applied. Gating the laser off for the ion isolation is one method to stop photodissociation.

In this experiment photodissociation is stopped by lowering the trapping potential. The FNF was applied at this lower potential so that ion isolated could be achieved without photodissociation also occurring. After the ion isolation step is complete, the trapping level is increased so that the fragment of interest is held at $q_z = 0.65$ for 1 s. The photon counting electronics are gated on for this time period and any fluorescence counts can be attributed to the fragment. The first few fragments of R6G corresponding to loss of CH_2, $2 \times CH_2$, $3 \times CH_2$, and OC_2H_4 are fluorescent.

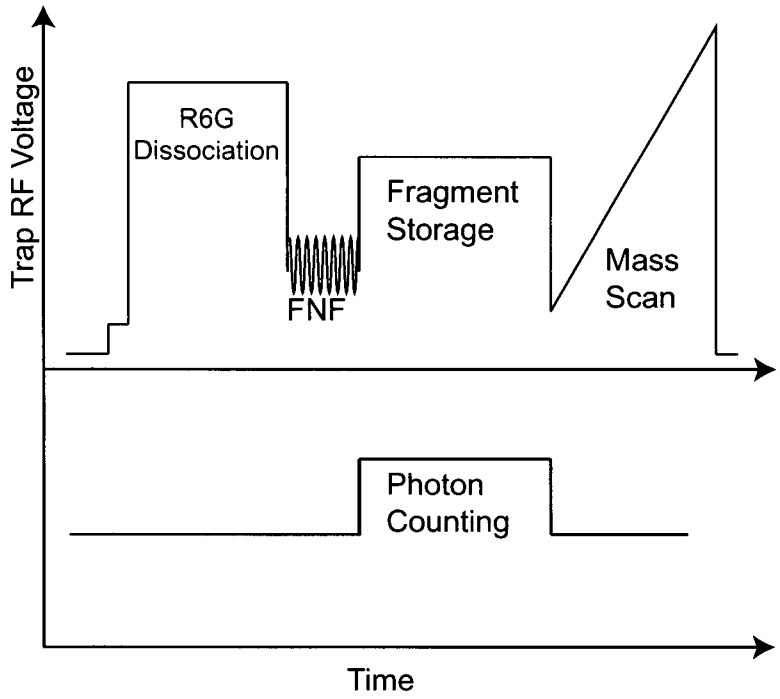

Figure 4.12: Timing diagram to test fragment ions for fluorescence.

4.10 Chopping Experiments

The idea of chopping the excitation laser was first presented in Section 3.4.2. Chopping the laser beam allows the ions more time to cool and higher laser powers can therefore be used. While chopping certainly permitted the use of higher laser powers, the experiment was unsuccessful when first attempted. The chopping experiment was revisited and reevaluated after fluorescence was detected using pulse counting experiments. The total fluorescence emission

collected for a given counting period was reduced by 66% by chopping the laser. The chopping wheel used for these experiments had a 50% duty cycle. Chopping the laser beam would only be useful for increasing the S/N ratio during the "on" phase of the chopping. If the fluorescence signal is already sufficiently above the background noise then a chopping experiment should not be used.

4.11 Conclusions

The main objective of building an instrument capable of detecting gas phase fluorescence emission from molecular ions has been achieved. An instrument has been developed to detect fluorescence emission from gas phase molecular ions confined in an ion trap. This is the first such instrument capable of making high S/N measurements of the fluorescence emission from large molecular ions. A S/N of 260:1 was measured for a 15 s experiment and larger S/N measurements could easily be achieved by increasing the counting period. The fluorescence experiment is optimized by using compact ion clouds and lower laser powers. A trapping potential corresponding to $q_z = 0.65$ gives the optimal fluorescence signal for R6G ions (2000-3000 CPS). Many significant

instrumental innovations were required to achieve this goal.

The ESI front-end allowed ions to be trapped without also filling the trapping volume with neutrals. A large, noisy neutral background and emission from filaments were the main disadvantages of using a thermal desorption probe with the first version of the instrument.

The most significant instrumental challenge was to reduce the amount of laser generated background. This background problem was not anticipated at the beginning of this work because the fluorescence emission was expected to be significantly Stokes shifted. The sensitivity of gas phase molecules to photodissociation also required the use of lower laser powers, thus decreasing the total amount of fluorescence that could be expected. The only way to make this fluorescence measurement was to significantly reduce the total amount of background light detected. The use of a fiber optic probe and the coating of the electrodes with carbon reduced the amount of background scatter collected by at least six orders of magnitude. This background reduction led to the successful detection of fluorescence from trapped gas phase molecular ions.

At the beginning of this chapter it was stated that separating the fluorescence emission of trapped ions from the laser generated background might not

be possible with a spectrograph. Wavelength dispersion was thought to be inadequate for separating the small fluorescence signal from the overwhelming laser background. Fluorescence was expected to be almost resonant with the excitation and wavelength dispersion would therefore not help. The dramatic reduction of background noise and the fact that a filter could be used to separate some of the fluorescence from the laser background prompted a re-evaluation of the wavelength dispersion experiment.

The next experimental goal and supplementary objective of this thesis was to collect a fluorescence emission spectrum of a gas phase molecular ion. An intensified CCD (ICCD) was provided for this purpose. The ICCD is an ideal detector for this ion trap fluorescence experiment.

4.12 Perspective

While many laboratories around the world have abandoned their attempts to detect fluorescence emission from trapped molecular ions, other groups are making progress. To put the instrumental accomplishments described in this chapter into perspective it is important to consider the progress made by these groups.

Joel Parks' group at the Rowland Institute (Harvard) has detected emission from trapped ionic dyes and has now moved on to gas phase FRET experiments.[16] Parks was able to detect an average of 1 photon for each pulse of a Nd:YAG laser. Two dielectric high reflectors, designed to attenuate the laser wavelength by $\approx 99\%$, and two long pass filters were used to reduce the background detected. Relying on several filters to reduce the background limits the excitation wavelengths that can be used and attenuates the fluorescence. Collecting a full emission spectrum is likely impossible when long pass filters are used. Also, a fluorescence excitation spectrum could only be collected if filters were purchased for every excitation wavelength measured.

Another group actively developing instrumentation in this field is Alan Marshall's group at the National High Magnetic Field Laboratory in Florida. Marshall's group has been able to detect fluorescence emission of $C_6F_6^+$ confined in an ICR trap.[15,49] Pulsed excitation (10 Hz) was also used for these experiments. $C_6F_6^+$ has an excited state lifetime that is long enough to allow a detector to be turned on after the excitation from the pulsed laser has passed. They were able to collect close to 2 photons per pulse. Also, since no filters were required to block the excitation wavelength, an excitation spectrum was recorded. For ions with sufficiently long fluorescent lifetimes a

pulse laser is a reasonable excitation source.

Chapter 5

Fluorescence Emission Spectroscopy

This chapter describes the first instrument capable of recording the gas phase emission spectrum of large molecular ions. The objective of the work described in this thesis was to develop an instrument capable of detecting fluorescence emission from large gas phase molecular ions confined in a quadrupole ion trap. This was demonstrated in Chapter 4. The possible future applications of the instrument included: probing the gas phase structure of biomolecules, identifying potential diffuse interstellar band carriers, and complementing other forms of molecular spectroscopy. Experiments based on the pulse counting detection methods and instrumentation presented in Chapter 4 demonstrate that the instrument can potentially be used for these applications. However, these pulse counting experiments only

record the quantity of fluorescence emitted by the trapped ions. The wavelength component of the emission is only roughly estimated by considering the transmittance of the filter used in the experiment.

The ability to record a complete emission spectrum of trapped ions would significantly enhance the versatility and effectiveness of the instrument. A fluorescence emission spectrum is recorded by spatial dispersion of the emission and recording of the fluorescence intensity as a function of wavelength. The spectroscopic information contained in an emission spectrum could be used help elucidate the structure of gas phase ions. Also, the design of pulse counting experiments could be improved with knowledge of the emission spectrum of the ion under investigation.

As well, it is likely that fluorescence experiments would be easier to optimize with prior knowledge of the emission spectrum of the ion to be studied. For example, a FRET experiment (Section 1.1) requires that the emission of the donor molecule correspond in energy to the absorption of the acceptor chromophore. In Chapter 3 it was shown that the gas phase absorption of ions differs from their solution absorbance (Section 3.4.1). Also, if emission of the donor is significantly different in the gas phase it may not excite the acceptor at all. FRET pairs that work well in solution experiments may

not be appropriate for gas phase investigation. An instrument capable of recording complete emission spectra of gas phase ions could be used to select suitable FRET pairs and provide a proof of principle for all gas phase FRET experiments.

The results from the pulse counting experiments suggest that the instrument might be capable of recording emission spectra because the laser background was significantly reduced. The fluorescence signal was two orders of magnitude higher than the laser generated background. However, the pulse counting experiments relied on a long pass filter to reduce the total amount of laser generated background detected. Earlier in this thesis it was hypothesized that fluorescence emission is very close in wavelength to the laser excitation, so a long pass filter may not be the best choice for fluorescence emission spectroscopy. A long pass filter would likely attenuate a significant proportion of the emission.

In order to evaluate the possibility of recording an emission spectrum of trapped ions, modifications to the instrument were necessary. The PMT used to detect photons in pulse counting experiments was replaced with a spectrograph. The same spectrograph used in previous experiments (Section 3.2) was coupled to the fiber optic probe. The CCD used in earlier work

(Section 3.2) was replaced with an ICCD (PI-Max 1024 × 256, Roper Scientific, Inc., Tucson, USA). Initially, a holographic notch filter was used to reduce the amount of laser scatter reaching the spectrograph.

5.1 Instrumentation

Most of the instrumentation used for the pulse counting experiments was also used to collect emission spectra. The excitation optics and fiber optic probe were not changed. The methods and instrumentation used to confine the ions also remained the same. The only change from the pulse counting experiments was how the fluorescence was separated from the excitation background and detected. The pulse counting PMT and long pass filter were exchanged for an ICCD mounted on a spectrograph. Other filters, including the one used for pulse counting, could easily be added if required. Figure 5.1 is a diagram showing the final version of the instrument.

5.1.1 Spectrograph and ICCD

The 0.150 m spectrograph has been previously described (Section 3.2). The ICCD uses a microchannel plate (MCP) to amplify light prior to CCD detec-

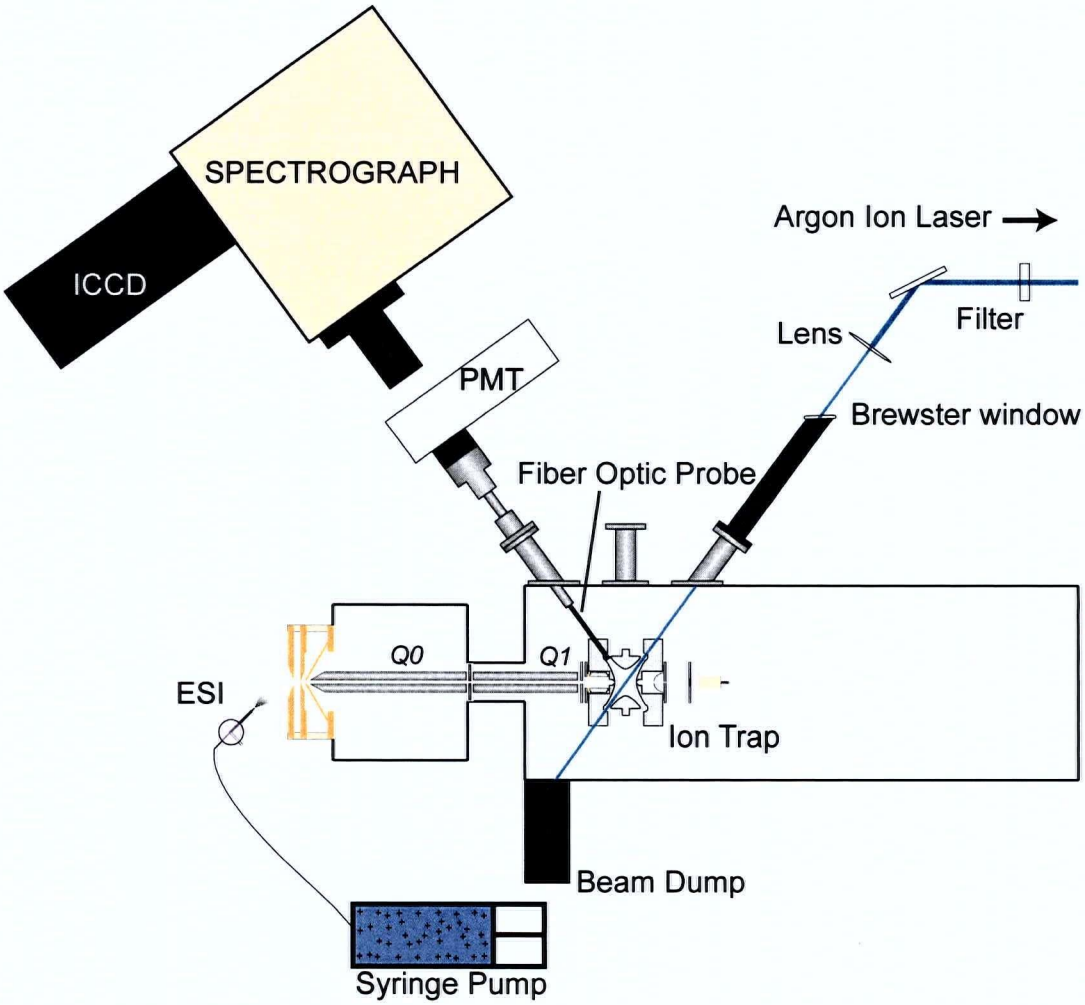

Figure 5.1: Final version of the instrument.

tion. The ICCD has five main components: photocathode, MCP, phosphor screen, fiber optic bundle, and CCD. Light hitting the photocathode will generate photoelectrons, which are accelerated towards the front of the MCP. A photoelectron then enters one channel of the MCP and becomes amplified via a cascade process. Amplified electron packets exiting the MCP strike the phosphor screen producing visible photons that are then coupled through the fiber optic bundle to the CCD where they are detected.

By gating both the photocathode and the MCP this ICCD can achieve off/on ratios of $10^6 : 1$. An ICCD can detect extremely low light levels that would otherwise be far below the read noise of a CCD. A gain setting of 200 was used for all emission experiments; according to manufacturer specifications this corresponds to an ≈ 7800 times amplification of the signal. The CCD was cooled to $-20°C$ for all experiments. The ICCD was controlled with commercial software supplied by the manufacturer (WinSpec V2.4.7, Roper Scientific, Inc.). Spectra shown in this thesis are plotted with a vertical axis in counts. These counts correspond to the intensified signal and have not been corrected to represent the number of photon incident on the detector.

The spectrograph was mounted on a kinematic platform which sits on a translation stage. After fluorescence emission was confirmed with a pulse

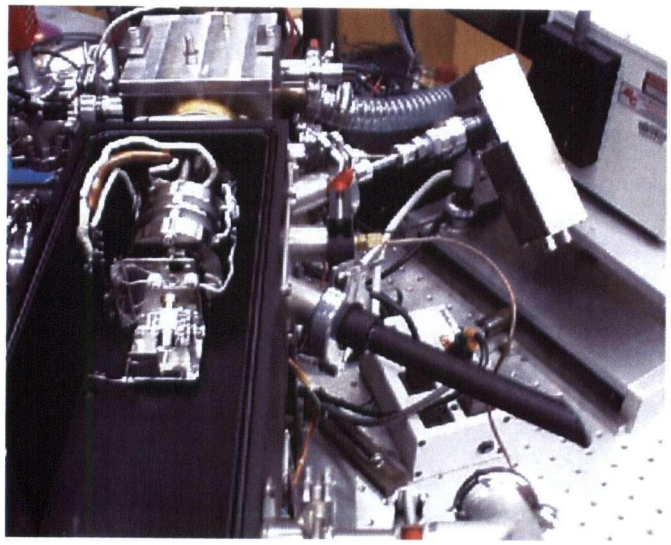

Figure 5.2: Photograph of the instrument with the PMT attached to the fiber optic probe and spectrograph ready to be connected.

counting experiment the PMT was removed from the fiber optic probe and the spectrograph was moved forward into place. The entrance flange of the spectrograph has been modified to couple directly to the fiber optic probe. The fine thread used in the tube lens coupling system aided in the alignment of the spectrograph. The translation stage allows the spectrograph to be moved on and off the probe without altering the alignment. Figure 5.2 is a photograph of the instrument with the PMT attached to the fiber optic probe and the pre-aligned spectrograph ready to be connected.

The entrance slit width used on the spectrograph was $760\,\mu m$ giving a

resolution of $\approx 14\,nm$ at the detector. Room temperature fluorescence emission from R6G and 5-CR 6G ions was expected to be diffuse and greater resolution unnecessary.

Filters and Optics

The 488.0 *nm* holographic notch filter (Chapter 4) was used as the output window of the fiber optic probe to reduce the scattered 488.0 *nm* excitation. The probe was designed so that only light exiting the fibers at small angles ($< 10°$) would reach the filter. Light exiting the fibers at greater angles would hit a beam stop built into the probe. To achieve optimum performance the light to be filtered must strike the notch filter with an angle of incidence of less than 10°.

After the collected light passes through the notch filter it was focused onto the entrance slit of the spectrograph with a 25 *mm* diameter plano-convex lens with a 100 *mm* focal length. This lens has an f-number of 4 to match the spectrograph. Since the output of the fiber optic probe does not illuminate the entire lens the grating was underfilled.

5.1.2 Methods

The instrumental parameters shown in Table 4.4.1 were used to trap ions of the ionic dyes R6G and 5-CR 6G. The only instrumental parameter changed was the buffer gas pressure. In these experiments the buffer gas pressure was 1 *mtorr*. Each dye was investigated separately and held at a trapping level corresponding to $q_z = 0.65$ for every experiment. Laser wavelength and laser power are specified for each experiment. The room lights were turned off for these experiments.

The ion storage time was 1 *s* and the total time for the complete mass scan was 1.065 *s*. Since the duty cycle for the storage time was 94%, the ICCD was operated asynchronously with the mass spectrometer and the total integration time was dictated by the light collected. For the PAH experiments described in Chapter 3, the CCD was usually gated on and off with every mass scan to avoid collecting light emitted by the filaments. Gating the detector on and off for each mass scan adds read noise to the measurement and should always be avoided if possible.

Full vertical binning of the ICCD was used to minimize read noise. The capacity of the readout pixel below every column of pixels on the ICCD is 1.2×10^6 electrons. To obtain the best possible S/N the integration time of the

ICCD was set so that the highest signal on the detector would be just below the maximum capacity of the read pixel. The relationship between total counts and S/N is basically the same as for the pulse counting experiments. The S/N will increase with the square root of the total number of counts. It is important not to saturate the pixels or charge will bloom into adjacent pixels.

5.1.3 Solution Spectra

R6G and 5-CR 6G are very similar dye molecules which have high fluorescent quantum efficiencies in solution ($\phi_f > 0.9$). The structures of the dyes are shown in Figure 3.7 and their solution absorption spectra are shown in Figure 5.3. The solution absorption spectra were recorded using a Hewlett Packard (Palo Alto, USA) 8452A diode array UV-Vis spectrophotometer.

Emission spectra for R6G and 5-CR 6G were recorded using the same fiber optic probe, spectrograph, and ICCD used with the ion trap experiments. A quartz cuvette filled with a $1\mu M$ solution of the dye was positioned approximately $25\,cm$ from the end of the fiber optic probe. The 488.0 nm output of the argon ion laser was directed through the cuvette and the emission spectrum was recorded. The solution emission spectra are shown in Figure 5.4.

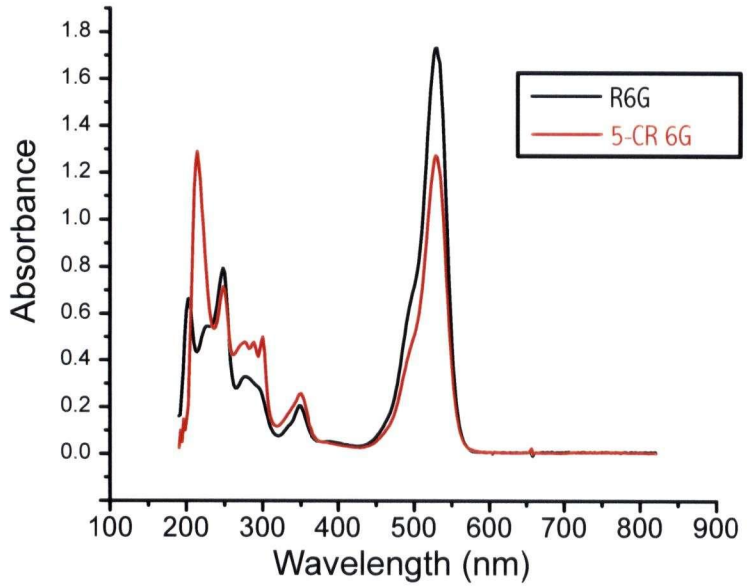

Figure 5.3: Solution absorbance spectra of R6G and 5-CR 6G.

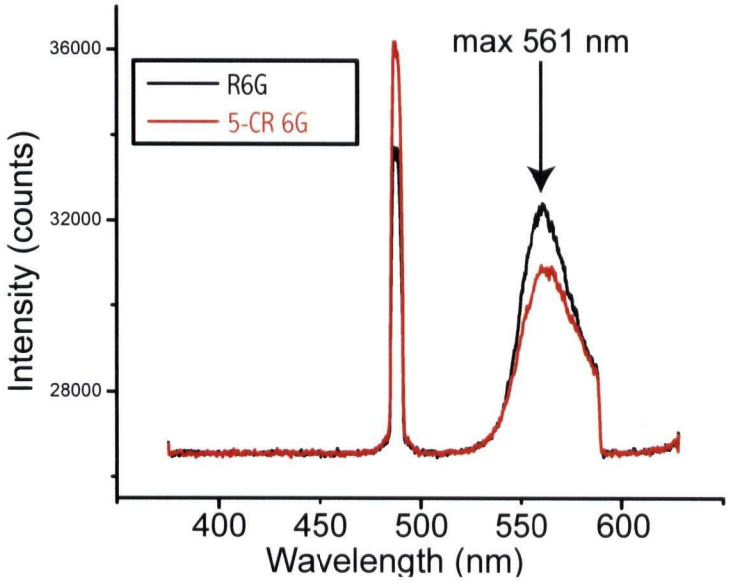

Figure 5.4: Solution emission spectra of R6G and 5-CR 6G. Fluorescence maximum is Stokes shifted 73 *nm*.

The emission spectra of R6G and 5-CR 6G are very similar. The emission maximum for both dyes is Stokes shifted 73 *nm* from the 488.0 *nm* excitation. The long wavelength side of the solution emission shows a sharp cutoff which corresponds to the edge of the ICCD. R6G and 5-CR 6G are expected to also have very similar gas phase emission spectra.

5.2 Emission Spectra with Notch Filter

The first emission spectrum collected was for R6G. R6G ions were excited with 66 *mW* of 488.0 *nm* laser light. The emission spectrum of R6G was recorded in three 60 minute integrations. One 60 minute background spectrum was recorded with no ions in the trap. The only change made in the experiment to collect the background spectrum was to disconnect the gate pulse and therefore prevent ions from reaching the ion trap. The full 180 minute fluorescence emission spectrum was obtained by adding the three 60 minute integrations and subtracting the background spectrum three times. Since the laser power was chosen to maximize the fluorescence emission, some photodissociation was occurring during this experiment. The recorded emission spectrum shown in Figure 5.5 must contain emission from the fragments

in addition to emission from the R6G ion.

Lower laser powers should be used when collecting emission spectra if any of the photodissociation fragments have a different emission spectrum from the precursor ion. The emission spectrum of R6G was collected again at a lower laser power. The laser was set to 32 mW so that almost no photodissociation would occur during the experiment. As before, three 60 minute integrations and one 60 minute background spectrum were recorded. The background subtracted sum of the three integration times is shown in Figure 5.5.

The emission spectrum of 5-CR 6G ions was also recorded. The total integration time was 105 minutes for 5-CR 6G. The background subtracted emission spectrum is shown in Figure 5.5. A laser power of 66 mW was used to excite the 5-CR 6G and some photodissociation occurred during this experiment. The emission spectra shown in Figure 5.5 were smoothed using a five point moving average.

5.2.1 Discussion

The two most obvious characteristics of the emission spectra shown in Figure 5.5 are that the fluorescence emission is very close to the excitation

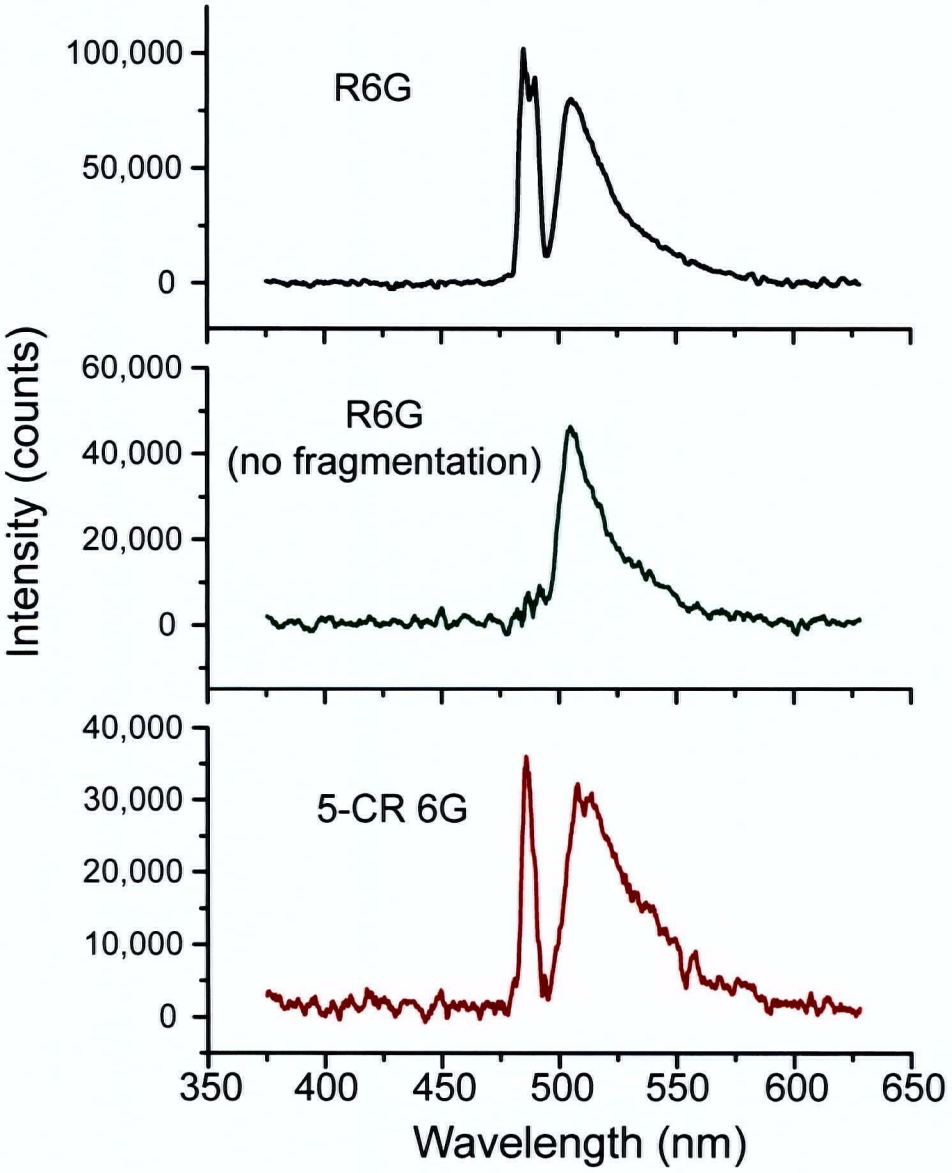

Figure 5.5: Emission spectra collected with the notch filter.

wavelength and that there is a gap in the spectrum between the excitation wavelength and the fluorescence. The holographic notch filter was supposed to provide a 10 *nm* notch centered at 488.0 *nm*.

The actual transmission of the notch filter was measured with a Hewlett Packard 8452A diode array UV-Vis spectrophotometer. The transmission of the notch filter was compared with the R6G emission spectrum. The results of this comparison are shown in Figure 5.6. The filter is not a 488.0 *nm* notch filter but a 496.5 *nm* notch filter which does little to attenuate the 488.0 *nm* excitation used for these experiments. The filter manufacturer (Kaiser Optical Systems, Inc., Ann Arbor, USA) had inadvertently shipped the wrong filter. While disappointing there was a positive aspect to discovering the incorrect filter had been used. The use of an expensive notch filter was unnecessary. A fluorescence excitation spectrum, for example, could now be measured without requiring a separate notch filter for every excitation wavelength measured. Experiments without the notch filter will be 20% more sensitive because the transmission of a notch filter is less than 80% outside the notch. Without the need for notch filters the instrument is more versatile, sensitive, and less expensive.

The use of an inappropriate notch filter interfered with the collection of

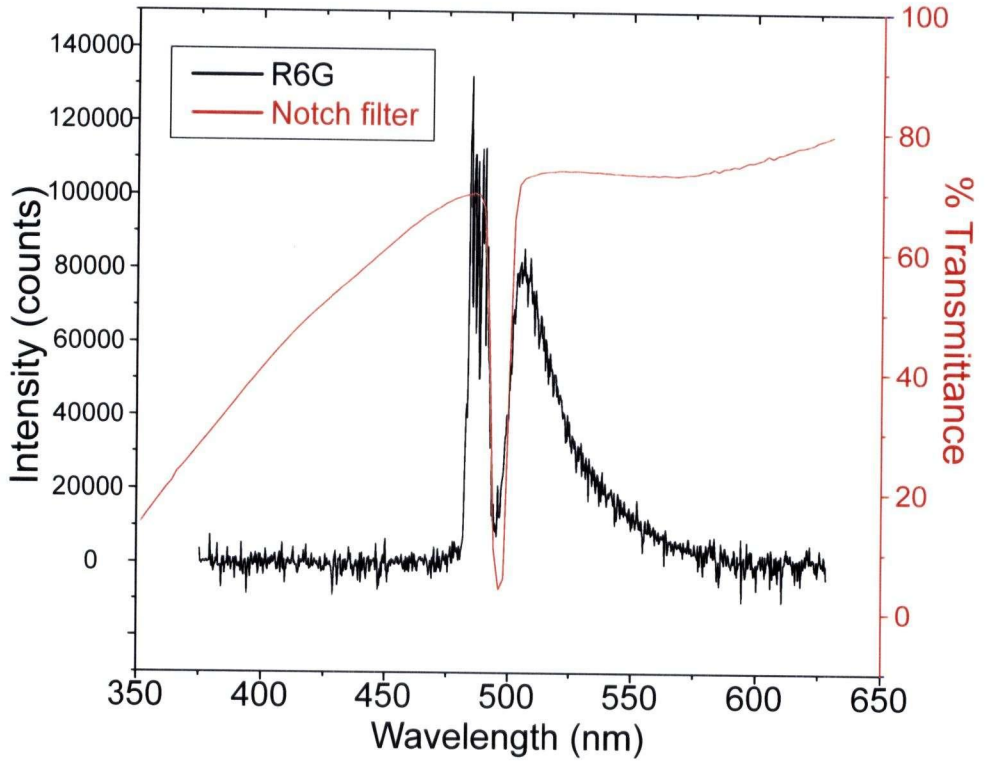

Figure 5.6: R6G emission (left axis) and notch filter transmittance (right axis).

the fluorescence emission spectra of R6G and 5-CR 6G. The edge of the notch filter was almost certainly defining the shape of the emission spectrum and experiments without this notch filter were necessary. Despite this, some useful information was extracted from these first emission spectra. Comparing the emission spectra collected for R6G with and without photodissociation and comparing the emission of R6G and 5-CR 6G is still possible.

The elastically scattered laser light appears in most of the emission spectra shown in this thesis. This collected laser scatter is $\approx$ 200 times larger than the maximum fluorescence signal. This laser scatter appears in the background subtracted emission spectra because there is more noise associated with subtracting two large signals. Drifting of the laser power during long experiments also contributed to this effect.

The normalized emission spectra of R6G with and without photodissociation are plotted together to aid in their comparison (Figure 5.7). At this resolution they appear to be identical and photodissociation will not have to be avoided in future experiments unless the information being sought is lost by fragmentation (*e.g.* FRET experiments).

The fluorescence emission spectra of R6G and 5-CR 6G are plotted together in Figure 5.8. The 5-CR 6G emission spectrum is broader and its

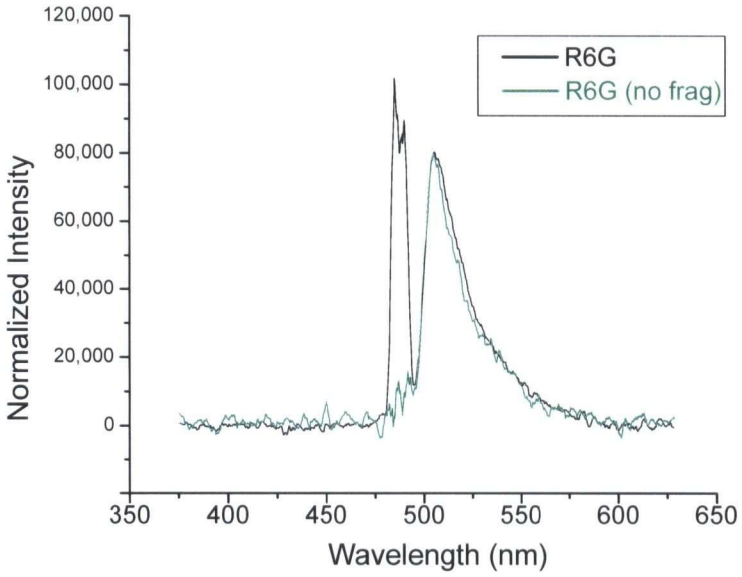

Figure 5.7: R6G emission spectra with and without photodissociation.

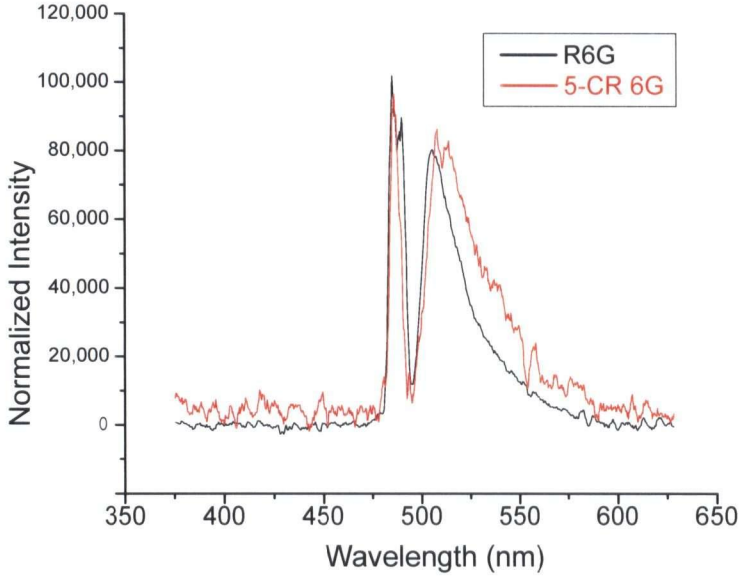

Figure 5.8: R6G and 5-CR 6G emission spectra.

emission maximum has a greater Stokes shift. One of the intended applications of the instrument is to investigate the conformations of gas phase biomolecular ions trapped in an ion trap. It was encouraging that differences in the emission spectra of two very similar ions can be observed even at such low resolution.

5.3 Emission Spectra without Filter

The inappropriate (and, in fact, unnecessary) notch filter was removed from the fiber optic probe and replaced with a quartz window. The emission spectra of trapped R6G and 5-CR 6G ions were collected using a laser power of 47 mW for both dyes. An 80 minute R6G ion emission spectrum was collected in eight 10 minute integrations with four 10 minute background integrations. A 90 minute 5-CR 6G ion emission spectrum was collected in six 15 minute integrations with two 15 minute backgrounds integrations. The emission spectra of R6G and 5-CR 6G are plotted together in Figure 5.9.

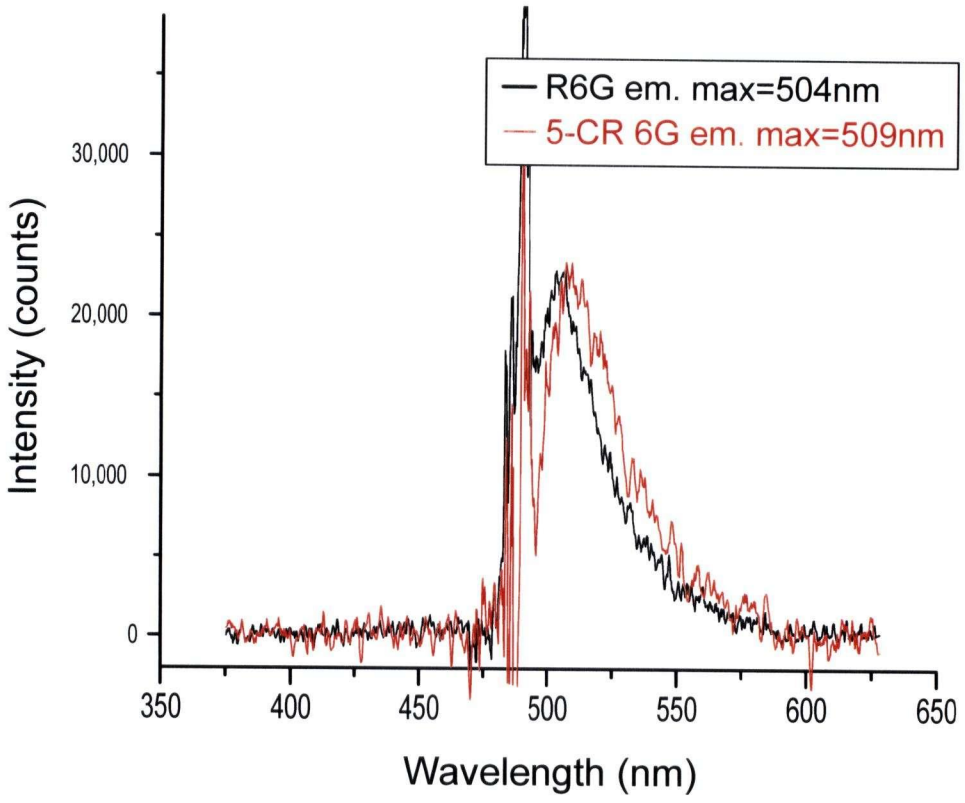

Figure 5.9: Fluorescence emission spectra for R6G (80 min integration time) and 5-CR 6G (90 min integration time).

5.3.1 Discussion

R6G has an emission maximum at 503 *nm* and 5-CR 6G has an emission maximum at 509 *nm*. As with the previous spectra of these two ions (Figure 5.8), the 5-CR 6G emission spectrum is more diffuse and has a greater Stokes shift than the R6G emission. The fluorescence emission from gas phase R6G ions is Stokes shifted 15 *nm* from the 488.0 *nm* excitation. The fluorescence emission from gas phase 5-CR 6G ions is Stokes shifted 21 *nm* from the 488.0 *nm* excitation. These Stokes shifts are small compared to the 73 *nm* Stokes shifts measured in solution (Figure 5.4).

In condensed phase experiments molecules excited to a high vibrational level of the excited state quickly lose excess vibrational energy to the surrounding solvent or matrix. Any fluorescence will therefore originate from the lowest vibrational energy level of the excited state. Franck-Condon factors are non-zero for a wide range of transition energies and the resulting emission is a diffuse band. After emission, some molecules will be in a high vibrational level of the ground state. The excess vibrational energy is again absorbed by the solvent and the molecules end up in the lowest vibrational energy level of the ground state. The Stokes shift observed in solution experiments is a consequence of vibrational relaxation of the excited state and

solvent rearrangements.

In the gas phase, no such relaxation of the excited state can occur between absorption and emission events. As a result, smaller Stokes shifts are observed in gas phase emission spectra. These small Stokes shifts make detecting gas phase fluorescence from trapped molecular ions difficult. In solution measurements the fluorescence is Stokes shifted away from the excitation and emission is detected against an almost zero background. In gas phase experiments the fluorescence emission is very close in energy to the excitation. Separating the weak fluorescence signal of trapped ions from the large excitation generated background is therefore challenging. Figure 5.10 shows the fluorescence signal dominated by the background laser scatter. Figure 5.11 is the same data with an expanded vertical scale so the small fluorescence signal can be observed. The data shown in Figure 5.10 was used to generate the R6G background-subtracted fluorescence emission spectrum shown in Figure 5.9.

Since the fluorescence emission spectrum of R6G ions has been collected it is possible to evaluate the effect of the long pass filter (CG-OG-530) used in the pulse counting experiments. The transmittance of the filter was measured using a Hewlett Packard 8452A diode array UV-Vis spectrophotometer.

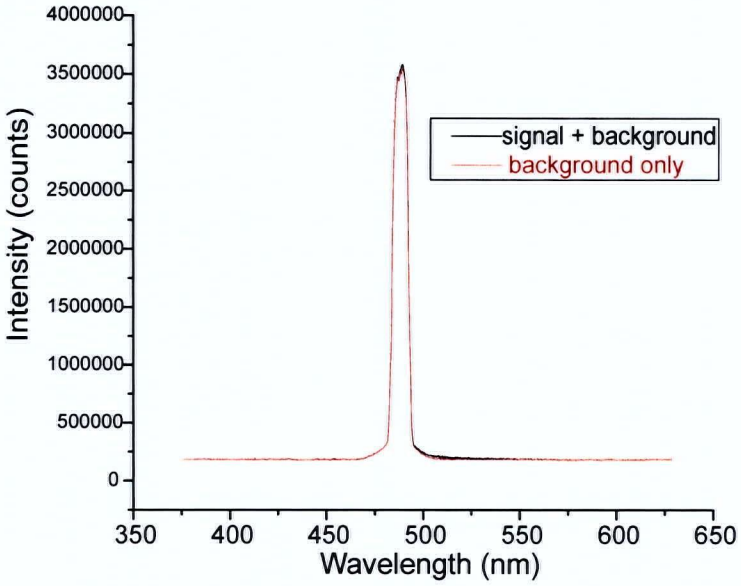

Figure 5.10: R6G fluorescence emission spectrum without background subtraction (black) and the corresponding background spectrum (red).

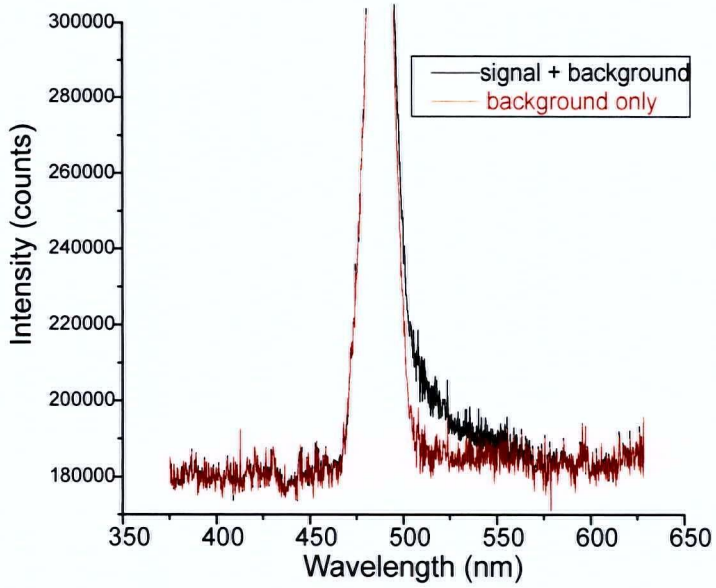

Figure 5.11: R6G fluorescence emission spectrum without background subtraction (black) and the corresponding background spectrum (red) with expanded vertical scale.

Figure 5.12 shows the filter transmittance plotted with the R6G ion emission spectrum. To calculate the attenuation the R6G emission spectrum was multiplied by the measured transmittance of the long pass filter. The result of this calculation is also shown in Figure 5.12.

Using the long pass filter was necessary for pulse counting experiments to reduce the amount of background light detected, but the fluorescence emission was attenuated as well. The long pass filter reduced the total amount of fluorescence by $\approx 83\%$. If this long pass filter was used for the collection of the emission spectrum, the peak fluorescence would have been erroneously measured at 547 *nm*. Now that the emission spectrum has been recorded, a more effective long pass filter could be selected for pulse counting experiments.

5.4 Anti-Stokes Fluorescence

Although the holographic notch filter was not required for the detection optics of the instrument, it was reinstalled into the fiber optic probe and evaluated using 496.5 *nm* excitation. Two 20 minute integrations and one 20 minute background were collected for R6G ions. The trapping level remained

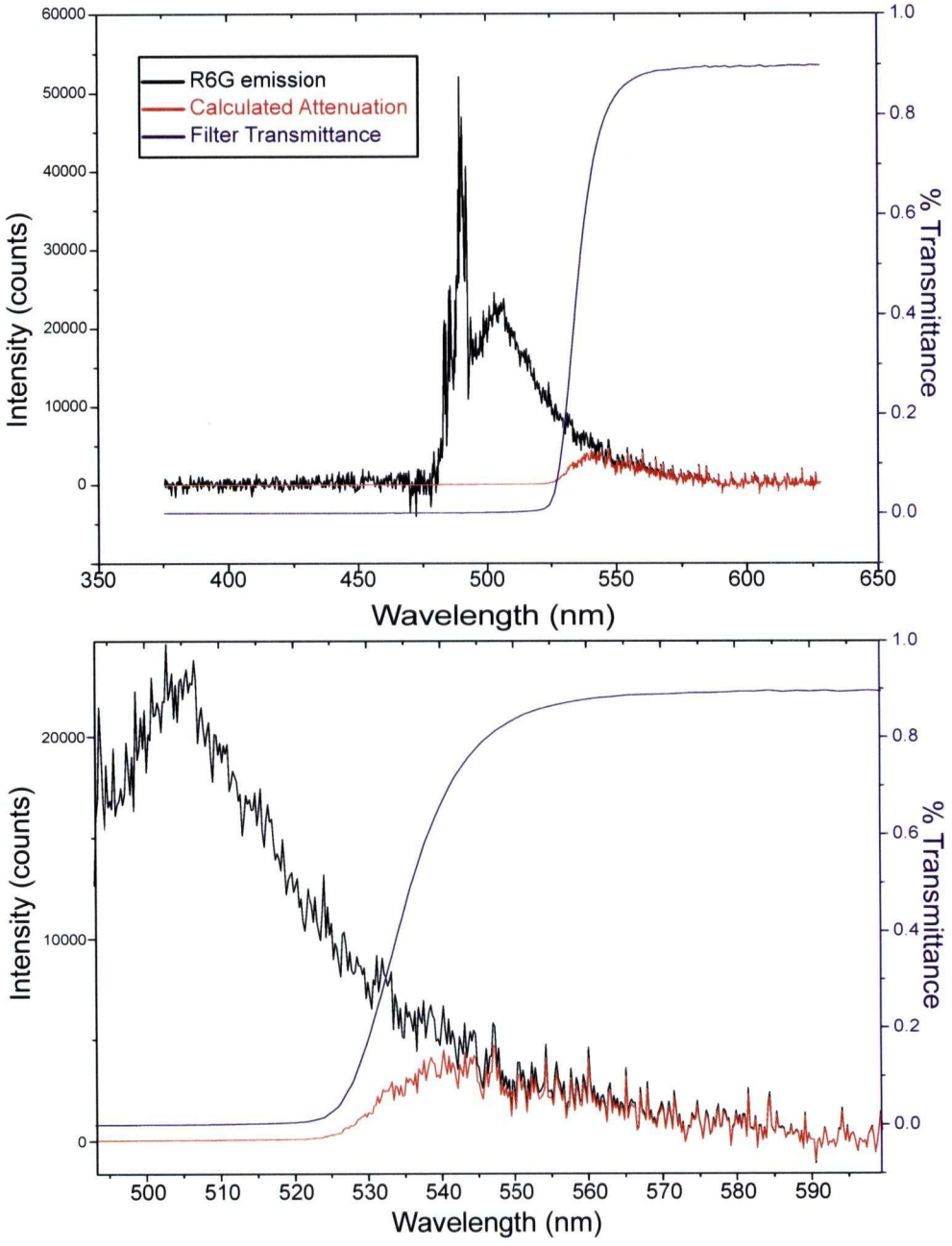

Figure 5.12: R6G emission (left axis), transmittance of the filter used for pulse counting experiments (right axis) and the calculated attenuation of the emission spectrum by the filter. The long pass filter used for pulse counting experiments attenuates the fluorescence significantly.

at $q_z = 0.65$, the laser power was 47 mW, and the buffer gas pressure remained at 1 $mtorr$. The background subtracted R6G emission was smoothed using a five point moving average and the resulting emission spectrum is shown in Figure 5.13.

Another instrumental change was required before 496.5 nm excitation could be used. The filter used to pass only the laser line and block all other argon ion plasma lines was removed. This filter was necessary in older versions of the instrument. Since the black carbon coating of the electrodes and the fiber optic probe reduced the total amount of scattered light collected this filter was no longer necessary.

5.4.1 Discussion

The emission spectrum of R6G ions is shown in figure 5.13. Excitation at 496.5 nm produced a smaller Stokes shift of 9.5 nm compared to the 15 nm Stokes shift measured for 488.0 nm excitation. The emission maximum is now 506 nm. This maximum is directly adjacent to the long wavelength side of the notch filter's attenuation and the notch filter is likely obscuring part of the fluorescence emission.

The fluorescence emission of molecules is usually easy to differentiate

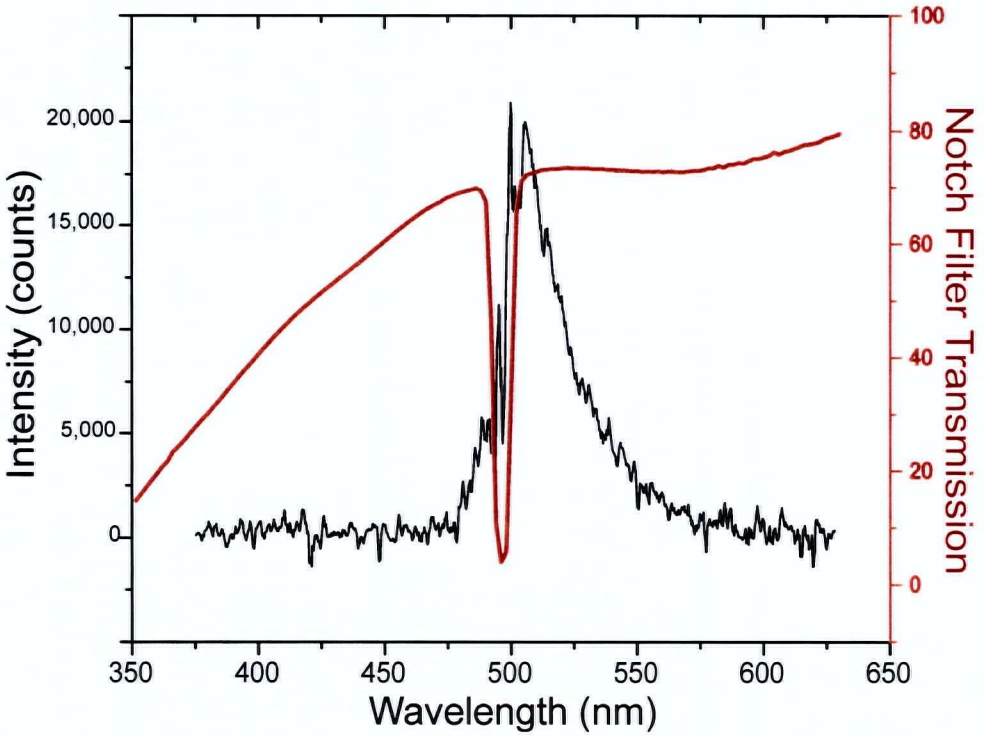

Figure 5.13: R6G emission from 496.5 *nm* excitation (left axis) and the notch filter transmission (right axis).

from Raman scattering. For sufficiently intense emission or long fluorescence lifetimes fluorescence can be temporally resolved from Raman scattering. In condensed phase experiments the fluorescence is often significantly Stokes shifted from the excitation and cannot be confused with Raman scattering (*e.g.* Figure 5.4).

In these gas phase experiments the fluorescence emission is very close to

the laser line and therefore involves transitions similar in energy to those expected in a resonance Raman spectrum. The emission observed for R6G ions excited at 488.0 nm and 496.5 nm is consistent with fluorescence emission. Resonance Raman scattering would have produced an emission spectrum with identical Stokes shifts (in energy units, *e.g.* cm^{-1}) at both excitation wavelengths. The observed Stokes shift in nanometers between excitation and emission was smaller for 496.5 nm excitation and therefore even smaller in energy units. The difference in the Stokes shifts observed for the two excitations is indicative of fluorescence.

For comparison, the emission from 488.0 nm and 496.5 nm excitation were plotted on the same graph (Figure 5.14). Within the noise and resolution limits of this measurement, it appears that the R6G emission is identical for excitation at both wavelengths . The R6G ion is excited from a low vibrational energy level of the ground state into a higher vibration level of the excited state. The excited ion will keep this vibrational energy when it returns to the ground state by fluorescence emission. The fluorescence emission wavelength therefore corresponds to the difference in energy of ground and excited states. The diffuseness of the fluorescence emission depends on Franck-Condon factors. Excitation of a gas phase molecule with 488.0 nm

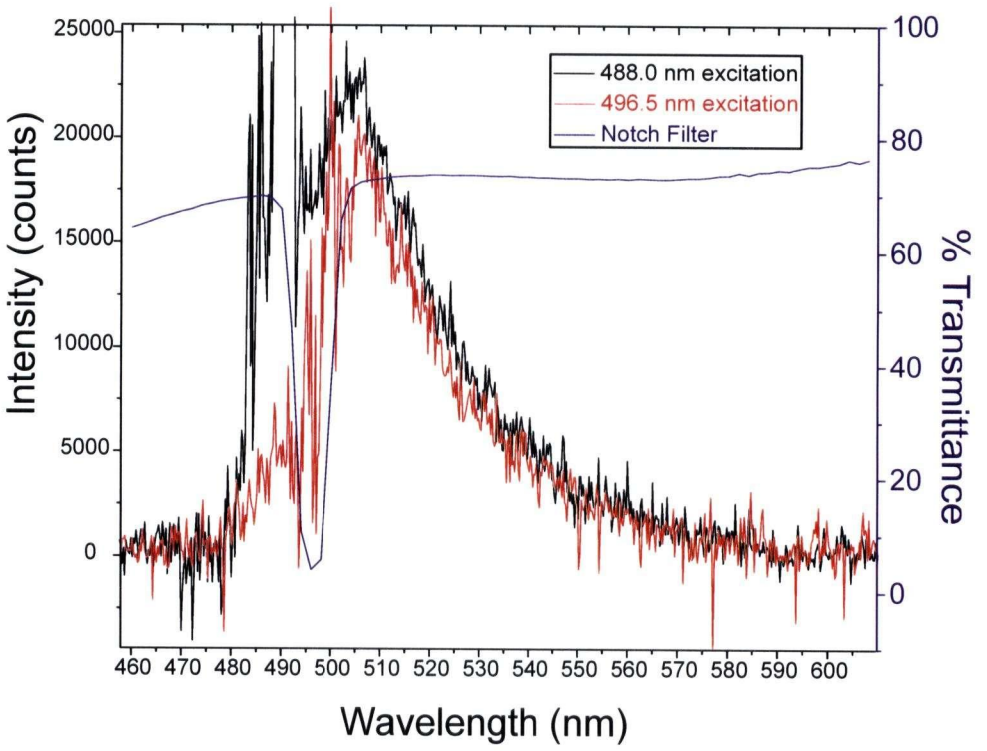

Figure 5.14: R6G ion emission from 488.0 *nm* and 496.6 *nm* excitation (left axis). The notch filter transmittance shown for reference (right axis).

and 496.5 *nm* radiation is expected to produce the same emission spectrum at this resolution.

Anti-Stokes emission can be observed in the R6G emission shown in Figure 5.13. Anti-Stokes emission can occur in the gas phase fluorescence spectrum because the ions are not vibrationally cooled effectively in the excited or ground state. Non-radiative relaxation of the excited state will obviously

lead to heating of the ion. However, a radiative transition will also cause heating of the ion. The Stokes shift observed in the gas phase emission is related to the amount of energy retained by the ion after one excitation and radiative emission. Heating of the ions will lead to photodissociation and anti-Stokes emission. Anti-Stokes emission occurs when a hot ground state ion absorbs a photon and then relaxes to a lower energy level of the ground state.

5.5 Conclusions

This chapter described the first instrument capable of recording gas phase emission spectra of large molecular ions. The instrument developed was not only able to collect emission spectra of large gas phase molecular ions, but the background light rejection of the instrument was even better than expected. Emission spectra were collected without filtering the excitation or collected emission. Without the need for a different pair of filters for every excitation wavelength used, fluorescence excitation spectra of ions can be recorded using this instrument. Simultaneously recording absorption spectra (by monitoring photodissociation) and fluorescence emission spectra can provide a wealth of

spectroscopic information.

Detecting differences in the fluorescence emission spectra of R6G and 5-CR 6G ions was very encouraging. The ability to detect such small structural differences supports the hypothesis that fluorescence emission spectroscopy can be a sensitive probe of gas phase molecular ion structure. Finally, knowledge of an ion's fluorescence emission spectrum would be very useful for selecting filters for pulse counting experiments.

5.6 Perspective

The results described in Chapter 4 and Chapter 5 were first reported at the 51st Annual ASMS Conference on Mass Spectrometry and Allied Topics (June 8-12, 2003, Montréal, Canada). At the same conference Alan Marshall's group at the National High Magnetic Field Laboratory in Florida reported the collection of the emission spectrum of $C_6F_6^+$ confined in an ICR trap. $C_6F_6^+$ has an excited state lifetime that is long enough to allow a detector to be turned on after the excitation from a pulsed laser has passed. Their emission experiment required 80 hours of integration time. However, temporally resolving the fluorescence from the background may limit this technique

to small or simple molecules. Since larger molecules have shorter fluorescence lifetimes their emission spectra are very difficult to measure in this way. Since most of the intended applications for the instrument described in this thesis involve large molecules, temporal separation methods are not desirable. Interestingly, this group also revealed plans for an instrument based on a linear quadrupole ion trap.

Chapter 6

Summary and Conclusion

6.1 Summary

This thesis described the first instrument capable of high S/N gas phase fluorescence measurements of large molecular ions. The instrument is also the first capable of recording the gas phase emission spectra of large gas phase molecular ions. This instrument was used with filters and a pulse counting PMT to detect fluorescence, or the fluorescence was dispersed with a spectrograph and an emission spectrum recorded with an ICCD. The instrument is versatile, sensitive and robust.

The two most significant experimental challenges associated with detecting the gas phase fluorescence of ions were discovered rather than anticipated. First, the susceptibility of gas phase ions to photodissociation was an unexpected problem. Photodissociation limited the laser power which could be used. Second, the fluorescence emission of gas phase ions was not significantly

Stokes shifted from the excitation. The lack of Stokes shift meant that small fluorescence signals must be detected in the presence of background scatter generated by the excitation. The technical difficulties associated with such a measurement are similar to those encountered in condensed phase Raman experiments. The background scatter recorded with the initial version of the instrument was $\approx 1.7 \times 10^7$ times larger than the fluorescence signal eventually detected.

Initial experiments were carried out on PAH cations. Although fluorescence from these cations was not detected, the experiments outlined in Chapter 3 were still very useful. The most obvious result from the PAH experiments was that molecules are more vulnerable to photodissociation in the gas phase. The emission of neutral molecules also suggested that ion emission may be significantly closer to the laser line than originally predicted. The lack of detectable emission indicated that the fluorescence was below the noise level, or not present at all. Changing the ion source to electrospray eliminated the neutral background problem, but the real challenge was to extract the fluorescence signal from the much larger laser background.

The ESI source permitted the investigation of molecules that were not accessible with the thermal desorption probe (Section 2.4.1). Initial exper-

iments were carried out on R6G and 5-CR 6G cations. Unfortunately, the fluorescence emission from these ions was still buried in the background noise and was undetectable. Photodissociation experiments with R6G and 5-CR 6G did however lead to a improved understanding of the gas phase photophysics of trapped ions. For fluorescence to be detected, the ion optics of the ESI front-end needed improvement and major changes to the optical collection system were necessary.

The innovative changes to the instrument reduced the background by six orders of magnitude. The internal beam dump was an addition that reduced some background noise; however, the carbon coating of the electrodes and the development of the fiber optic probe were the key elements introduced to reduce the background. As a result, background noise was reduced without limiting the versatility of the instrument.

For fluorescence experiments, the 3D ion trap is an excellent device for confining ions. Optically, the ion volume is well shielded from the rest of the instrument. As a result, much of the unwanted light scattered off of the vacuum manifold does not reach the inside of the trap. With inside surfaces of the electrodes coated black the ion trap makes a good "ion cuvette".

The pulse counting experiments described in Chapter 4 were used to

optimize fluorescence detection. The greatest fluorescence signals were measured for compact ion clouds and lower laser powers. A trapping potential corresponding to $q_z = 0.65$ gave the best fluorescence signal for R6G ions. With the fluorescence experiment optimized, the emission spectra of R6G and 5-CR 6G ions were collected. It was possible to collect the emission spectra discussed in Chapter 5 for two reasons. First, the background was reduced 1.3×10^6 times with the instrumental innovations detailed in Chapter 4. Second, the signal was amplified $\approx$ 7800 times using an ICCD. Finally, anti-Stokes fluorescence was detected from R6G excited at 496.5 nm.

6.2 Conclusion

In condensed phase experiments molecules excited to a high vibrational level of the excited state quickly lose excess vibrational energy to the surrounding solvent or matrix. Any fluorescence will therefore originate from the lowest vibrational energy level of the excited state. Franck-Condon factors are non-zero for a wide range of transition energies and the resulting emission is a diffuse band. After emission, some molecules will be in a high vibrational level of the ground state. The excess vibrational energy is again absorbed by

the solvent and the molecules end up in the lowest vibrational energy level of the ground state.

Since all fluorescence emission in the condensed phase originates from the lowest vibrational level of the excited state, excitation at different wavelengths produces the same fluorescence emission spectrum. The Stokes shift observed in solution experiments is a consequence of vibrational relaxation of the excited state and solvent rearrangements. In the gas phase, no such relaxation of the excited state can occur between absorption and emission events. As a result, smaller Stokes shifts are observed in gas phase emission spectra. Furthermore, without a solvent or matrix to remove excess vibrational energy, gas phase ions remain vibrationally hot after emission occurs.

To detect fluorescence from gas phase ions confined in an ion trap an instrument must be capable of separating the emission from the excitation. For atomic ions this is very easy. Figure 6.1 shows two different excitation schemes that are used to detect atomic fluorescence. Multiphoton absorption will produce an emission that is at least half the wavelength of the excitation. Alternatively, emission from a lower energy transition of the atomic ion can be monitored. In both cases the excitation and emission transitions are well separated in wavelength; thus fluorescence is detected against a zero

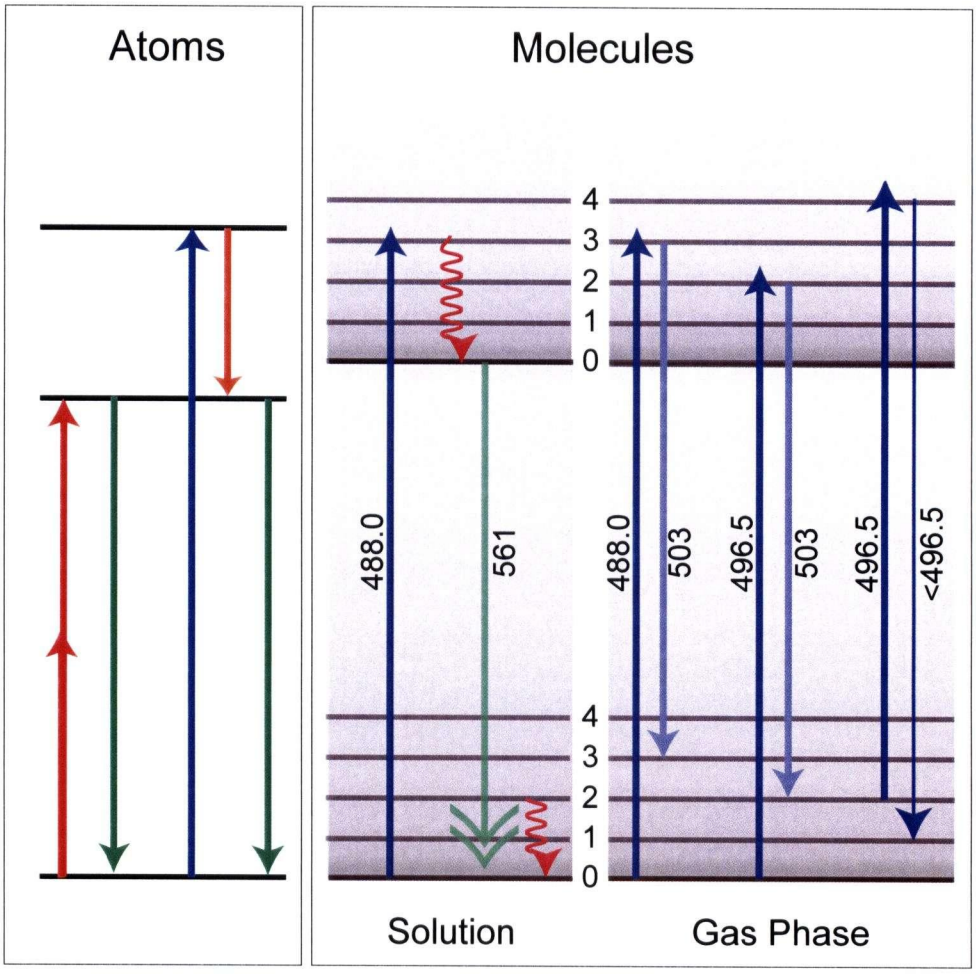

Figure 6.1: Energy level diagrams for fluorescence experiments.

background. Furthermore, the excitation laser power is not limited by photodissociation.

Fluorescence from atomic and small molecular ions can also be detected using a pulsed laser source. These ions typically have long fluorescence lifetimes and their emission can be detected after an excitation pulse. For larger molecules excited state lifetimes are usually 1 to 3 ns and their fluorescence must be detected in the presence of the excitation background. The limitation in this case is not the length of the laser pulse, but the time required to gate a detector. The best intensifiers currently require several nanoseconds to turn on. Therefore, in the time it takes to gate on the detector the signal will have almost completely decayed.

For a large gas phase molecular ion, excitation places the ion in a high vibrational level of the excited state. The ion cannot lose energy before emission occurs so it retains this vibrational energy when it emits a photon. A π-$\pi^{\star}$ transition is not expected to induce a significant distortion in a large dye molecule and the Franck-Condon factors will therefore be greatest for transitions to the same vibrational level of the ground state. Figure 6.1 illustrates why excitation of R6G at 488.0 nm and 496.5 nm produces the same emission spectrum. The emission is mainly dependent on the difference in

energy between the ground state and the excited state. Anti-Stokes fluorescence can be detected when a vibrationally hot ion in the ground state absorbs a photon and then relaxes to a lower vibrational level of the ground state.

Since the fluorescence is not Stokes shifted far from the excitation wavelength the fluorescent measurement is no longer made against a zero background. Without a zero background, the main sensitivity advantage of fluorescence spectroscopy is lost. However, difficulties associated with measuring the fluorescence emission of trapped ions do not detract from the desired benefits of such a measurement.

6.3 Future Directions

6.3.1 Improvements to the Instrument

A tunable laser for excitation would be very useful for molecular spectroscopic investigations and for optimizing the fluorescence experiment. It would allow the fluorescence excitation spectrum of an ion to be collected. A tunable laser would also allow the optimization of the fluorescence experiment with respect to excitation energy. The optimal excitation wavelength will likely be a trade

off between increasing the molar absorptivity and decreasing the Stokes shift.

A spectrograph with improved resolving power would also enhance this instrument. The spectrograph initially acquired for this instrument has a 600 grooves/mm grating. Since the fluorescence emission is not significantly Stokes shifted from the excitation a grating with a higher groove density (e.g. 1200 grooves/mm) would be more effective in separating the fluorescence emission from the excitation at the detector. A greater physical separation at the detector will decrease the amount of stray light contaminating the emission signal. The original grating would still be useful for solution measurements where greater spectral coverage is required at the focal plane.

More modest gains in instrument performance could be realized by increasing the size of the fiber optic probe and using a buffer gas that would more efficiently cool the ions. Increasing the number of fibers will improve collection efficiency. However, this must be accomplished without degrading the capabilities of the ion trap as a mass spectrometer. Sulphur hexafluoride (SF_6) should be evaluated as a collision gas during a fluorescence experiment. SF_6 will likely be more effective at cooling ions during collisions and allow the use of higher laser powers.

For an improved understanding of the experiment pulse counting tech-

niques should be applied to the ion trap detector. Currently, the ion trap uses analog detection but pulse counting could help estimate the total number of ions in the trap. The maximum capacity for an ion trap similar to the one used in this work is thought to be approximately one million ions. Pulse counting the output of the ion trap during a mass scan would help refine this approximation. This would be a first step towards quantifying gas phase molar absorptivities and fluorescent quantum efficiencies.

6.3.2 Applications

Future work will involve applications of the instrument. Gas phase structure of proteins could be investigated using fluorescent tags or by detecting native fluorescence from tryptophan or green fluorescent protein (GFP). GFP has been cloned and purified for this purpose. Fluorescence emission detection could also be used to complement other molecular spectroscopies.

PAH cations are potential DIB carriers that could be evaluated using fluorescence spectroscopy. Photodissociation is commonly used to measure the gas phase absorption of PAH ions. However, if the fluorescence quantum efficiency of particular transition is very high it may appear to have a lower absorption in a photodissociation experiment. Fluorescence experiments may

help refine absorption measurements based solely on photodissociation.

In addition, FRET experiments may help determine the structures of gas phase proteins. FRET experiments rely on the emission of one molecule to be resonant with the absorption of the second molecule. FRET pairs that work well in solution may not be appropriate for gas phase experiments. As demonstrated in this work, the absorption and fluorescence emission of a molecule is very different in the gas phase. Methods and instrumentation developed in this thesis could be used to select suitable molecules for gas phase FRET experiments.

6.3.3 Concluding Remarks

The instrumental innovations described in this thesis permitted high S/N fluorescence detection and fluorescence emission spectroscopy of large gas phase molecular ions. Others wishing to investigate the fluorescence emission of trapped molecular ions will be able to duplicate these innovations in a straightforward manner. Detecting fluorescence emission from large gas phase ions was an experimental problem that had frustrated many groups over the past twenty or thirty years. With the knowledge gained during the development of the instrument described this problem has now been solved.

Bibliography

[1] L. Stryer and R.P. Haugland. Energy transfer: A spectroscopic ruler. *Proc. Natl. Acad. Sci. U.S.A.*, 58(2):719–726, 1967.

[2] Paul R. Selvin. The renaissance of fluorescence energy transfer. *Nature Struct. Biol.*, 7(9):730–734, 2000.

[3] Guo-Zhong Li, Bryan A. Vining, Shenheng Guan, and Alan G. Marshall. Laser-induced fluorescence of Ba^+ ions trapped and mass-selected in a fourier transform ion cyclotron resonance mass spectrometer. *Rapid Communications in Mass Spectrometry*, 10:1850–1854, 1996.

[4] C. Moutou, L. Verstraete, P. Brechignac, S. Piccirillo, and A. Leger. Laser induced fluorescence spectroscopy of jet-cooled molecular species:a tool to identify diffuse interstellar band carriers. *Astronomy and Astrophysics*, 319:331–339, 1997.

[5] D. Romanini, L. Biennier, F. Salama, A. Kachanov, L. J. Allamandola, and F. Stoeckel. Jet-discharge cavity ring-down spectroscopy of ionized polycyclic aromatic hydrocarbons: progress in testing the pah hypothesis for the diffuse interstellar band problem. *Chemical Physical Letters*, 303(1-2):165–170, 1999.

[6] J.J. Thomson. *Rays of Positive Electricity.* Longmans Green and Co., London, 1913.

[7] W Paul and H Steinwedel. Apparatus for separating charged particles of different specific charges. *German Patent*, 944,900, 1956.

[8] W. Neuhauser, M. Hohenstatt, P.E. Toschek, and H. Dehmelt. Localized visible Ba^+ mono-ion oscillator. *Phys. Rev. A*, 22(3):1137, 1980.

[9] Fred J. Grieman, Bruce H. Mahan, and Anthony O'Keefe. The laser induced fluorescence spectrum of trapped BrCN cations. *J. Chem. Phys.*, 74(2):857–861, 1981.

[10] Cecilia C. Martner, Jurgen Pfaff, Neil H. Rosenbaum, Anthony O'Keefe, and Richard J. Saykally. Radiative lifetimes of trapped molecular ions:HCl^+ and HBr^+. *J. Chem. Phys.*, 78(12):7073–7076, 1983.

[11] Alexander Baldwin Young, Raymond Evans March, and Richard James Hughes. Studies of infrared multiphoton dissociation rates of protonated aliphatic alcohol dimers. *Can. J. Chem.*, 63:2324–2331, 1985.

[12] F. Diedrick, J.C. Bergquist, Wayne M. Itano, and D.J. Wineland. Laser cooling to the zero-point energy of motion. *Physical Review Letters*, 62 (4):403–406, 1989.

[13] R.C. Thompson. Spectroscopy and quantum optics with trapped ions. *Comments At. Mol. Phys.*, 27(6):349–364, 1992.

[14] D.J. Wineland, Wayne M. Itano, and R.S. Jr. Van Dyck. High-resolution spectroscopy of stored ions. In *Advances in Atomic and molecular Physics*, volume 19, pages 135–186. Academic Press, New York, 1983.

[15] Yang Wang, Christopher L. Hendrickson, and Alan G. Marshall. Direct optical spectroscopy of gas-phase molecular ions trapped and mass-selected by ion cyclotron resonance: laser -induced fluorescence excitation spectrum of hexafluorobenzene ($C_6F_6^+$). *Chemical Physical Letters*, 334:69–75, 2001.

[16] Joseph T. Khoury, Sandra E. Rodriguez-Cruz, and Joel H. Parks. Pulsed fluorescence measurements of trapped molecular ions with zero background detection. *J. Am. Soc. Mass Spectrom.*, 13:696–708, 2002.

[17] Michael D. Barnes, William B. Whitten, and Micheal J. Ramsey. Detecting single molecules in liquids. *Analytical Chemistry*, 67(13):418A, 1995.

[18] Raymond E. March and John F.J. Todd, editors. *Practical Aspects of Ion Trap Mass Spectrometry: Fundamentals of Ion Trap Mass Spectrometry*, volume I. CRC Press, New York, 1995.

[19] Raymond E. March and John F.J. Todd, editors. *Practical Aspects of Ion Trap Mass Spectrometry: Ion Trap Instrumentation*, volume II. CRC Press, New York, 1995.

[20] Raymond E. March. Quadrupole ion trap mass spectrometry: a view at the turn of the century. *International Journal of Mass Spectrometry*, 200:285–312, 2000.

[21] M. Nappi, C. Weil, C.D. Cleven, L.A. Horn, H. Wollnik, and R.G. Cooks. Visual representations of simulated three-dimensional ion trajectories in

an ion trap mass spectrometer. *International Journal of Mass Spectrometry and Ion Processes*, 161:77–85, 1997.

[22] E. Mathieu. Memoire sur le mouvement vibratoire d'une membrane de forme elliptique. *J. Math. Pures Appl.*, 13:137, 1868.

[23] Raymond E. March. An introduction to quadrupole ion trap mass spectrometry. *Journal of Mass Spectrometry*, 32:351–369, 1997.

[24] J.E.P. Syka, J.N. Louris, P.E. Kelly, G.C. Jr. Stafford, and W. Reynolds. Method of operating an ion trap. *U.S. Patent*, 738,018, 1985.

[25] Raymond E. Kaiser, John N. Jr. Louris, Jonathan W. Amy, and R. Graham Cooks. Extending the mass range of the quadrupole ion trap using axial modulation. *Rapid Communications in Mass Spectrometry*, 3(7): 225–229, 1989.

[26] J. Louris. Presentation WOB 10:45. In *40th ASMS*, Washington, D.C., 1992.

[27] P.E. Kelley, G.C. Jr. Stafford, and D.R. Stephens. Method of mass analyzing a sample by use of a quadrupole ion trap. *U.S. Patent*, 4,540,884, 1985.

[28] Scott Gronert. Estimation of effective ion temperatures in a quadrupole ion trap. *J. Am. Soc. Mass Spectrom.*, 9:845–848, 1998.

[29] D.J. Douglas and J.B. French. Collisional focusing effects in radio frequency quadrupoles. *J. Am. Soc. Mass Spectrom.*, 3:398–408, 1992.

[30] Paul Kebarle and Liang Tang. From ions in solution to ions in the gas phase. the mechanism of electrospray mass spectrometry. *Analytical Chemistry*, 65(22):972A–986A, 1993.

[31] Terri L. Constantopoulos, George S. Jackson, and Christie G. Enke. Challenges in achieving a fundamental model for ESI. *Analytica Chimica Acta*, 406:37–52, 2000.

[32] Scott T. Quarmby and Richard A. Yost. Fundamental studies of ion injection and trapping of elctrosprayed ions on a quadrupole ion trap. *International Journal of Mass Spectrometry*, 187:1–23, 1999.

[33] Richard B. Cole, editor. *Electrospray Ionization Mass Spectrometry. Fundamentals, Instrumentation & Applications.* John Wiley & Sons, Inc., Toronto, 1997.

[34] R.P.A. Hartman, D.J. Brunner, D.M.A. Camelot, J.C.M. Marijnissen, and B. Scarlett. Electrohydrodynamic atomization in the cone-jet mode physical modeling of the liquid cone and jet. *J. Aerosol Sci.*, 30(7): 823–849, 1999.

[35] A. Jaworek and A. Krupa. Classification of the modes of EHD spraying. *J. Aerosol Sci.*, 30(7):873–893, 1999.

[36] Th Dulcks and R. Juraschek. Electrospray as an ionization method for mass spectrometry. *J. Aerosol Sci.*, 30(7):927–943, 1999.

[37] Scott A. McLuckey, Gary J. Van Berkel, Douglas E. Goeringer, and Gary L. Glish. Ion trap mass spectrometry of externally generated ions. *Analytical Chemistry*, 66(13):689A–696A, 1994.

[38] David Rendell. *Fluorescence and Phosphorescence.* Analytical Chemistry by Open Learning. John Wiley & Sons, Toronto, 1987.

[39] L.H. Kieth and W.A. Telliard. ES&T special report: Priority pollutants: I-a perspective view. *Environ. Sci. Technol.*, 13(4):416–423, 1979.

[40] Tadamasa Shida, editor. *Electronic absorption spectra of radical ions*, volume 34 of *Physical sciences data.* Elsevier, New York, 1988.

[41] Robert E. Buckles, Arthur Serianz, and David Naffziger. Dibenzo(g.p)chrysene: A challenging experiment in organic synthesis. *Proc. Iowa Acad. Sci.*, 80:45–49, 1973.

[42] Steven C. Hill, Michael D. Barnes, Noah Lermer, William B. Whitten, and J. Michael Ramsey. Simulation of single-molecule photocount statistics in microdroplets. *Analytical Chemistry*, 70:2964–2971, 1998.

[43] John P. Maier. Spectroscopic studies of open-shell organic cations in the gas phase. *Chimia*, 34(5):219–231, 1980.

[44] C. L. Hunter, A. G. Mauk, and D. J. Douglas. Dissociation of heme from myoglobin and cytochrome b5: Comparison of behavior in solution and in the gas phase. *Biochemistry*, 36:1018, 1997.

[45] Robert C. Dunbar, Jyh Horung Chen, Hun Young So, and Bruce Asamoto. Infrared fluorescence relaxation of photoexcited gas-phase ions by chopped-laser two-photon dissociation. *J. Chem. Phys.*, 86(4): 2081–2086, 1987.

[46] James D. Faulk and Robert C. Dunbar. Photodissociation spectroscopy of gas-phase ferrocene cation. *J. Am. Soc. Mass Spectrom.*, 2:97–102, 1991.

[47] Robert C. Dunbar. Photodissociation of trapped ions. *International Journal of Mass Spectrometry*, 200:571–589, 2000.

[48] Melvin B. Comisarow and Alan G. Marshall. Fouier transform ion cyclotron resonance spectroscopy. *Chemical Physical Letters*, 25(2):282–283, 1974.

[49] B. Cage, M.A. McFarland, C.L. Hendrickson, N.S. Dalal, and A.G. Marshall. Resolution of individual component fluorescence lifetimes from a mixture of trapped ions by laser-induced fluorescence/ion cyclotron resonance. *J. Chem. Phys. A.*, 106:10033–10036, 2002.